AN EXPERIMENTAL STUDY OF SPIN INTERACTIONS AT VERY LOW TEMPERATURES

A thesis submitted for the Degree of Doctor of Philosophy in the University of Oxford

by

R.H.B. EXELL, B.A.

BODLEIAN LIBRARY OXFORD
DEPOSITED THESIS
27. iii. 62

Magdalen College. Hilary Term, 1961.

Enlarged Michaelmas Term, 1961.

Contents

Abstract 5

Acknowledgements 12

PART ONE 14

THE MEASUREMENT OF MAGNETIZATION ENTROPY
–
LOW TEMPERATURE PROPERTIES OF
FERRIC METHYLAMMONIUM ALUM

CHAPTER ONE 15

DETERMINATION OF ABSOLUTE TEMPERATURES BELOW 1°K - introduction - absolute temperatures below 1°K - calculation of magnetization entropy - experimental measurement of magnetization entropy.

PROPERTIES OF FERRIC METHYLAMMONIUM ALUM - crystalline Stark effect - thermodynamic properties.

CHAPTER TWO 27

APPARATUS - cryostat - magnet - sample - thermometers.

EXPERIMENTAL DETERMINATION OF MAGNETIZATION ENTROPY - technique - measurements in small fields - results.

CHAPTER THREE 43

CALCULATION OF THE MAGNETIZATION ENTROPY - introduction - small magnetic fields - large magnetic fields.

CHAPTER FOUR 61

DETERMINATION OF ABSOLUTE TEMPERATURES BELOW 1°K - adiabatic demagnetizations - S/R-T* relation - specific heat - absolute temperatures below 1°K.

CONCLUSION - further applications.

PART TWO 71

HYPERFINE COUPLING IN FERROMAGNETIC MATERIALS

CHAPTER ONE 72

HYPERFINE COUPLING IN TRANSITION METALS - introduction - the transition metals - effective magnetic field at the nuclei.

EXPERIMENTAL DETERMINATIONS OF H_{eff} - gamma-ray anisotropy - heat capacity - nuclear resonance - Mössbauer experiments - some results for iron-cobalt alloys.

CHAPTER TWO 88

APPARATUS AND ASSEMBLY OF SAMPLES - a modification to the vacuum jacket - cooling salt - hysteresis heating - carbon thermometer - electrical heater.

EXPERIMENTS - procedure - calculation of results.

CHAPTER THREE 105

RESULTS - ordered and disordered iron-cobalt alloy - other iron-cobalt alloys - summary of results.

DISCUSSION OF RESULTS - effective magnetic field at the nuclei - electronic heat capacity.

CHAPTER FOUR 128

URANIUM HYDRIDE - introduction - heat capacity measurements above 1°K - heat capacity measurements below 1°K - discussion.

APPENDIX - electrical resistivity of uranium hydride.

CHAPTER FIVE 143 A

THE INTERPRETATION OF HFC RESULTS IN FERROMAGNETIC MATERIALS - introduction - the conduction electrons - the 3d electrons - the pure metals - iron cobalt alloys - close packed alloys - iron impurities in other metals.

PART THREE 144

LOW TEMPERATURE HEAT CAPACITY OF TITANIUM-IRON AND ZINC-MANGANESE FLUORIDE

CHAPTER ONE 145

HEAT CAPACITY OF TiFe - introduction - the experiments - discussion.

CHAPTER TWO 154

ZINC-MANGANESE FLUORIDE - introduction - experiments - discussion.

References 164

Further references 168 A

Abstract

This thesis is divided into three parts. Part One contains a description of a method for measuring the magnetization entropy of a paramagnetic salt near $1^{\circ}K$, and a study of the low temperature thermal and magnetic properties of ferric methylammonium alum. Part Two contains an account of heat capacity measurements below $1^{\circ}K$ made to examine the hyperfine coupling in ferromagnetic materials. Results are given for a range of iron-cobalt alloys, and for uranium hydride. Part Three contains an account of low temperature heat capacity measurements for titanium-iron, and for mixed zinc-manganese fluoride crystals.

Part One. The isothermal magnetization entropy of paramagnetic salts is needed for the standard method of determining the absolute temperatures reached by magnetic cooling. If the crystalline Stark splittings of the paramagnetic ions are $\sim k \times 1^{\circ}K$, the magnetization entropy deviates from ideal behaviour, and cannot be calculated easily. A method is described for determining the magnetization entropy of a cooling salt by measuring the heat absorbed during isothermal demagnetizations near $1^{\circ}K$ (Kurti, 1955; Croft and Exell, 1961).

The sample bearing a heater and a carbon thermometer is placed in a demagnetization cryostat. The sample is magnetized isothermally

at 1°K with a solenoid. It is then isolated and, while heat is introduced at a constant rate, the magnetic field is so diminished that the temperature shown by the carbon thermometer remains constant. Since the magnetic field is proportional to the solenoid current, and since the heat input is proportional to time, a recorder graph of the solenoid current gives the entropy as a function of field. The experimental arrangement is also suitable for making adiabatic demagnetizations at intervals of a few minutes.

The method has been used with ferric methylammonium alum, $Fe(NH_3CH_3)(SO_4)_2 \cdot 12H_2O$, whose overall Stark splitting is k x 1.6°K (Bleaney and Trenam, 1954). At 1.15°K and in fields below 1 kG the magnetization entropy was found to be close to that for an ideal paramagnetic substance with J = 5/2, while in fields of about 10 kG it was found to be about 10% less than the "ideal" value.

The entropy of this salt in small fields has been calculated approximately by a series expansion method, and found to be nearly ideal. In addition, the energy levels of the ferric ion in the trigonal crystalline field for a range of magnetic field strengths and orientations have been used to obtain a complete table of entropies for this salt by computer methods. Values of the entropy have been obtained for temperatures from 0.9°K to 1.2°K, and for magnetic fields from zero to 16 kG, both for use in single crystals and for a powder. The computed entropies for a powder are in

agreement with the experimental values.

Specific heat measurements below 1°K were found to agree with those of Cooke, Meyer, and Wolf (1956). The computed entropies have been used to determine the absolute temperatures below 1°K reached by adiabatic demagnetizations of this salt. The results differed from those of Cooke, Meyer, and Wolf, who used cerium magnesium nitrate as a thermometer. The results of this thesis agree above 0.4°K with the curve calculated from the Stark splittings, but deviate from it at lower temperatures.

Part Two. In ferromagnetic materials the magnetic electrons produce an effective magnetic field H_{eff} at the nuclei, usually of the order 10^2 to 10^3 kG. This field, which has an orienting effect on nuclei carring a magnetic moment, may be measured at low temperatures from the anisotrop y of gamma-ray emission from radioactive nuclei, and from a Schottky anomaly in the specific heat. H_{eff} may also be determined by nuclear resonance, and from Mössbauer experiments. The specific heat method has been used in the present work to measure H_{eff} at the cobalt nuclei in bcc iron-cobalt alloys, and to look for hyperfine coupling between the magnetic electrons and the hydrogen nuclei in uranium hydride, UH_3.

The samples were mounted in the cryostat with an electrical heater, a carbon thermometer, and cerium magnesium nitrate for magnetic cooling. The heat capacity was measured electrically from

0.4°K to 1.2°K in the Fe-Co alloys, and from 0.5°K to 5°K in UH_3. Hysteresis heating in the samples, which hindered the attainment of very low temperatures, was offset by the addition of extra amounts of cooling salt.

The measurements for the Fe-Co alloys were made initially to investigate a discrepancy (now resolved) between values of H_{eff} found from gamma-ray anisotropy experiments at Oxford and specific heat measurements at Berkeley. In the present work H_{eff} was found to be 293 kG for 47.5 %Co both in the ordered crystal structure and in the disordered structure. In other compositions H_{eff} was found to vary from 301 kG for 30 %Co to 244 kG for 70 %Co. The present results, while not conflicting with those of Arp, Edmonds, and Petersen (1959), provide the additional information that H_{eff} at the cobalt nuclei does not follow the simple linear function of composition suggested by their work. The present results show higher values of H_{eff} near 35 %Co, where there is a maximum in the Slater-Pauling curve of saturation magnetization for these alloys.

The measurements also give the conduction electron contribution to the heat capacity in these alloys, and from this an indication of the density of electronic states at the Fermi surface. In the Fe-Co alloys the electronic term was found to vary from 2.1 T millijoules/mol.deg for 30 %Co to 4.9 T millijoules/mol.deg for 70 %Co. These results agree with those of Cheng, Wei, and Beck (1960).

They suggest partial filling of an energy band of electrons whose spins are opposite to those responsible for the ferromagnetism.

In UH_3 the electronic heat capacity was found from the measurements above $1^{\circ}K$ to be 27 T millijoules/mol.deg. This value agrees within the experimental errors with that of Flotow, Lohr, Abraham, and Osborne (1959) obtained at higher temperatures, and is higher than that for uranium metal. No hyperfine Schottky anomaly was detected in UH_3 from the measurements below $1^{\circ}K$. An upper limit for the value of H_{eff} at the hydrogen nuclei was estimated at about 30 kG. Some electrical resistivity measurements for UH_3 made by Goitein and Richards from $93^{\circ}K$ to $241^{\circ}K$ are also quoted. UH_3 conducts like a metal and has a slight anomaly in the resistivity-temperature curve near the ferromagnetic Curie point ($\sim 170^{\circ}K$).

Part Three. At liquid helium temperatures there is a temperature independent contribution to the heat capacity of titanium-iron, TiFe (Schroder and Cheng, 1960). In the present work the heat capacity of TiFe has been measured from $1.4^{\circ}K$ to $0.3^{\circ}K$, and this contribution has been found to decrease with decreasing temperature in this region. Magnetic measurements show that TiFe is super-paramagnetic and contains ferromagnetic clusters of atoms. Schroder has proposed that the specific heat of such clusters can be approximated at low temperatures by an Einstein function. The results of this thesis indicate that the characteristic temperature of such

a function for TiFe is 1.3°K.

Finally, low temperature heat capacity measurements have been made on mixed crystals of zinc-manganese fluoride, Zn-MnF_2. In these crystals the Néel temperatures, below which the crystals become antiferromagnetic, depend on the composition. An attempt was made by Baker, Lourens, and Stevenson (1961) to determine these Néel temperatures from the temperature at which the nuclear magnetic resonance of the fluorine nuclei disappears on cooling from room temperature. Since the temperatures at which nuclear resonance disappears are not always equal to the Néel temperatures, a search was made for heat capacity anomalies at the transitions from the paramagnetic state to the antiferromagnetic state. As a contribution to this work the present thesis contains an account of measurements from 0.5°K to 2.5°K made on Zn-MnF_2 crystals in the composition range 11 %Mn to 43 %Mn. The results show that there are no sharply defined lambda anomalies marking the Néel temperatures in these crystals, but broad anomalies do occur. Measurements down to 0.3°K of the anomaly caused by the magnetic interaction of the Mn nuclei in the 43 %Mn sample indicate that the nuclear spin-lattice relaxation time in this crystal is not as long as in pure MnF_2 (Cooke and Edmonds, 1958).

Arp, V., Edmonds, D., and Petersen, R. Phys. Rev. Letters 3 212 (1959).

Baker, J.M., Lourens, J.A., and Stevenson, R.W.H. Accepted for publication in Proc. Phys. Soc. (1961). 77, 1038.

Bleaney, B., and Trenam, R.S. Proc. Roy. Soc. A 223 1 (1954).

Cheng, C.H., Wei, C.T., and Beck, P.A. Phys. Rev. 120 426 (1960).

Cooke, A.H., and Edmonds, D.T. Proc. Phys. Soc. 70 517 (1958).

Cooke, A.H., Meyer, H. and Wolf, W.P. Proc. Roy. Soc. A 237 404 (1956).

Croft, A.J., and Exell, R.H.B. Accepted for publication in Proc. Roy. Soc. (1961). A 262 110.

Flotow, H.E., Lohr, H.R., Abraham, B.M., and Osborne, D.W. J. Amer. Chem. Soc. 81 3529 (1959).

Kurti, N. Conf. Phys. Basses Temp. Paris (1955), p.187.

Schroder,K. and Cheng, C.H. J. App. Phys. 31 2154 (1960).

Acknowledgements

I have much pleasure in expressing here my gratitude towards -

Professor B. Bleaney for offering me the facilities of the Clarendon Laboratory, and for his interest in the work;

Dr. N. Kurti, my supervisor, for his generous help and instruction at all times, and for many stimulating ideas;

Dr. A.J. Croft, who introduced me to research work, taught me how to use the cryostat, and helped me with the experiments on ferric methylammonium alum; and

Dr. J.H.E. Griffiths, my former college tutor, whose good natured tuition formed an indispensable preparation for this work.

The ferric methylammonium alum sample was prepared and analysed by Dr. P.F.D. Shaw; the Fe-Co alloys were supplied by Mr. A.D. LeClaire, Professor P.A. Beck, and Dr. D.M.S. Bagguley; the TiFe sample was supplied by Professor Beck; the uranium hydride was supplied by Dr. A. Kussner; and the Zn-MnF_2 crystals were supplied by Dr. J.M. Baker.

Jarrett's data used in the computing work was given to me by Dr. W.P. Wolf. Dr. L. Fox kindly helped me with the computing and gave me the use of the Mercury Computer at Oxford.

Dr. J.W. Christian kindly examined one of the Fe-Co alloys by X-ray diffraction.

I thank Mr. Tilbury and the staff of the Low Temperature Workshop, and Mr. Saxton and the members of the Glassblowing Workshop for construction and repairs on the apparatus; Mr. Hazel, Mr. Band, and Mr. Day for the supply of cold liquids; Mr. Newbold for assistance in many of the experiments; Miss Bunnag for most of the typing; and all others who have helped from time to time and are not mentioned above.

Finally, I express my debt to the Department of Scientific and Industrial Research for financial support in the form of a Research Studentship.

PART ONE

THE MEASUREMENT OF MAGNETIZATION ENTROPY - LOW TEMPERATURE PROPERTIES OF FERRIC METHYLAMMONIUM ALUM

CHAPTER ONE

DETERMINATION OF ABSOLUTE TEMPERATURES BELOW 1°K

Introduction

Paramagnetic salts suitable for use in magnetic cooling experiments have entropy diagrams similar to that sketched in figure 1. The entropy is a function of temperature and magnetic field. To cool the salt one applies a field H_i isothermally at the initial temperature T_i. In passing from a to b on the diagram the entropy removed from the salt is ΔS. The salt is then thermally isolated and the magnetic field is removed. During this isentropic process from b to c the temperature of the salt falls to T_f. This method is quite standard and is carried out in a helium cryostat (see for example White, 1959). In practice T_i is usually about 1°K. It is determined on the helium vapour pressure scale. T_f is usally between 0.2°K and 0.01°K. Here gas thermometry cannot be used, for below 0.8°K even helium has a vapour pressure less than 0.01 mm H_g. The absolute temperature must be measured in other ways.

The magnetic susceptibility χ is a suitable thermometric property for magnetic cooling salts below 1°K. In an ideal paramagnetic substance, that is to say one whose paramagnetic ions have no interactions with a crystal field or with neighbouring ions,

Figure 1 Entropy diagram for paramagnetic salts.

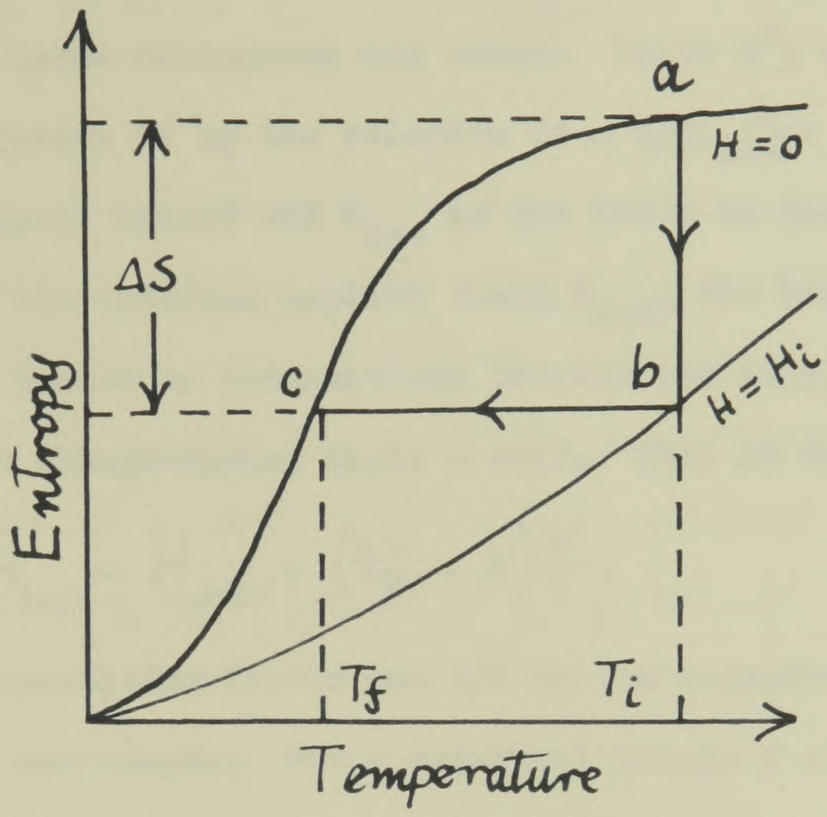

Figure 2 Paramagnetic resonance data for ferric methylammonium alum.

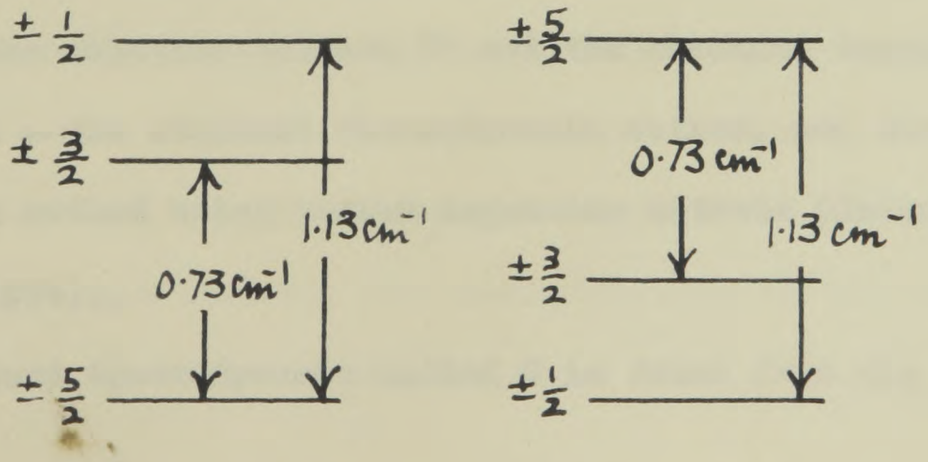

(a) D negative (b) D positive

χ obeys Curie's law : $\chi = c/T$, where c is Curie's constant. Salts used in practice obey Curie's law well above 1°K, but at lower temperatures large deviations may occur. Below 1°K we define the magnetic temperature T* by the relation $T^* = c/\chi_{loc} = M/H_{loc}$, where M is the magnetic moment and H_{loc} is the field at the ions. H_{loc} is the sum of the external applied field H_{ext}, the Lorentz field $(4\pi/3)(M/V)$ caused by interactions between the ions, and the shape dependent demagnetizing field $-NM/V$. That is to say

$$H_{loc} = H_{ext} + \left(\frac{4\pi}{3} - N\right)\frac{M}{V},$$

where N is the demagnetizing factor and M/V is the magnetic moment per unit volume of the sample. For a spherical sample $N = 4\pi/3$ and $H_{loc} = H_{ext}$, so T* is called the magnetic temperature corrected to spherical shape. Some experiments and calculations for determining the relation between T* and the absolute temperature T are described in this part of the thesis.

Absolute temperatures below 1°K

Two of the various methods (for a short survey see Kurti, 1957) for determining the relation between T* and the absolute temperature will be mentioned - the standard thermodynamic method, and the concentric sphere method using cerium magnesium nitrate (Cooke, Meyer and Wolf, 1956).

In the standard thermodynamic method T is found from the relation

$$T = \frac{dQ}{dS} = \frac{(\partial Q/\partial T^*)}{(\partial S/\partial T^*)}$$

in the following way. When one knows how much entropy ΔS is removed from the salt by the application of a magnetic field H_i at the temperature T_i (fig.1), one also knows the entropy difference of the salt between the temperatures T_i and T_f in zero field. If the final temperature is measured on the magnetic scale we write $T_f = T^*$. By making demagnetizations from the temperature T_i and different fields H_i, and hence different entropy reductions ΔS, one obtains a curve of entropy as a function of T^*. From this curve $(\partial S/\partial T^*)$ is found. $(\partial Q/\partial T^*)$ is obtained from specific heat measurements. The absolute temperature at temperatures T^* may then be calculated.

In the concentric sphere method of determining the relation between T^* and T developed by Cooke, Meyer and Wolf (1956), cerium magnesium nitrate is used as a thermometric standard. This salt obeys Curie's law down to $0.006^{\circ}K$, and is anisotropic. A single crystal sphere of cerium magnesium nitrate is surrounded by a spherical shell made from a powdered sample of the substance to be examined. After magnetic cooling, the susceptibility of the compound specimen is measured parallel and perpendicular to the magnetic axis

of the cerium magnesium nitrate crystal. The susceptibilities of the two parts may be separated, and hence the relation between T* and T for the material of the shell is found.

Calculation of magnetization entropy

For the standard thermodynamic method the entropy of magnetization ΔS may be found by a theoretical calculation or by experiment. If the salt behaves ideally at the temperature T_i, ΔS may be calculated from simple paramagnetic theory.

The partition function Z for N free paramagnetic ions with spin J in a field H at a temperature T is given by

$$Z = \left[\sum_{m=-J}^{+J} \exp\left(\frac{-mg\beta H}{kT}\right) \right]^N,$$

where g is the spectroscopic splitting factor, β is the Bohr magneton, k is Boltzmann's constant, and m is the magnetic quantum number. If N is Avogadro's number and R is the gas constant per mole, the magnetic moment and entropy are given by

$$\frac{M}{R} = \left(\frac{\partial}{\partial H} T \ln Z\right)_T, \quad \frac{S}{R} = \left(\frac{\partial}{\partial T} T \ln Z\right)_H.$$

Tables of these functions have been published (Hull and Hull, 1941, J = 1/2, 3/2, 5/2. Giaque, Stout, Egan and Clark, 1941, J = 7/2. Schmid and Smart, 1954, J = 1/2, 1,...9/2). In small magnetic fields this calculation gives Curie's law :

$$\frac{M}{R} = \frac{1}{3}J(J+1)\frac{g^2\beta^2 H}{k^2 T} = c\frac{H}{T},$$

where c is Curie's constant. The entropy is given by

$$\frac{S}{R} = \ln(2J+1) - \frac{1}{6}J(J+1)\frac{g^2\beta^2}{k^2}\left(\frac{H}{T}\right)^2$$

$$= \ln(2J+1) - \frac{c}{2}\left(\frac{H}{T}\right)^2.$$

The lattice entropy is negligible at the usual starting temperatures.

If there are deviations caused by the stark splitting of the ground state of the paramagnetic ion in a crystalline electric field, corrections to the ideal values of ΔS may be calculated provided that the separation of the ground state levels is small compared with T_i. These deviations may be calculated from the spin Hamiltonian $\mathcal{H}$ (Daniels and Kurti, 1954). The calculation is outlined here for a small magnetic field. The partition function is then given by

$$Z = \Sigma_i \exp\left(\frac{-E_i}{kT}\right) = \Sigma_i \left(1 - \frac{E_i}{kT} + \frac{E_i^2}{2k^2T^2} - \ldots\right)$$

or

$$Z = \mathrm{Tr}\,\mathcal{J} - \frac{\mathrm{Tr}\,\mathcal{H}}{kT} + \frac{\mathrm{Tr}\,\mathcal{H}^2}{2k^2T^2} - \ldots,$$

provided that the traces ($\mathrm{Tr}\,\mathcal{H}$, $\mathrm{Tr}\,\mathcal{H}^2$) are small compared with

kT, $2k^2T^2$,.....etc. $\mathcal{J}$ is the unit matrix of the same order as $\mathcal{H}$. LnZ may now be expanded in a series from which the entropy is obtained:

$$\frac{S}{R} = \ln(2J+1) - \frac{c}{2}\left(\frac{H}{T}\right)^2 - \frac{A}{2T^2} + \text{terms containing higher powers}$$

of H and A and their products. A is proportional to the square of the Stark splitting of the ground state. To the approximation given $\Delta S/R$ is independent of A. The first term containing A gives rise to the tail of a Schottky anomaly in the specific heat: $c/R = A/T^2$.

When the Stark splittings of the ground state are of the same order of magnitude as kT_i, which in practice is k x 1°K, the series expansions diverge. To calculate $\Delta S/R$ one must obtain the energy matrix for the field H_i from the spin Hamiltonian, and diagonalize it to get the energy levels E_i. The entropy in the field H_i may then be calculated from the partition function, $Z = (\sum_i \exp(-E_i/kT))^N$, with the help of the formula

$$\frac{S}{R} = \ln\left(\sum_i \exp\left(\frac{-E_i}{kT}\right)\right) + \frac{\sum_i \left(\frac{E_i}{kT}\right)\exp\left(\frac{-E_i}{kT}\right)}{\sum_i \exp\left(\frac{-E_i}{kT}\right)}.$$

The energy levels, and hence the entropy, depend on the orientation of the magnetic field relative to the axis of symmetry of the crystalline field. To calculate $\Delta S/R$ for powdered material an average has to be made over all directions of the magnetic field.

Calculations for a range of temperatures and field strengths are too long to do at the desk and must be carried out on an electronic computer. An experimental determination of $\Delta S/R$ in this case is desirable. Later an application of this method will be described in detail.

Experimental measurement of magnetization entropy

There are two simple ways of determining ΔS directly by experiment. One may measure the amount of evaporation from the surrounding helium bath as the magnetic field is applied, or one may measure the heat absorbed during an isothermal demagnetization. In the first method a sample of the cooling salt is put into thermal contact with a helium bath boiling at about $1^{\circ}K$. The additional amounts of helium evaporating are measured as the magnetic field is increased in steps. Unfortunately this method does not give the entropy of magnetization accurately (Kurti, Lainé and Simon, see Kurti, 1958).

The principle of the method using an isothermal demagnetization is as follows. The paramagnetic salt specimen bearing an electrical heater and a carbon resistance thermometer is placed in a demagnetization cryostat. The specimen is magnetized isothermally at $1^{\circ}K$ by means of a solenoid. Then the specimen is isolated, and while heat is introduced at a constant rate the magnetic field is diminished at such a rate that the temperature, as shown by the carbon thermometer,

remains constant. Since the magnetic field is proportional to the current in the solenoid, and since the heat input is proportional to time, a recorder graph of the magnet current gives the isothermal entropy of magnetization, $\Delta S/R = (\Delta Q/R)/T$, as a function of the field (Croft and Kurti, see Kurti, 1955). The usefulness of carbon thermometers for entropy determinations near $1^{\circ}K$ has been emphasised by Giauque (1953). A detailed account of the method described in this section forms the main subject of Part One of this thesis.*

PROPERTIES OF FERRIC METHYLAMMONIUM ALUM

Crystalline Stark effect

We now discuss the properties of ferric methylammonium alum, $Fe(NH_3CH_3)(SO_4)_2 \cdot 12H_2O$, paramagnetic salt whose entropy of magnetization has been determined in the present work. For brevity we shall refer to this salt as FMA. The paramagnetic resonance spectrum of FMA was accurately measured by Bleaney and Trenam (1954). They used single crystals dilut ed with the isomorphous aluminium salt to reduce the line width caused by spin-spin interactions between the ferric ions. Their results showed that the ground state $^6S_{5/2}$ of the ferric ion Fe^{3+} is split into three doublets by the Stark effect of the crystalline field. This field has trigonal symmetry with a small contribution of cubic symmetry (about 5%). Figure 2 shows the levels obtained by Bleaney and Trenam. Their measurements did not decide which of the two diagrams

*See also Croft and Exell (1961).

is correct. If we neglect the cubic term, the energy levels of the ferric ion may be described by the following spin Hamiltonian :

$$\mathcal{H} = g\beta H \cdot S + D\left(S_z^2 - \tfrac{1}{3}S(S+1)\right),$$

where $g = 2$ and $S = 5/2$. D is the parameter which describes the magnitude of the splitting of the ground state caused by the trigonal field. Bleaney and Trenam found $D = 0.188 \pm 0.014$ cm^{-1}, but the absolute sign was uncertain.

The overall splitting of the ground state of the paramagnetic ions in FMA is k x 1.6°K, which is large compared with that of other alums commonly used in magnetic cooling experiments. For example in iron ammonium alum the overall splitting is k x 0.18°K.

The Stark effect in FMA gives rise to a large Schottky specific heat from 0.2°K to 1°K. This salt might therefore be useful for cooling other substances and maintaining them at temperatures in this range. For this reason Cutler made a theoretical study of FMA to predict its performance as a cooling salt (1955). He calculated the entropy, specific heat, and magnetic moment of the salt both as a single crystal and in powder form at 1°K in magnetic fields of 10 kG and 15 kG. Since the Stark splittings are large the thermodynamic functions were evaluated numerically by diagonalising the energy matrix as described earlier. The lengthy nature of the work, which was done on a desk calculator, prevented Cutler from obtaining

enough data for general use in experiments; but his work showed that FMA would be a useful cooling salt for experiments at temperatures between 0.3°K and 1°K.

Thermodynamic properties

Cooke, Meyer and Wolf (1956) have measured the specific heat of FMA from 0.2°K to 20°K. The results below 1°K agreed with the theoretical curve calculated from the second of the two diagrams in fig. 2, thus showing that the $\pm \frac{1}{2}$ levels of the ferric ion have the lowest energy in the crystalline field. Cooke, Meyer and Wolf also determined the relation between T* and T by the concentric sphere method using cerium magnesium nitrate as a thermometer.

At about the same time Croft and Kurti (see Kurti, 1955) had been developing the method of measuring $\Delta S/R$ as outlined earlier. These experiments were resumed and completed by myself and Croft. The experiments were done in three parts: measurements of $\Delta S/R$ in field strengths from zero to 13 kG by isothermal demagnetizations at 1.15°K; measurements of the temperatures T* reached by adiabatic demagnetizations from different initial fields H_i up to 13 kG; and measurements of the specific heat $C^*/R = dQ/RdT^*$ from 0.15°K to 1.2°K by electrical heating in steps. In this way all the information necessary for determining the T* - T relation by the standard method was obtained. The specific heat measurements agreed with those of Cooke, Meyer and Wolf. The T* - T relation did not agree with

that of Cooke, Meyer and Wolf, but lay closer to the theoretical curve calculated from the Stark splittings (see Bleaney and Trenam, 1954, appendix).

The energy levels E_i of the spin Hamiltonian $\mathcal{H} = g\beta H.S + D(S_z^2 - \frac{1}{3}S(S+1))$ for $S = 5/2$ were calculated recently on a computer by Jarret (1957). The levels E_i, which depend on the angle θ between the magnetic field H and the z-axis, were obtained in the form $E/2D$ for values of θ every 10°, and for values of $g\beta H/4D$ from 0 to 2. Using this data (kindly supplied by Dr. Wolf) and the value of D given by Bleaney and Trenam, I calculated the entropy of FMA. This work was done on the Ferranti Mercury computor in the Oxford University Computing Laboratory. A table of entropies was obtained for temperatures from $0.9^\circ K$ to $1.2^\circ K$, and for magnetic fields from zero to 16 kG, both for a powder and for selected values of θ in single crystals. This table covers the range of conditions normally used in magnetic cooling experiments. The experimental values of $\Delta S/R$, obtained from the isothermal demagnetizations, were in good agreement with those derived from the table.

CHAPTER TWO

APPARATUS

Cryostat

We shall now describe the general features of the apparatus converted from that described by Croft (1952). As shown in figure 3, a vacuum case containing the specimen to be studied was surrounded by liquid helium. This was shielded by liquid hydrogen. Both the helium and the hydrogen dewars were made of glass with slits in the silvering allowing one to see the liquid levels. Although the inside of the dewar was made of Monax glass, the least permeable to helium, it was necessary to have the vacuum space repumped after five or six experiments. The helium dewar was fixed at the top with a Kovar-glass seal and connected by two short tubes and a long 2-inch line to a pulsometer 8-inch pump. The helium could be pumped down to a temperature of 1.15°K.

The vapour pressure of the helium bath was used as a temperature standard on the T_{55E} scale (Clement, Logan and Gaffney, 1955. An abbreviated table is given by White, 1959). It was measured on oil and mercury manometers connected by a 2 mm diameter tube to the top of the helium dewar. The thermomolecular correction was negligible at and above 1.2°K. Above the helium lambda point measurements were made with the temperature steady or falling slowly

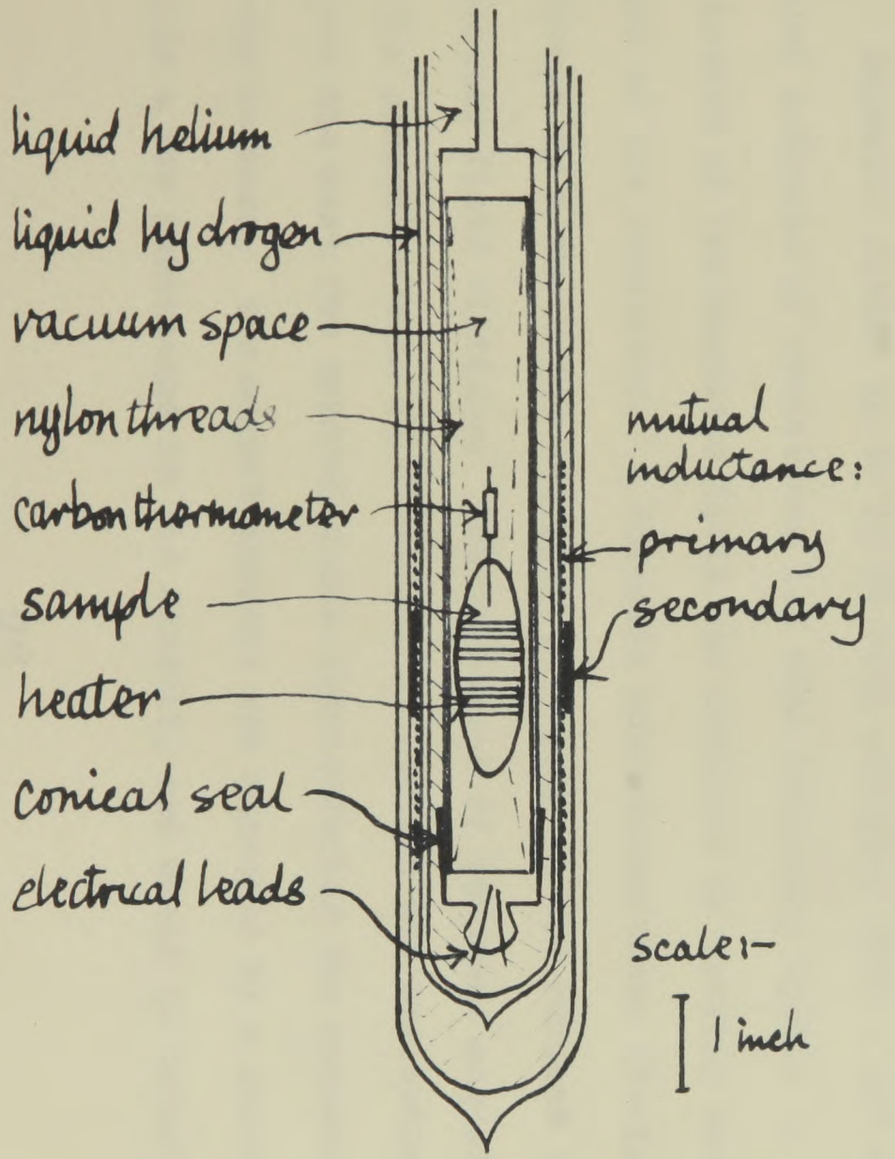

Figure 3 Cryostat

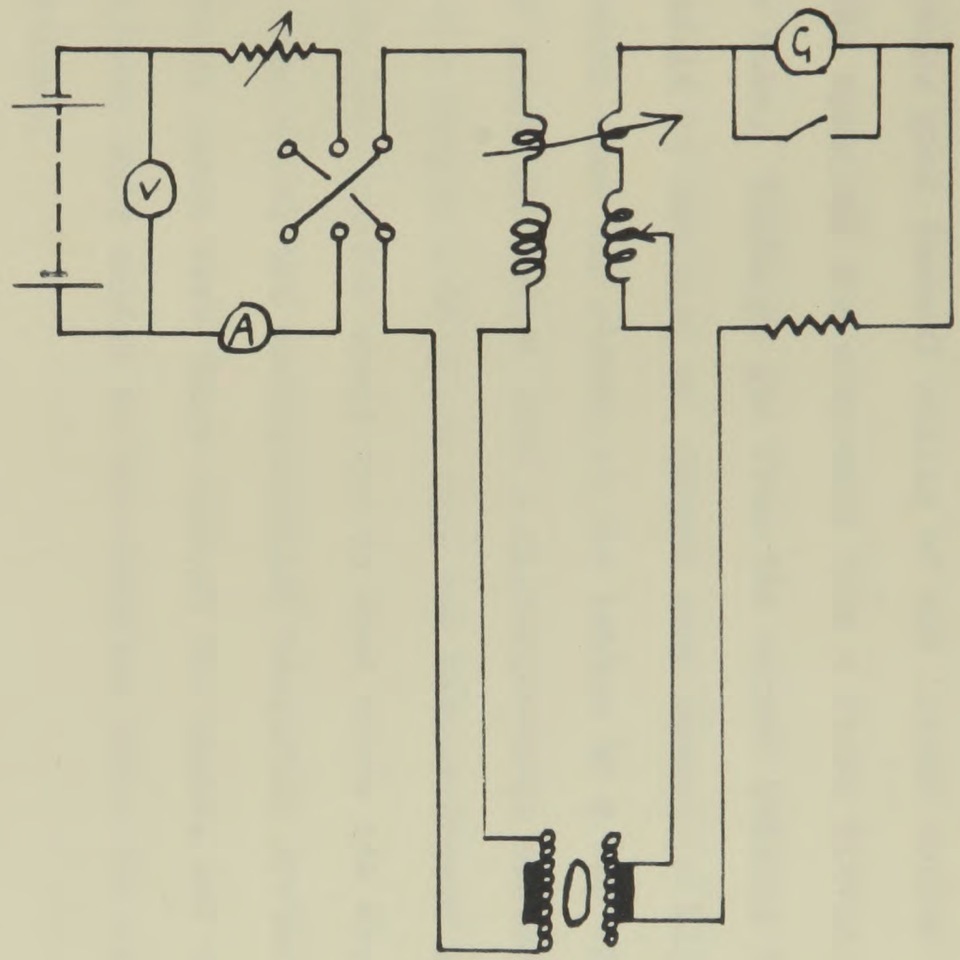

Figure 4 Susceptibility bridge

to ensure good thermal mixing of the liquid helium by boiling.

The specimen was suspended from a frame fitting into the brass vacuum case. Exchange gas from the vapour boiling off the helium bath could be admitted or pumped away through a high vacuum system. The vacuum case was closed at the bottom by a cap with a conical ground joint and sealed with a glycerine-soap mixture. The copper tube of a copper - 08 glass seal was hard-soldered into the cap. Ordinary soft solder could not be used since its superconductivity would have upset the susceptibility measuring system. Four tungsten electrical leads were taken through the glass, and small pieces of platinum were welded on the tungsten wires for soldering connections.

Magnet

Magnetic fields up to 13 kG were obtained with a 100 kW water-cooled solenoid of resistance 1.3 ohms (Daniels, 1950). A smooth variation of the magnetic field was obtained by varying the excitation of the generator. A variable auto-transformer (Variac) followed by a rectifier was used to supply direct current to the generator field windings. The existence of remanent magnetism in the generator made it necessary to reverse the excitation to remove the last few hundred gauss when reducing the magnetic field slowly to zero. The magnet current was measured by a galvanometer across a low resistance in the circuit, and could be recorded on

a pen recorder. The calibration of the magnet, measured with a flip-coil and flux meter, was 0.0525 kG amp^{-1} $\pm$ 1% in a length of 6 cm at the centre of the solenoid. Outside this region the field decreased rapidly with increasing distance from the centre.

Sample

The specimen contained about 18 gm (i.e. 0.04 gm ions) of FMA in the form of a highly compressed powder of filling factor 0.95. The shape was an ellipsoid of revolution with a 2 cm minor axis and a 6 cm major axis along the applied magnetic field. It was suspended by six nylon threads of diameter 0.01 in. Chemical analysis of the specimen after the experiments showed that 3.2% of the water of crystallization had been lost. Since the susceptibilities of anhydrous ferric salts are temperature independent at helium temperatures, the weight of anhydrous salt in our specimen was subtracted from the total weight before the results were calculated.

Some care has to be taken when making up a specimen of FMA. As soon as the powder has been obtained, by grinding the crystals, it must be put in an air-tight bottle. Warm moist air from one's breath makes the powder sticky, or if it is left in the open in a dry atmosphere its water of crystallisation is soon lost. The moistened powder is pressed into a cylinder with a force of several tons and allowed to set overnight. The cylinder is then shaped into an ellipsoid on a lathe. During this process it must be kept

cold with liquid air. The pill is then varnished and kept below 0°C in an airtight bottle.

A heater coil of 46 swg constantan, wound non-inductively on the specimen had a resistance of 885 ohms at 1.2°K. This includes a small correction (19 ohms) for the resistance of the leads inside the vacuum jacket. It was assumed that half of the heat developed in the leads flowed into the specimen. The resistance of the coil an d the leads inside the vacuum space at 1.2°K was found from current and voltage measurements.

Thermometers

For a carbon thermometer an Aerovox 1097 ½ watt 470 ohm resistor (Nicol and Soller, 1957) was used. It was attached by gluing one of its copper leads with GE 7031 varnish into a hole drilled 1 cm deep into the specimen. This was found to give good heat contact at 1°K, but a comparison between the temperature indicated by the carbon thermometer and the magnetic temperature T* showed that the heat contact was poor below 0.3°K.

The resistance of the thermometer was measured with a post office box. To avoid heating up the specimen it was necessary to use a small current of 5 μA and a sensitive galvanometer with telescope and scale to balance the bridge. The carbon resistance R was calibrated against the helium vapour pressure scale from 4°K to 1.2°K, and the two constant ad hoc empirical calibration formula

$T = a/(R - b)$ was used near 1.2°K. This formula has the advantage of simplicity and sufficient accuracy over a few tenths of a degree at this temperature. This technique of carbon thermometry, though good for the isothermal demagnetization experiments, was afterwards improved as described in Part Two of this thesis. A separate experiment with the carbon thermometer alone in the cryostat showed that the applied magnetic field reduced the value of the carbon resistance at constant temperature. The approximate characteristics of the thermometer at 1.2°K were : R = 1600 ohm, $(\partial R/\partial T)_{H=0} = -700$ ohm deg^{-1}, $(\partial R/\partial H)_{T=1.15^{\circ}K} = -2$ ohm kG^{-1}, so that a magnetic field of 13 kG produced a change in resistance equivalent to 0.04°K. This small effect was allowed for during the experiments.

To obtain T* from the magnetic susceptibility of the specimen a standard bridge was used with a critically damped ballistic galvanometer. The arrangement allowed one to observe every thirty seconds the deflection δ of the galvanometer produced by reversing the primary current of the mutual inductance. The primary and secondary coils in the hydrogen bath surrounding the specimen were compensated externally (see figure 4). Calibration was made against the helium vapour pressure scale using the formula

$$\frac{\delta}{i} = \frac{a}{T-\Delta} + b,$$

where δ is the galvanometer deflection, i is the primary current (1 amp), a and b are constants determined during the calibration

and T is the temperature. Δ is the term for correcting to spherical shape;

$$\Delta = \left(\frac{4\pi}{3} - N\right)\frac{J(J+1)g^2\beta^2R\rho}{3mk^2}$$

where ρ is the density of the pill, and m is the gram ionic weight of the salt.

EXPERIMENTAL DETERMINATION OF MAGNETIZATION ENTROPY

Technique

The experimental method of determining the entropy of magnetization was as follows. A magnetic field of about 13 kG was applied to the specimen with exchange gas in the cryostat and the liquid helium at its lowest temperature 1.15°K. When thermal equilibrium between the specimen and the helium bath has been reached, the exchange gas was pumped out until a pressure of less than 10^{-5} mm Hg was obtained. Then the specimen was heated electrically and the magnetic field was reduced by hand to keep the temperature constant, as shown by the galvanometer in the carbon thermometer bridge. The heating power was adjusted so that this took about eight minutes, a time which made a good compromise between two extremes. A large heating power and a rapid demagnetization of, say, one or two minutes makes it too difficult to keep the temperature constant with the required precision, but it has the advantage of reducing errors caused by imperfect heat insulation. With a small heating power

and a very slow demagnetization the converse is true.

It was necessary during these measurements to allow for the effect mentioned earlier of the magnetic field on the carbon thermometer. The galvanometer reading in the carbon thermometer bridge was noted for various external fields when the specimen was in thermal equilibrium with liquid helium bath. During the isothermal demagnetizations the galvanometer was kept at the reading appropriate to the actual field strengths present.

To check the thermodynamic reversibility of the demagnetization process the specimen was demagnetized and remagnetized adiabatically in a time of about two minutes. The carbon thermometer showed that after the remagnetization the original temperature had been restored to within $\sim 0.003^{\circ}K$, no irreversible heating having taken place. The insulation was checked by heating the specimen to a temperature above that of the helium bath and observing the temperature drift rate. The observations showed that the heat leak was $\sim 2 \times 10^{-6}$ watts for a temperature difference of $0.1^{\circ}K$ between the specimen and the helium bath.

Fig.5 shows a reproduction of one of the recorder graphs obtained for FMA. The entropy of magnetization $\Delta S/R$ as a function of H_{loc}/T was obtained from the experimental recorder traces by the following steps. First the applied fields H_{ext} were obtained by converting the horizontal scale of the recorder trace from inches to kilogauss

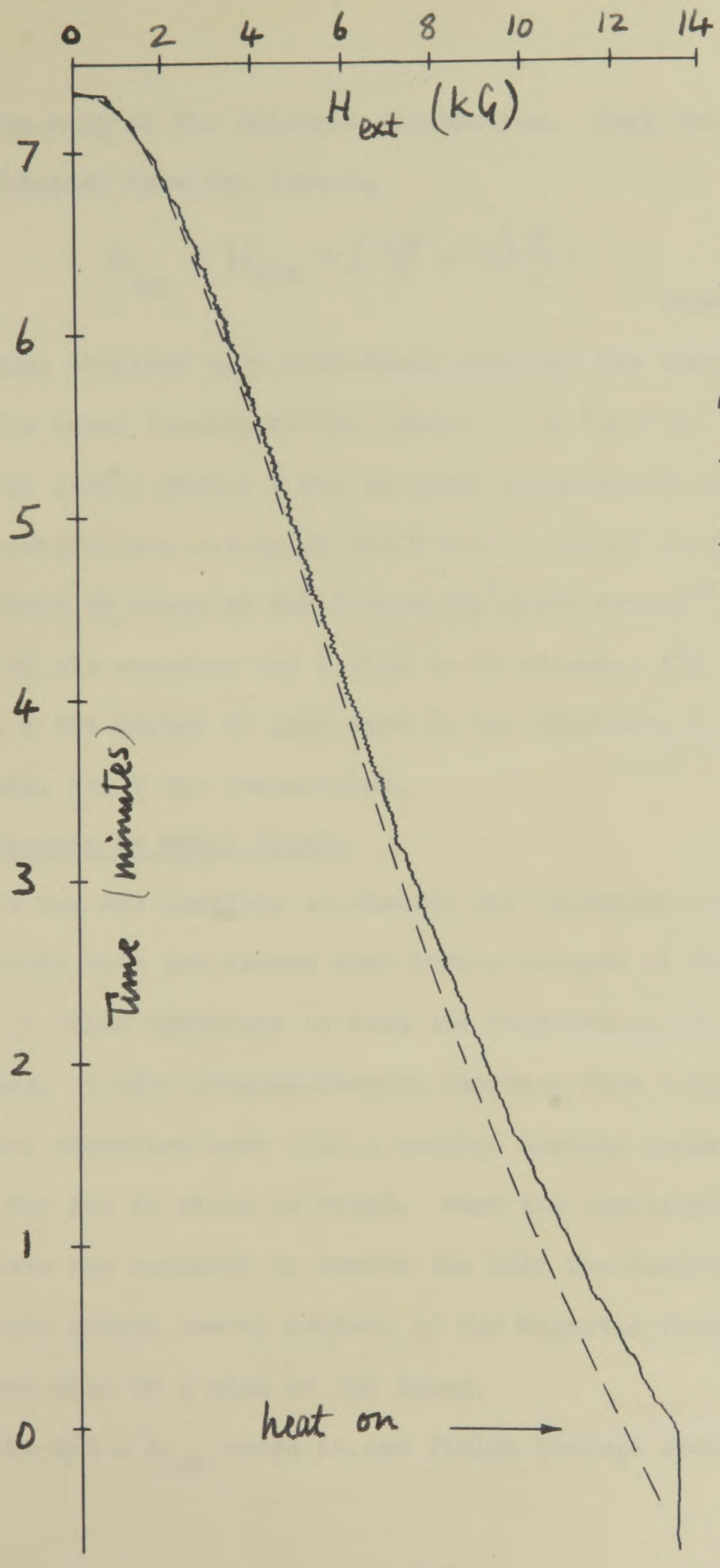

Figure 5

Record of an isothermal demagnetization of 0.04 gm ions of FMA.

$T = 1.19\ ^{\circ}K$.

Heating power $= 8.0 \times 10^{-4}$ watts.

– – – "ideal" curve for $J = 5/2$.

with the help of the solenoid calibration. Next the local fields H_{loc} were obtained from the formula

$$H_{loc} = H_{ext} + \left(\frac{4\pi}{3} - N\right)\frac{M}{V},$$

(see Chapter One)

M/V being obtained with sufficient accuracy for this small correction from the known density of the specimen and from the tables of Hull and Hull (1941) giving M for an ideal paramagnetic substance. Next the magnetization entropies $\Delta S/R$ were obtained from the vertical time scale by means of the factor $30i^2r/nRT$ inches^{-1}, since the speed of the recorder was 1 inch in 30 seconds, i^2r was the heating power, n the number of gram ions in the specimen, R the gas constant per mole, and T the temperature.

Measurements in small fields

It was not possible to observe the low-field end of the graph accurately with the larger heat inputs because of the rapid change of magnetic field necessary to keep the temperature of the specimen constant. A slow demagnetization starting from a field of about 2 kG was therefore made with a smaller heating power. The recorder trace for FMA is shown in fig.6. When the excitation of the magnet generator was reversed to remove the last few hundred gauss the otherwise smooth manual control of the magnetic field was interrupted and gave rise to a kink in the trace.

The $S/R - H_{loc}$ curve in low fields derived from the trace

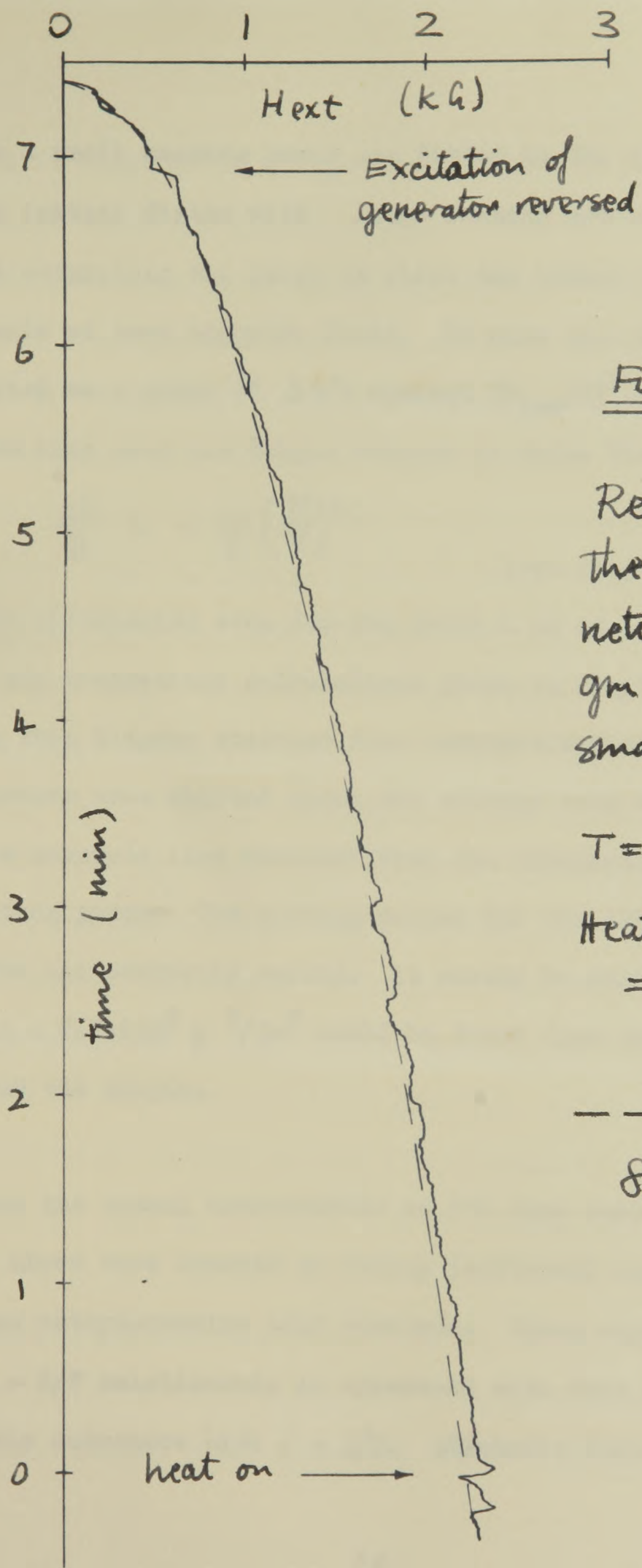

Figure 6

Record of an isothermal demagnetization of 0.04 gm ions of FMA in small magnetic fields.

T = 1.15°K

Heating power = 0.8×10^{-4} watts

– – – "ideal" curve for J = 5/2

made with a small heating power was fitted to the curves obtained from high initial fields with large heating powers in order to determine accurately the point at which the latter curves cut the entropy axis at zero magnetic field. To make this fit, the results were plotted on a graph of $\Delta S/R$ against $(H_{loc}/T)^2$. This produced a straight line near the origin because in small fields

$$\frac{\Delta S}{R} = -\frac{c}{2}\left(\frac{H}{T}\right)^2$$

(see Chapter One),

a relation which holds even for FMA below 1 kG at 1.2°K as we shall see from the theoretical calculations given in Chapter Three. The curves on this diagram obtained from demagnetizations with large heating powers were shifted along the entropy axis where necessary to fit the accurate line obtained from the demagnetization with a small heating power. The entropy scales for the different runs were then all correctly zeroed. It should be mentioned that the value of $c = J(J+1)g^2\beta^2/3k^2$ could be found from the slope of the curves near the origin.

Results

Before the actual measurements on FMA were made, the techniques described above were checked by making isothermal demagnetizations of a chrome methylammonium alum specimen. These experiments gave a $\Delta S/R - H/T$ relationship in agreement with that for an ideal paramagnetic substance with $J = 3/2$. Adiabatic demagnetizations

gave final T* readings which agreed with those of Gardner and Kurti (1954) and de Klerk and Hudson (1953).

We now give details of the actual results obtained for FMA. As expected, from the fact that part of the total magnetic entropy $\ln(2S + 1)$ is removed by the large crystalline Stark effect, the observed values of the entropy of magnetization $\Delta S/R$ in large fields were smaller than those for an ideal paramagnetic substance with $J = 5/2$. This is clearly shown in fig.5, where the curve which would have been obtained with an ideal paramagnetic substance has been included. Fig.7 shows the smoothed results of five isothermal demagnetizations of the FMA specimen, two at 1.15°K and three at 1.19°K. The graph shows the deviation of the measured entropy from that for an ideal paramagnetic substance. The heating powers used in different demagnetisations varied between 5.6×10^{-4} watts and 8.9×10^{-4} watts. To compare the results, the values obtained at 1.19°K were corrected to 1.15°K with the help of table 2 (Chapter Three). The accuracy of these entropy determinations, estimated from the possible systematic errors and the fluctuations in the recorder traces, was 2%, that is to say $\pm$ 0.02 in $\Delta S/R$ at 10 kG deg^{-1}. Fig.7 also shows the entropy curve computed on the assumption that the interaction between the ferric ions and the crystalline field has the same magnitude as that found from paramagnetic resonance in the diluted salt. Fairly close agreement exists between this theoretical

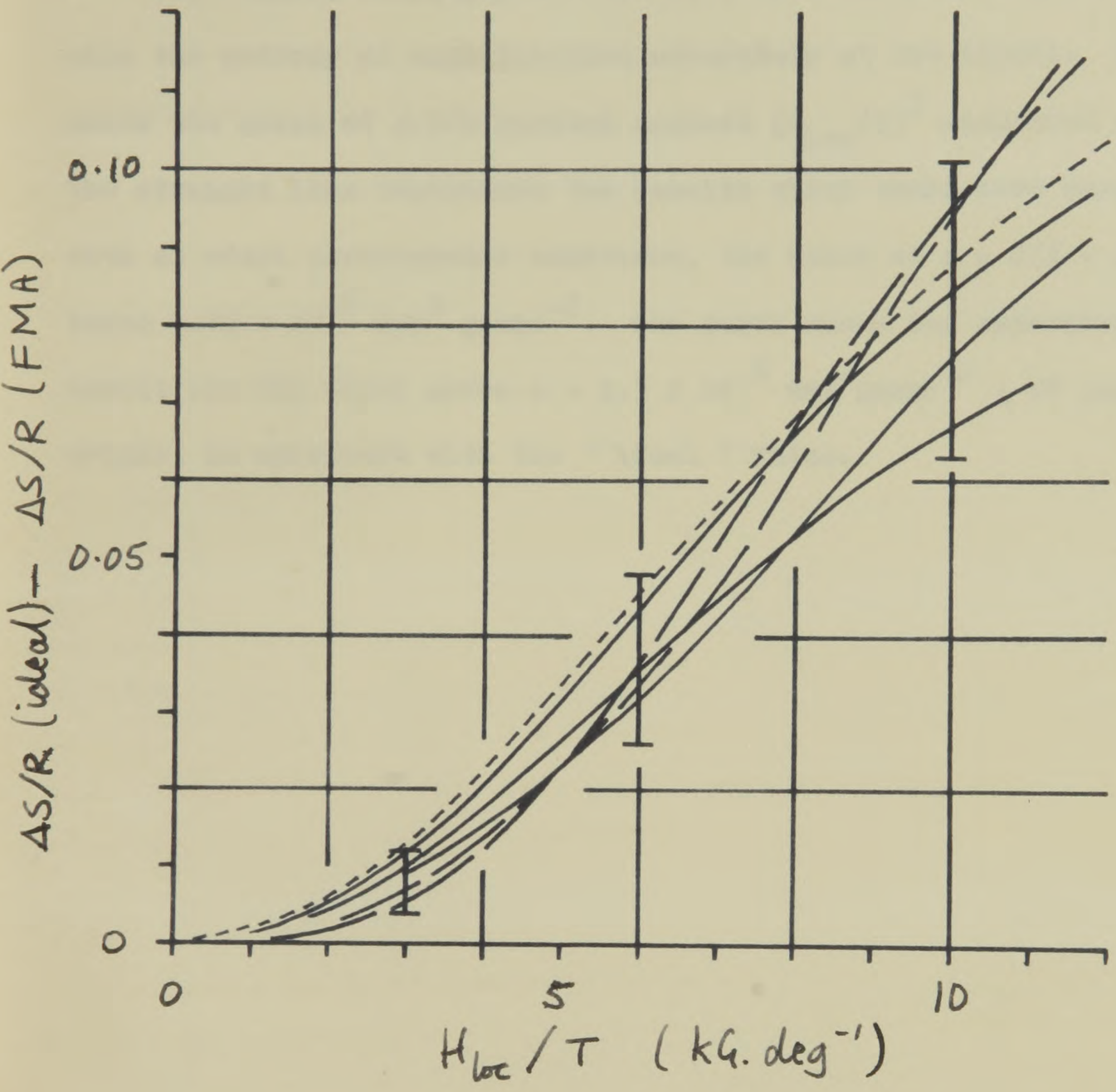

Figure 7 Deviation of magnetization entropy of FMA from the "ideal" ($J = 5/2$) as a function of H_{loc}/T. — — — experimental results at 1.15°K, ——— experimental results for 1.19°K, ------ theoretical curve. Experimental error (2% of total magnetization entropy) shown thus: I

curve and the experimental results.

The smaller heating power of 0.8×10^{-4} watts was used to determine the entropy of magnetization accurately at low fields. Figure 8 shows the graph of $\Delta S/R$ plotted against $(H_{loc}/T)^2$ mentioned earlier. The straight line represents the results which would have been obtained with an ideal paramagnetic substance, the value of $c = J(J+1)g^2\beta^2/3k^2$ being 5.26×10^{-8} deg^2 gauss^{-2}. The curve shows the experimental result for FMA which gives $c = 5.3 \times 10^{-8}$ deg^{2}gauss^{-2} $\pm$ 2% near the origin, in agreement with the " ideal " value.

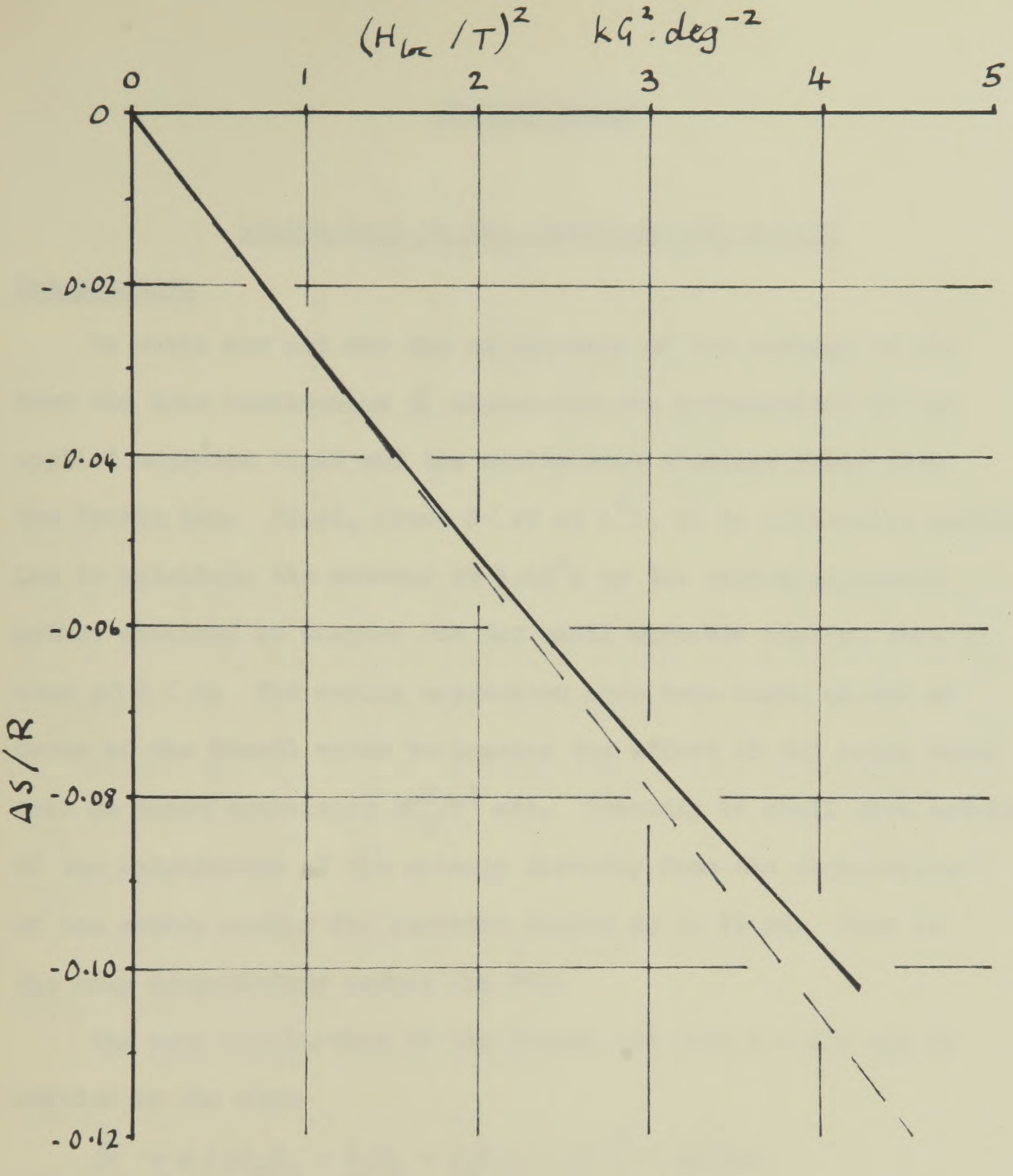

Figure 8 Magnetization entropy of FMA in small fields.

——— experimental result (smoothed) 1.15°K

— — — theoretical line for an ideal paramagnetic substance ($J = 5/2$)

CHAPTER THREE

CALCULATION OF THE MAGNETIZATION ENTROPY

Introduction

We shall now set out the calculation of the entropy of FMA from the spin Hamiltonian $\mathcal{H}$ containing the interactions of the applied magnetic field and the crystalline electric field with the ferric ion. First, since $D < kT$ at $1^{\circ}K$, it is worthwhile attempting to calculate the entropy at $1.15^{\circ}K$ by the series expansion method outlined in Chapter One for small magnetic fields, that is when $g\beta H < D$. The series expansions have been taken as far as terms of the fourth order to examine the effect of the cross terms such as those containing DH_z^2/T^3 etc. Secondly we shall give details of the calculation of the entropy directly from the eigen-values of the energy matrix for magnetic fields up to 16 kG. This is the only satisfactory method for FMA.

The spin Hamiltonian of the ferric ion with $S = 5/2$ may be written in the form

$$\mathcal{H} = g\beta(H_x S_x + H_y S_y + H_z S_z) + D(S_z^2 - 35/12).$$

The energy matrix derived from this operator is -

$$
\begin{array}{c|cccccc}
 & \frac{5}{2} & \frac{3}{2} & \frac{1}{2} & -\frac{1}{2} & -\frac{3}{2} & -\frac{5}{2} \\
\frac{5}{2} & a_{11} & a_{12} & 0 & 0 & 0 & 0 \\
\frac{3}{2} & a_{21} & a_{22} & a_{23} & 0 & 0 & 0 \\
\frac{1}{2} & 0 & a_{32} & a_{33} & a_{34} & 0 & 0 \\
-\frac{1}{2} & 0 & 0 & a43 & a_{44} & a_{45} & 0 \\
-\frac{3}{2} & 0 & 0 & 0 & a_{54} & a_{55} & a_{56} \\
-\frac{5}{2} & 0 & 0 & 0 & 0 & a_{65} & a_{66}
\end{array}
$$

where -

$$
a_{11} = \frac{10}{3}D + \frac{5}{2}g\beta H_z, \quad a_{12} = \frac{\sqrt{5}}{2}g\beta(H_x - iH_y), \quad a_{21} = \frac{\sqrt{5}}{2}g\beta(H_x + iH_y),
$$

$$
a_{22} = -\frac{2}{3}D + \frac{3}{2}g\beta H_z, \quad a_{23} = \frac{\sqrt{8}}{2}g\beta(H_x - iH_y), \quad a_{32} = \frac{\sqrt{8}}{2}g\beta(H_x + iH_y),
$$

$$
a_{33} = -\frac{8}{3}D + \frac{1}{2}g\beta H_z, \quad a_{34} = \frac{\sqrt{9}}{2}g\beta(H_x - iH_y), \quad a_{43} = \frac{\sqrt{9}}{2}g\beta(H_x + iH_y),
$$

$$
a_{44} = -\frac{8}{3}D - \frac{1}{2}g\beta H_z, \quad a_{45} = \frac{\sqrt{8}}{2}g\beta(H_x - iH_y), \quad a_{54} = \frac{\sqrt{8}}{2}g\beta(H_x + iH_y),
$$

$$
a_{55} = -\frac{2}{3}D - \frac{3}{2}g\beta H_z, \quad a_{56} = \frac{\sqrt{5}}{2}g\beta(H_x - iH_y), \quad a_{65} = \frac{\sqrt{5}}{2}g\beta(H_x + iH_y),
$$

$$
a_{66} = \frac{10}{3}D - \frac{5}{2}g\beta H_z.
$$

This result has been given by Cutler (1955).

Small magnetic fields

To simplify the calculations of the entropy by the power series expansions let us choose axes so that $H_z = H_\parallel$, $H_x = H_\perp$, and $H_y = 0$, where $H_\parallel$ and $H_\perp$ are the components of the magnetic field parallel and perpendicular to the trigonal axis of the crystalline field. We are able to combine the components H_x and H_y into one term $H_\perp$ because in the algebra they always appear in the form $H_x^2 + H_y^2 = H_\perp^2$. To simplify the form of the matrix elements, we

put $2D/3 = d$, $g\beta H_z/2 = Z$, and $g\beta H_x/2 = X$. The matrix elements then become -

$$a_{11} = 5d + 5Z, \quad a_{12} = \sqrt{5}X = a_{21},$$
$$a_{22} = -d + 3Z, \quad a_{23} = \sqrt{8}X = a_{32},$$
$$a_{33} = -4d + Z, \quad a_{34} = \sqrt{9}X = a_{43},$$
$$a_{44} = -4d - Z, \quad a_{45} = \sqrt{8}X = a_{54},$$
$$a_{55} = -d - 3Z, \quad a_{56} = \sqrt{5}X = a_{65},$$
$$a_{66} = 5d - 5Z.$$

Next we need the values of $\mathrm{Tr}\,\mathcal{J}$, where $\mathcal{J}$ is the 6 x 6 unit matrix, and $\mathrm{Tr}\,\mathcal{A}$, $\mathrm{Tr}\,\mathcal{A}^2$, $\mathrm{Tr}\,\mathcal{A}^3$, and $\mathrm{Tr}\,\mathcal{A}^4$ to get terms of the fourth order in the expansions. By substituting the expressions for the matrix elements we obtain -

$$\mathrm{Tr}\,\mathcal{J} = 6,$$
$$\mathrm{Tr}\,\mathcal{A} = 0,$$
$$\mathrm{Tr}\,\mathcal{A}^2 = 84d^2 + 70Z^2 + 70X^2,$$
$$\mathrm{Tr}\,\mathcal{A}^3 = 120d^3 + 672dZ^2 - 336dX^2,$$
$$\mathrm{Tr}\,\mathcal{A}^4 = 1764d^4 + 7800d^2Z^2 + 1414Z^4 + 1414X^4 + 3912d^2X^2 + 2828Z^2X^2.$$

The partition function Z may then be found from the series expansion -

$$Z = \mathrm{Tr}\,\mathcal{J} - \frac{\mathrm{Tr}\,\mathcal{A}}{kT} + \frac{\mathrm{Tr}\,\mathcal{A}^2}{2k^2T^2} - \frac{\mathrm{Tr}\,\mathcal{A}^3}{6k^3T^3} + \frac{\mathrm{Tr}\,\mathcal{A}^4}{24k^4T^4} \cdots$$

which we shall write in the form $Z = 6(1 + x)$. Here x is less than 1 when the values of D and the magnetic field H are not large. The entropy is then obtained from the expressions -

$$\ln Z = \ln 6 + \left(x - \frac{1}{2}x^2 + \frac{1}{3}x^3 - \frac{1}{4}x^4 + \dots\right), \quad |x| < 1,$$

$$S/R = \ln Z + T(\partial \ln Z/\partial T).$$

When the necessary algebra has been done, and terms higher than the fourth order have been rejected, one obtains -

$$\frac{S}{R} = \ln 6 - \frac{1}{12k^2T^2}\left(84d^2 + 70z^2 + 70x^2\right)$$

$$+ \frac{1}{18k^3T^3}\left(120d^3 + 672dz^2 - 336dx^2\right)$$

$$+ \frac{1}{48k^4T^4}\left(1764d^4 - 1920d^2z^2 + 1036z^4 + 1036x^4 + 1968d^2x^2 + 2072z^2x^2\right),$$

which has the form -

$$\frac{S}{R} = \ln 6 + C_1\frac{D^2}{T^2} + C_2\frac{H_\parallel^2}{T^2} + C_3\frac{H_\perp^2}{T^2} + C_4\frac{D^3}{T^3} + C_5\frac{DH_\parallel^2}{T^3} + C_6\frac{DH_\perp^2}{T^3}$$

$$+ C_7\frac{D^4}{T^4} + C_8\frac{D^2H_\parallel^2}{T^4} + C_9\frac{D^2H_\perp^2}{T^4} + C_{10}\frac{H_\parallel^4}{T^4} + C_{11}\frac{H_\parallel^2H_\perp^2}{T^4} + C_{12}\frac{H_\perp^4}{T^4},$$

where the c_i's are constant coefficients. This expression taken as far as the second order terms is -

$$\frac{S}{R} = \ln 6 - \frac{28D^2}{9k^2T^2} - \frac{35g^2\beta^2}{24k^2T^2}\left(H_\parallel^2 + H_\perp^2\right).$$

The first and second terms represent the entropy in zero field, and the third term is identical with the magnetic entropy reduction $\Delta S/R$ of an ideal paramagnetic substance without Stark splittings.

Table 1 shows the contribution of each term up to those of the fourth order in the series expansion for S/R calculated from the

magnetic field	ln 6	second order terms			third order terms		
		$C_1\frac{D^2}{T^2}$	$C_2\frac{H_{\parallel}^2}{T^2}$	$C_3\frac{H_{\perp}^2}{T^2}$	$C_4\frac{D^3}{T^3}$	$C_5\frac{DH_{\parallel}^2}{T^3}$	$C_6\frac{DH_{\perp}^2}{T^3}$
0	1.792	-0.172	0	0	0.026	0	0
$H_{\parallel}$ = 1 kG	1.792	-0.172	-0.020	0	0.026	0.020	0
H_{45^0} = 1 kG	1.792	-0.172	-0.010	-0.010	0.026	0.010	-0.005
$H_{\perp}$ = 1 kG	1.792	-0.172	0	-0.020	0.026	0	-0.010
$H_{\parallel}$ = 4 kG	1.792	-0.172	-0.319	0	0.026	0.320	0
$H_{\perp}$ = 4 kG	1.792	-0.172	0	-0.319	0.026	0	-0.160
H = 10 kG - the series diverges							

	fourth order terms						total
	$C_7\frac{D^4}{T^4}$	$C_8\frac{D^2H_{\parallel}^2}{T^4}$	$C_9\frac{D^2H_{\perp}^2}{T^4}$	$C_{10}\frac{H_{\parallel}^4}{T^4}$	$C_{11}\frac{H_{\parallel}^2H_{\perp}^2}{T^4}$	$C_{12}\frac{H_{\perp}^4}{T^4}$	S/R
0	0.022	0	0	0	0	0	1.668
$H_{\parallel}$ = 1 kG	0.022	-0.003	0	0.000	0	0	1.665
H_{45} = 1 kG	0.022	-0.001	0.002	0.000	0.000	0.000	1.652
$H_{\perp}$ = 1 kG	0.022	0	0.004	0	0	0.000	1.642
$H_{\parallel}$ = 4 kG	0.022	-0.054	0	0.064	0	0	1.679
$H_{\perp}$ = 4 kG	0.022	0	0.055	0	0	0.064	1.308

Table 1. Terms in the series expansion for S/R.

above formulae with the values $g = 2$, $\beta = -0.927 \times 10^{-20}$ erg.gauss^{-1}, $D = 0.188$ cm^{-1}, $k = 1.38 \times 10^{-16}$ erg.deg^{-1}, $T = 1.15^{\circ}$K. When the field H is 1 kG, the third order terms containing H give an appreciable contribution to the entropy, but the fourth order terms give only a small contribution. In the table we have, for this field strength, values of S/R for θ, the angle between H and the trigonal axis, equal to 0°, 45°, and 90°. One may calculate roughly the value of S/R for a powder from these results by estimating the value of the integral $S(\text{powder})/R = \int_0^{\pi/2} S(\theta)\sin\theta\, d\theta/R$, where $S(\theta)/R$ is the entropy with the field at the angle θ. We obtain $S/R = 1.650$ at 1 kG and 1.15°K. The entropy of magnetization $\Delta S/R$ is then $\Delta S/R = S(1kG)/R - S(H=0)/R = 1.650 - 1.668 = -0.018$. This result is close to the value -0.020 for an ideal paramagnetic substance, and shows why the experimental measurement of $\Delta S/R$ given in Chapter Two lies close to the "ideal" curve in low magnetic fields. When the applied field is 4 kG the series expansion for S/R converges too slowly for this method to be used. When the field strength is 10 kG the series diverges.

Large magnetic fields

As mentioned in Chapter One, Jarrett's tables for the eigenvalues E_i of the Hamiltonian matrix contained the quantities $E_i/2D$ ($i = 1, 2 \ldots 6$) for values of θ every 10° up to 90°, and for values of $g\beta H/4D$ equal to 0.1, 0.2, 0.3 ... 1.2, 1.5, and 2.0.

The eigenvalues are shown graphically for $\theta = 0^\circ$ and 90° in figure 9. When D is known one may calculate for a chosen temperature the entropy S/R for different values of H, and for values of θ every 10°.

For practical use, one needs tables of S/R for the values of θ obtained when H is applied along one of the recognizable directions of a single crystal, and also for a powdered sample with S/R averaged over all values of θ. FMA probably has the beta-alum structure (Lipson, 1935. Bagguley and Griffiths, 1950) in which there are four equivalent paramagnetic ions per unit cell. The trigonal axes of the crystalline field at the ions lie in the directions of the four body diagonals of the cube. Figure 10 shows that if the magnetic field is applied along the 100 axis, $\theta = \tan^{-1}\sqrt{2} = 54.74^\circ$ for all four ions. If the magnetic field is applied along the 110 axis, $\theta = \tan^{-1}1/\sqrt{2} = 35.26^\circ$ for two of the ions and 90° for the other two. If the magnetic field is applied along the 111 axis, $\theta = 2\tan^{-1}1/\sqrt{2} = 70.53^\circ$ for three of the ions and 0° for the fourth ion. It is therefore more useful to have values of S/R for the angles 0°, 35.26°, 54.74°, 70.53°, and 90° than for every 10° (the values of θ given in Jarrett's data). The entropies for these angles were obtained by interpolation between the values for every 10° with the help of Newton's interpolation formula.

In order to calculate the entropy for a powdered sample one

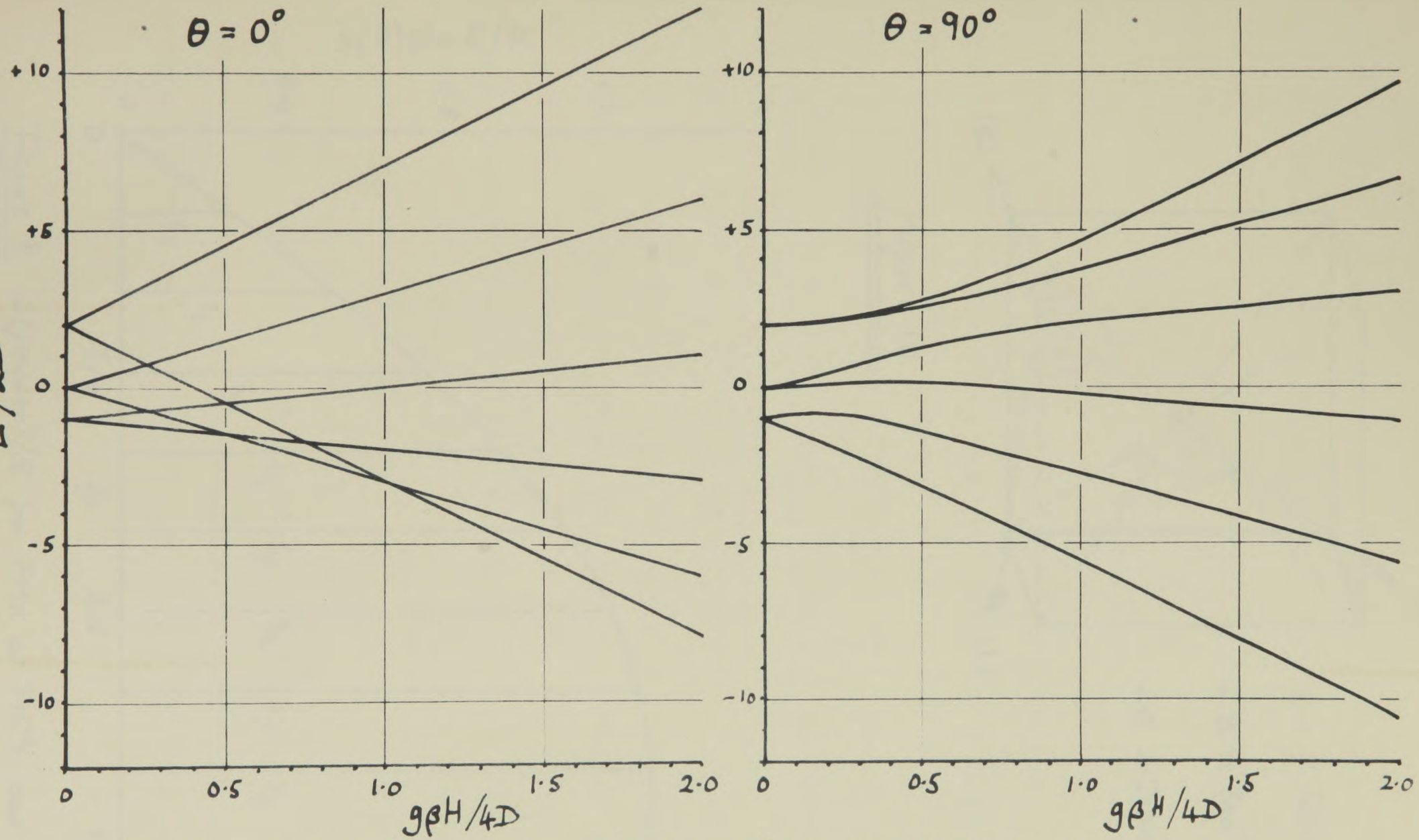

Figure 9 Energy levels as a function of magnetic field (Jarrett).

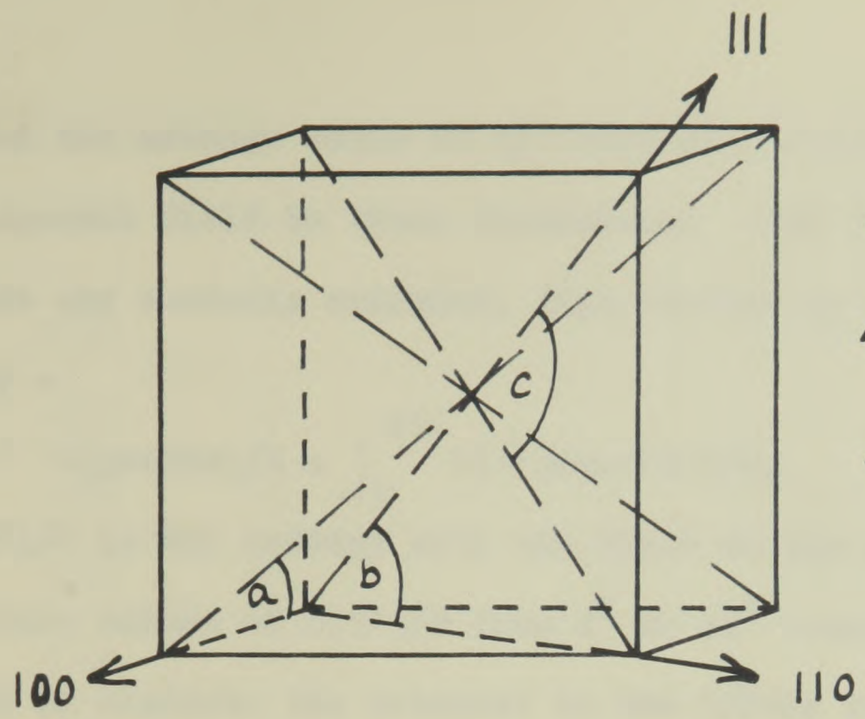

$\angle a = \tan^{-1}\sqrt{2}$

$\angle b = \tan^{-1} 1/\sqrt{2}$

$\angle c = 2\tan^{-1} 1/\sqrt{2}$

Figure 10

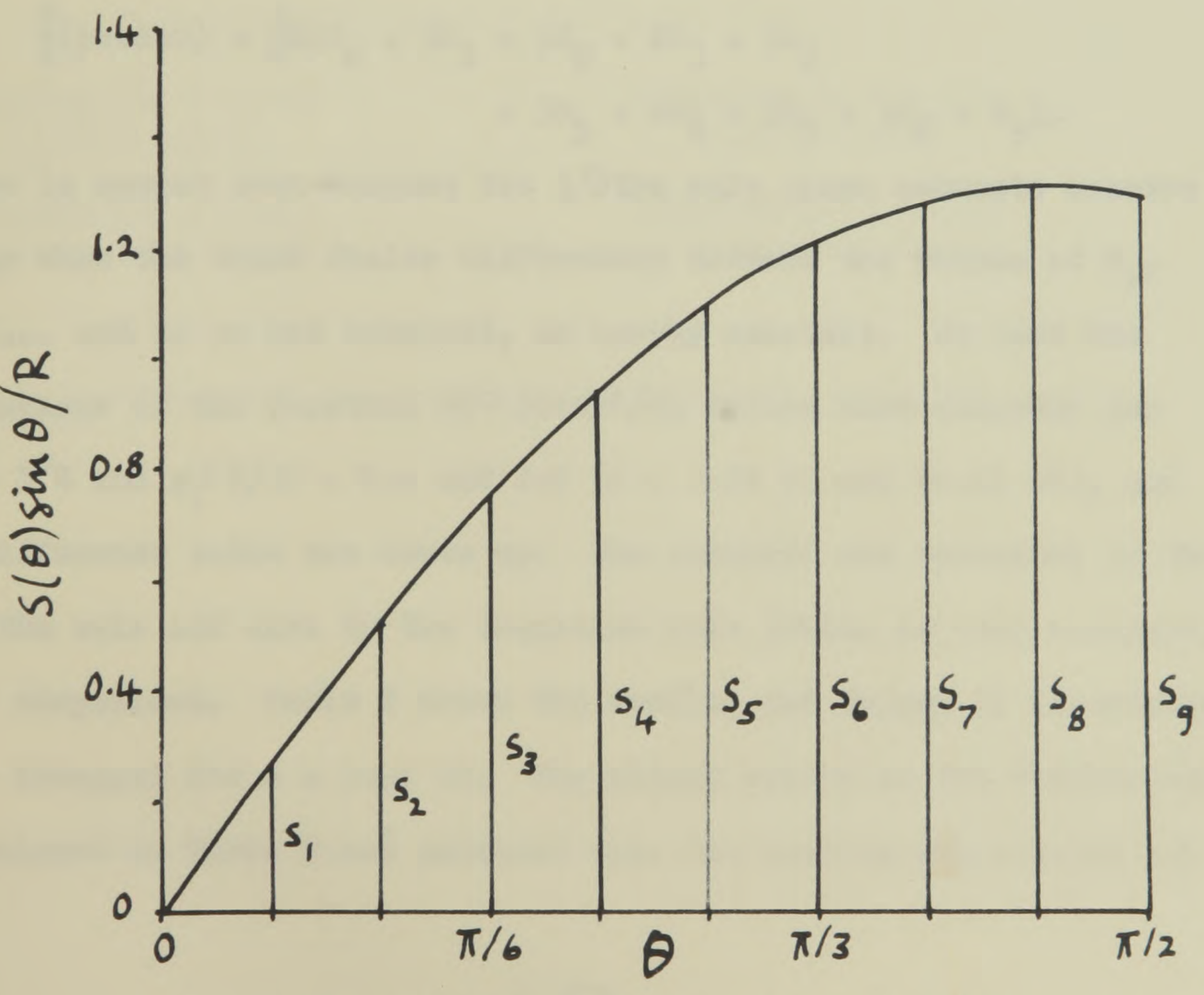

Figure 11 S(powder)/R for FMA at 1·15°K and ? 22 kG = area under curve.

has to find the average value of S/R over all orientations of the applied magnetic field in three dimensions. When the crystal axes of the ions are randomly oriented, this average is given as mentioned already by -

$$S(\text{powder})/R = \int_0^{\pi/2} S(\theta)\sin\theta\, d\theta/R,$$

where $S(\theta)/R$ is the entropy with the field at the angle θ. Since we have values of $S(\theta)/R$ from 0° to 90° every 10° it is convenient to evaluate the integral by the 3/8ths rule, taking the 10° steps of θ in three groups of three. Putting $S(0^\circ)\sin 0^\circ/R = S_0$, $S(10^\circ)\sin 10^\circ/R = S_1$, and so on, and h equal to the difference in θ between successive values of $S(\theta)$, we have -

$$\frac{S}{R}(\text{powder}) = \tfrac{3}{8}h(S_0 + 3S_1 + 3S_2 + 2S_3 + 3S_4 + 3S_5 + 2S_6 + 3S_7 + 3S_8 + S_9).$$

Care is needed here because the 3/8ths rule gives accurate answers only when the third finite differences between the values of S_1, S_2 ... and so on are constant, or nearly constant. To test the behaviour of the function $S(\theta)\sin\theta/R$, values were computed for $T = 1^\circ K$ and $g\beta H/4D = 0.4$ and 2.0 ($H = 3.22$ kG and 16.11 kG), and a difference table was drawn up. The integral was evaluated by the 3/8ths rule and also by the trapezium rule (which is less accurate) for comparison. Table 2 shows the result, and figure 11 illustrates the integral for $H = 3.22$ kG. The slight errors in the differences tabulated in Table 2 are produced when the numbers are rounded off

$T = 1^{\circ}K$, $H = 3.22$ kG

	Δ	Δ^2	Δ^3
$S_1 = 0.271$			
	+255		
$S_2 = 0.526$		−29	
	+226		−8
$S_3 = 0.753$		−37	
	+189		−3
$S_4 = 0.942$		−40	
	+150		+1
$S_5 = 1.092$		−38	
	+111		+3
$S_6 = 1.203$		−35	
	+76		+3
$S_7 = 1.279$		−32	
	+44		−40
$S_8 = 1.323$		−69	
	−25		
$S_9 = 1.298$			

S(powder)/R = 1.408
(3/8ths rule)

S(powder)/R = 1.403
(trapezium rule)

$T = 1^{\circ}K$, $H = 16.11$ kG

	Δ	Δ^2	Δ^3
$S_1 = 0.127$			
	+94		
$S_2 = 0.220$		−42	
	+52		+10
$S_3 = 0.272$		−32	
	+20		+14
$S_4 = 0.293$		−18	
	+3		+10
$S_5 = 0.295$		−7	
	−5		+6
$S_6 = 0.291$		−1	
	−6		+3
$S_7 = 0.285$		+1	
	−4		+1
$S_8 = 0.280$		+3	
	−2		
$S_9 = 0.279$			

S(powder)/R = 0.386
(3/8ths rule)

S(powder)/R = 0.384
(trapezium rule)

Table 2. Values of the function $S(\theta)\sin\theta/R$, for FMA.

to the third decimal place. The results of the test show that the entropies computed in this way are subject to unavoidable errors of not more than one or two units in the third decimal place. The entropy values obtained are therefore sufficiently accurate for practical use.

We are now in a position to follow the details of the programme for calculating the entropy from Jarrett's data. The values of $E_i/2D$ were taken to six decimal places. The work was done on the Ferranti Mercury computer of the Oxford University Computing Laboratory using the Autocode system of programming.

(a) Magnetic field strengths were calculated from the values of $g\beta H/4D$ by means of the substitutions $g = 2$, $\beta = 0.92712 \times 10^{-20}$ erg.gauss^{-1}, $D = 0.188$ cm^{-1}, and the conversion factor from cm^{-1} to ergs $= 1.9857 \times 10^{-16}$ erg.cm.

(b) The sixty energy levels $E_i/2D$ for the first value of the magnetic field were taken (six levels for θ every 10^0 up to 90^0), and the values of E_i/k were calculated, where k is Boltzmann's constant $= 1.3803 \times 10^{-16}$ erg.deg^{-1}.

(c) Next, with the temperature $T = 0.9^0$K, the values of the entropy for the ten values of θ were calculated from the partition function by means of the formula -

$$\frac{S(\theta)}{R} = \ln \sum_i \exp\left(\frac{-E_i}{kT}\right) + \frac{\sum_i \left(\frac{E_i}{kT}\right) \exp\left(\frac{-E_i}{kT}\right)}{\sum_i \exp\left(-\frac{E_i}{kT}\right)},$$

where the summations are taken over the six levels at each value of θ.

(d) Next, for the interpolations, the first, second, and third finite differences between the entropies were calculated -

$\Delta S(10^\circ)/R = S(20^\circ)/R - S(10^\circ)/R$ etc.,

$\Delta^2 S(10^\circ)/R = \Delta S(20^\circ)/R - \Delta S(10^\circ)/R$ etc.,

$\Delta^3 S(10^\circ)/R = \Delta^2 S(20^\circ)/R - \Delta^2 S(10^\circ)/R$ etc.,

The values of the entropy at $\theta = 35.2644^\circ$, 54.7356°, and 70.5288°, which are required for single crystals, were then found by interpolation between the entropies for each 10° with the help of the following forms of Newton's interpolation formula -

$$\frac{S}{R}(35.26^\circ) = \frac{S(20^\circ)}{R} + 1.5264\,\frac{\Delta S(20^\circ)}{R} + 0.4016\,\frac{\Delta^2 S(20^\circ)}{R} - 0.0634\,\frac{\Delta^3 S(20^\circ)}{R},$$

$$\frac{S}{R}(54.74^\circ) = \frac{S(40^\circ)}{R} + 1.4736\,\frac{\Delta S(40^\circ)}{R} + 0.3489\,\frac{\Delta^2 S(40^\circ)}{R} - 0.0612\,\frac{\Delta^3 S(40^\circ)}{R},$$

$$\frac{S}{R}(70.53^\circ) = \frac{S(60^\circ)}{R} + 1.0529\,\frac{\Delta S(60^\circ)}{R} + 0.02784\,\frac{\Delta^2 S(60)}{R}.$$

The values of $S(0^\circ)/R$ and $S(90^\circ)/R$ were also recorded.

(e) Next the value of S(powder)/R was evaluated by averaging the value of S/R over all directions of the magnetic field as already explained.

(f) The above steps (c, d, and e) were then repeated for the temperatures T = 0.95, 1.00, 1.05, 1.10, 1.15, and 1.20°K.

(g) The whole calculation was then repeated (from steps a to f) with the next value of $g\beta H/4D$, that is the next magnetic field strength. In this way the entropy was calculated for field strengths from zero to 16.11 kG.

The results are given in Table 3. As already mentioned in Chapter Two, and shown in figure 7, the theoretical entropies at 1.15°K agree with the experimental results within about 2% of the values of the total entropy of magnetization $\Delta S/R$.

From Table 3 one may obtain values of S/R for certain limited ranges of temperature and magnetic field even when D differs from 0.188 cm^{-1}. Since the partition function, and hence the entropy, is a function of E_i/kT, and since the entropy has been calculated from the energy levels E_i given in the form E_i/D as a function of H/D, the calculated values of S/R are unchanged if D, H, and T are simultaneously multiplied by a constant factor, say α. Therefore the entropy S/R given in the table for a temperature T and a magnetic field H when D = 0.188 cm^{-1} is equal to the entropy at a temperature αT and a magnetic field αH when D = 0.188α cm^{-1}. The table may therefore still be used if the value of D, here taken equal to that for the magnetically dilute salt, is later found to be slightly different in the undiluted salt. In addition it is possible to correlate the spread of the experimental entropy determinations, shown in figure 7, with a possible departure of the value of D

ENTROPY OF FMA - EXELL 1/3

H = 0.00 kG	Values of θ						
T (°K)	0°	35.26°	54.74°	70.53°	90°	powder	
0.90	1.597	1.597	1.597	1.597	1.597	1.597	
0.95	1.613	1.613	1.613	1.613	1.613	1.613	
1.00	1.626	1.626	1.626	1.626	1.626	1.626	
1.05	1.639	1.639	1.639	1.639	1.639	1.639	
1.10	1.650	1.650	1.650	1.650	1.650	1.650	
1.15	1.660	1.660	1.660	1.660	1.660	1.660	
1.20	1.669	1.669	1.669	1.669	1.669	1.669	1.667
0.81							
0.90	1.594	1.586	1.578	1.573	1.570	1.578	
0.95	1.609	1.602	1.595	1.590	1.588	1.595	
1.00	1.623	1.617	1.610	1.606	1.604	1.611	
1.05	1.635	1.630	1.624	1.621	1.619	1.624	
1.10	1.646	1.641	1.637	1.633	1.632	1.637	
1.15	1.656	1.652	1.648	1.645	1.643	1.648	
1.20	1.665	1.661	1.657	1.655	1.654	1.658	1.656
1.61							
0.90	1.583	1.552	1.523	1.503	1.494	1.523	
0.95	1.599	1.571	1.545	1.528	1.519	1.545	
1.00	1.612	1.588	1.565	1.549	1.542	1.565	
1.05	1.625	1.603	1.582	1.569	1.562	1.583	
1.10	1.636	1.617	1.598	1.586	1.580	1.598	
1.15	1.646	1.629	1.612	1.601	1.596	1.612	
1.20	1.655	1.640	1.625	1.615	1.610	1.625	1.622
2.42							
0.90	1.566	1.500	1.439	1.401	1.383	1.441	
0.95	1.581	1.523	1.469	1.434	1.418	1.470	
1.00	1.595	1.543	1.494	1.464	1.449	1.496	
1.05	1.607	1.561	1.518	1.490	1.476	1.518	
1.10	1.619	1.577	1.538	1.513	1.501	1.539	
1.15	1.629	1.592	1.557	1.534	1.522	1.557	
1.20	1.639	1.605	1.573	1.552	1.542	1.574	1.570
3.22							
0.90	1.542	1.433	1.339	1.282	1.212	1.340	
0.95	1.557	1.460	1.375	1.323	1.257	1.376	
1.00	1.571	1.485	1.407	1.360	1.298	1.408	
1.05	1.584	1.506	1.436	1.393	1.335	1.436	
1.10	1.595	1.526	1.462	1.422	1.368	1.462	
1.15	1.606	1.544	1.486	1.449	1.398	1.485	
1.20	1.616	1.560	1.507	1.473	1.426	1.506	1.502

Table 3(a)

H=4.03 kG	Values of θ 0°	35.26°	54.74°	70.53°	90°	powder	
T (°K) 0.90	1.511	1.357	1.230	1.158	1.125	1.239	
0.95	1.526	1.388	1.272	1.205	1.174	1.280	
1.00	1.541	1.417	1.310	1.248	1.219	1.316	
1.05	1.554	1.442	1.345	1.287	1.260	1.350	
1.10	1.566	1.465	1.376	1.322	1.297	1.380	
1.15	1.577	1.486	1.404	1.355	1.331	1.408	
1.20	1.588	1.505	1.430	1.384	1.362	1.433	1.428
4.83							
0.90	1.474	1.274	1.121	1.037	1.000	1.135	
0.95	1.490	1.310	1.168	1.089	1.053	1.180	
1.00	1.505	1.342	1.211	1.136	1.102	1.220	
1.05	1.518	1.371	1.250	1.179	1.147	1.258	
1.10	1.531	1.398	1.285	1.219	1.189	1.292	
1.15	1.543	1.422	1.318	1.256	1.227	1.324	
1.20	1.554	1.444	1.348	1.290	1.263	1.352	1.347
5.64							
0.90	1.432	1.191	1.017	0.927	0.887	1.036	
0.95	1.448	1.229	1.067	0.980	0.941	1.083	
1.00	1.463	1.265	1.112	1.029	0.992	1.126	
1.05	1.478	1.297	1.155	1.075	1.040	1.166	
1.10	1.491	1.327	1.194	1.118	1.084	1.204	
1.15	1.504	1.354	1.230	1.158	1.126	1.238	
1.20	1.516	1.379	1.263	1.196	1.165	1.270	1.264
6.44							
0.90	1.385	1.108	0.921	0.827	0.787	0.945	
0.95	1.402	1.149	0.971	0.880	0.841	0.992	
1.00	1.418	1.187	1.019	0.931	0.892	1.037	
1.05	1.433	1.222	1.063	0.978	0.940	1.079	
1.10	1.448	1.254	1.105	1.023	0.986	1.118	
1.15	1.461	1.284	1.143	1.065	1.030	1.155	
1.20	1.474	1.311	1.179	1.104	1.070	1.189	1.182
7.25							
0.90	1.333	1.027	0.833	0.739	0.700	0.861	
0.95	1.351	1.071	0.884	0.791	0.752	0.909	
1.00	1.369	1.110	0.932	0.841	0.802	0.954	
1.05	1.385	1.147	0.977	0.889	0.850	0.996	
1.10	1.400	1.181	1.020	0.934	0.896	1.036	
1.15	1.415	1.213	1.060	0.977	0.940	1.074	
1.20	1.429	1.242	1.097	1.018	0.982	1.110	1.103

Table 3(b)

H = 8.05 kG	Values of θ 0°	35.26°	54.74°	70.53°	90°	powder	
T (°K) 0.90	1.278	0.951	0.754	0.662	0.624	0.785	
0.95	1.298	0.995	0.804	0.712	0.674	0.832	
1.00	1.316	1.036	0.852	0.761	0.723	0.877	
1.05	1.334	1.075	0.897	0.808	0.770	0.919	
1.10	1.350	1.110	0.941	0.853	0.815	0.960	
1.15	1.366	1.144	0.981	0.896	0.859	0.999	
1.20	1.382	1.175	1.020	0.937	0.901	1.035	1.028
8.86							
0.90	1.221	0.879	0.683	0.594	0.557	0.716	
0.95	1.242	0.924	0.732	0.642	0.605	0.762	
1.00	1.261	0.966	0.779	0.690	0.652	0.806	
1.05	1.280	1.005	0.824	0.735	0.698	0.849	
1.10	1.298	1.042	0.867	0.780	0.742	0.889	
1.15	1.315	1.076	0.908	0.822	0.785	0.928	
1.20	1.332	1.108	0.947	0.863	0.826	0.965	0.958
9.66							
0.90	1.162	0.812	0.619	0.534	0.499	0.654	
0.95	1.184	0.857	0.667	0.580	0.545	0.699	
1.00	1.205	0.899	0.713	0.626	0.590	0.742	
1.05	1.225	0.938	0.757	0.670	0.634	0.783	
1.10	1.245	0.976	0.800	0.713	0.677	0.824	
1.15	1.263	1.011	0.840	0.755	0.718	0.862	
1.20	1.281	1.044	0.879	0.795	0.759	0.899	0.892
12.08							
0.90	0.980	0.637	0.465	0.392	0.364	0.500	
0.95	1.007	0.680	0.507	0.433	0.403	0.540	
1.00	1.033	0.721	0.549	0.472	0.441	0.580	
1.05	1.057	0.761	0.590	0.512	0.480	0.618	
1.10	1.080	0.798	0.629	0.550	0.518	0.656	
1.15	1.103	0.834	0.667	0.588	0.555	0.692	
1.20	1.124	0.869	0.705	0.625	0.592	0.728	0.721
16.11							
0.90	0.700	0.421	0.292	0.240	0.219	0.320	
0.95	0.732	0.459	0.326	0.270	0.249	0.353	
1.00	0.763	0.496	0.360	0.302	0.279	0.387	
1.05	0.793	0.532	0.393	0.333	0.309	0.419	
1.10	0.821	0.567	0.427	0.364	0.339	0.452	
1.15	0.848	0.601	0.460	0.396	0.370	0.484	
1.20	0.873	0.634	0.492	0.427	0.400	0.515	0.509

Table 3(c)

from 0.188 cm^{-1}. Calculations by this method show that the range of D values compatible with the experimental results is from 0.15 cm^{-1} to 0.20 cm^{-1}. Therefore the present experimental accuracy does not permit one to say definitely whether the value of D depends on the dilution of this salt.

CHAPTER FOUR

DETERMINATION OF ABSOLUTE TEMPERATURES BELOW 1°K

Adiabatic demagnetizations

The absolute temperatures as a function of T* below 0.7°K were obtained for FMA by the usual method from the relation $T = (dQ/dT^*)/(dS/dT^*)$. To determine the S/R - T* relation a series of adiabatic demagnetizations were made from known fields, that is with known entropy reductions. The value of (dQ/dT^*) was obtained directly from specific heat measurements.

In the usual method for determining the S/R - T* relation by adiabatic demagnetizations one starts with a small initial field and, after demagnetizing and measuring T*, one applies a slightly larger field. The specimen reaches a temperature higher than that of the helium bath and is brought back into equilibrium with exchange gas which must be pumped out before the next demagnetization is made. The time interval between demagnetizations is usually forty to fifty minutes.

The experimental arrangement described in this thesis made it possible to complete a series of measurements in a relatively short time without having to let in and pump out exchange gas between each demagnetization. The maximum field used in the experiments was applied first. When thermal equilibrium between the specimen and the helium bath had been reached the exchange gas was

pumped away. Before the demagnetization the magnetic field could be adjusted slightly to make the temperature of the specimen, as shown by the carbon thermometer, equal within certain limits to a previously chosen value. The magnetic field was reduced from its initial value to zero in a few seconds, and T* was measured in the usual way. Without admitting exchange gas a smaller field was then applied and heat was supplied electrically to bring the specimen back to the original starting temperature ready for the next demagnetization. It was possible with this method to make a demagnetization every six or seven minutes.

After each adiabatic demagnetization the temperature T* was measured every thirty seconds by reading the deflection δ of the ballistic galvanometer in the mutual inductance bridge. The value of δ at the time of demagnetization was found by extrapolation, and T* at this time was calculated from the formula $\delta/i = a/(T^* - \Delta) + b$, (see Chapter Two). The term Δ for correcting to spherical shape was calculated thus:

$$\Delta = \left(\frac{4\pi}{3} - N\right)\frac{J(J+1)Rg^2\beta^2\rho}{3mk^2}$$

(see Chapter Two)

where N = 1.365 (3:1 ellipsoid), J = 5/2, R = 8.310×10^7 erg ~~gauss~~ $^{-1}$ mol.$^{-1}$ deg^{-1}, g = 2, $\beta = 9.27 \times 10^{-21}$ erg gauss^{-1}, $k = 1.380 \times 10^{-16}$ erg deg^{-1}, m = 496.2 gm mol^{-1}, and ρ (the density of the pill) = 1.594 gm cm^{-3}. This gave Δ = 0.040 deg. The actual values of T* obtained after

adiabatic demagnetizations from various fields are shown in fig.12. The results are given of three runs with initial temperatures T_i = 1.15°K, 1.19°K, and 1.14°K respectively.

Calculations show that the slight magnetic anisotropy of FMA would cause thermally isolated grains in a powder to reach different temperatures after an adiabatic demagnetization. Suppose,for example, that a field of 12 kG is applied along the 100 axis of a single crystal of FMA at 1.15°K. Then θ = 54.74° for each ion (see Chapter Three), and Table 3 shows that S/R = 0.667. If the field is applied along the 111 axis, θ = 70 .53° for three ions per unit cell and 0° for the fourth. Then

$$\frac{S}{R} = \frac{3}{4}(0.588) + \frac{1}{4}(1.103) = 0.717.$$

Fig.13 (described later) shows that in these two cases adiabatic demagnetizations would produce final magnetic temperatures T* of 0.172 deg and 0.198 deg respectively, that is approximately 0.092°K and 0.118°K on the absolute scale (see fig.18 described later). The difference between these temperatures ΔT = 0.026°K represents the approximate temperature differences between isolated grains in a powder after being magnetically cooled to 0.1°K. A similar calculation shows that adiabatic demagnetizations from a field of 8.86 kG at 1.15°K would produce a final temperature of 0.2°K and ΔT = 0.015°K. These temperature inhomogeneities extend over a few grains, that is over about 10^{-2} cm. Using a typical value for

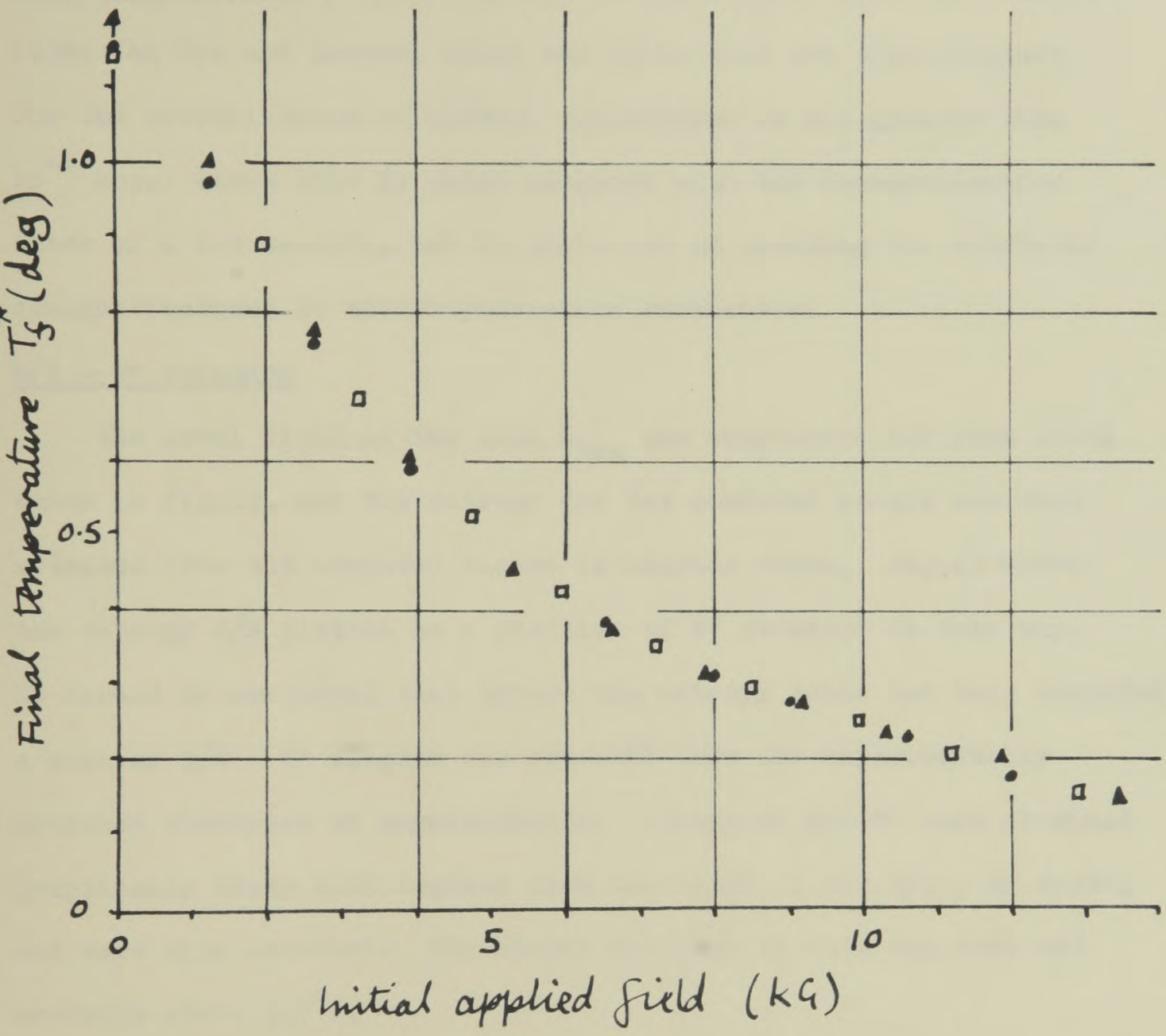

Figure 12 Temperatures reached by the adiabatic demagnetization of FMA.

Initial temperatures T_i – ● 1·15°K
▲ 1·19°K
□ 1·14°K

the heat conductivity of a compressed pill of paramagnetic salt at these temperatures (~50^0 erg/cm.sec.deg, Kurti, Rollin and Simon, 1936; Van Dyk and Keesom, 1940) one finds that the time constant for the establishment of thermal equilibrium is not greater than 10^{-1} sec. Since this is short compared with the demagnetization times of a few seconds, one is justified in treating the adiabatic demagnetizations as thermodynamically reversible.

S/R - T* relation

The local field at the ions H_{loc} was calculated for each point shown in fig.12, and the entropy for the powdered sample was then obtained from the computed tables in Chapter Three. Fig.13 shows the entropy S/R plotted as a function of T* obtained in this way. It should be mentioned that before the entropy table had been computed a similar S/R - T* diagram was obtainad from the experimentally measured entropies of magnetization. Values of dS/dT* were obtained graphically every 0.05 degrees from the slope of the S/R - T* curve, and were then smoothed. The slopes obtained in this way were not accurate above 0.7°K.

Specific heat

The specific heat of the specimen C* = dQ/dT* was measured from 0.1°K to 1.2°K by introducing heat electrically ih steps and measuring the temperature rise each step on the magnetic thermometer. The carbon thermometer was not used because heat contact with the

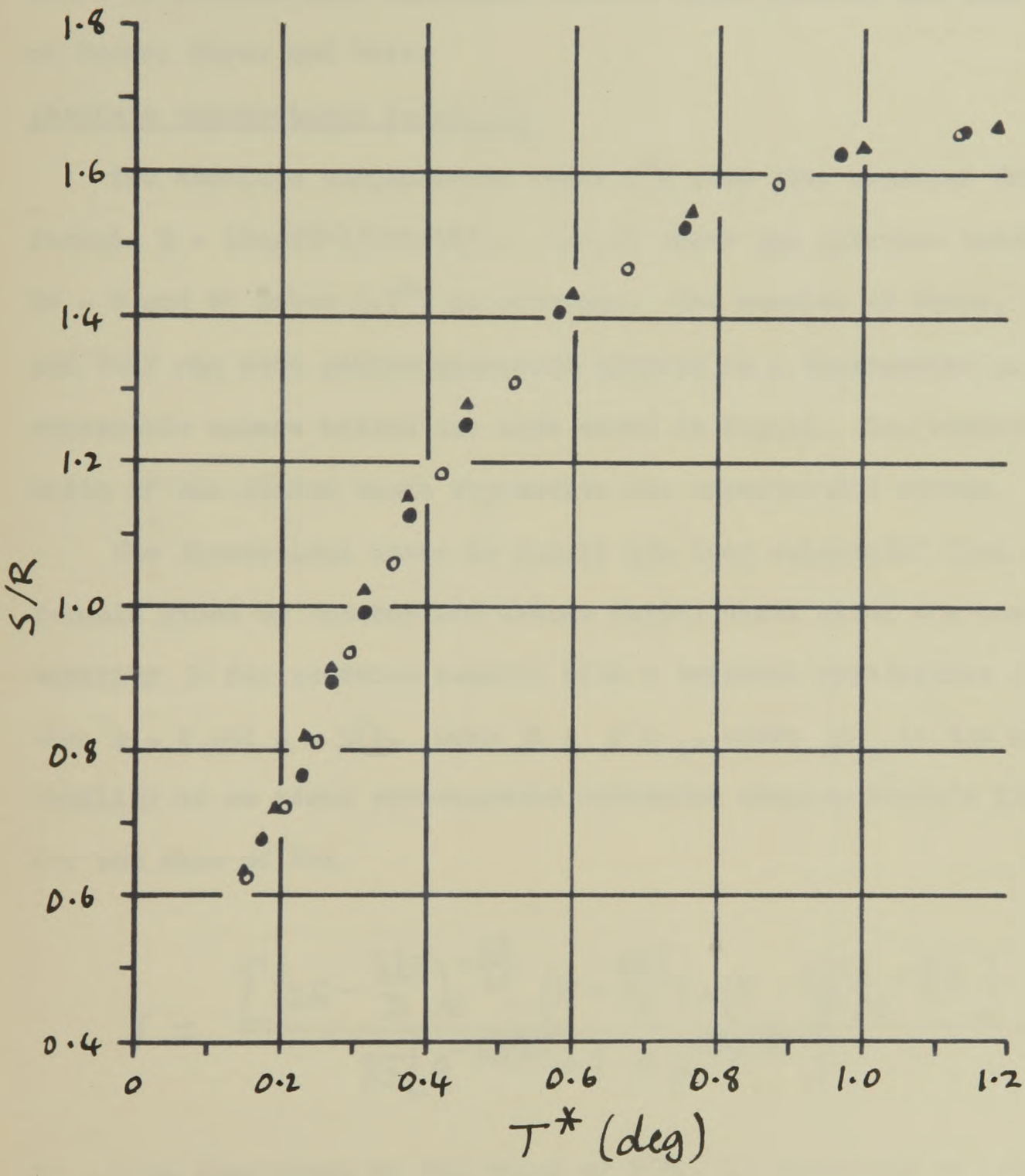

Figure 13 Entropy of FMA as a function of T*

specimen was poor below 0.3°K. The results are shown in fig.14. There is satisfactory agreement between these results and those of Cooke, Meyer and Wolf.

Absolute temperatures below 1°K

The absolute temperatures below 1°K were then obtained from the formula $T = (dQ/dT^*)/(dS/dT^*)$. Fig.15 shows the relation between $T^* - T$ and T^* below 0.7°K so obtained. The results of Cooke, Meyer and Wolf who used cerium magnesium nitrate as a thermometer in the concentric sphere method are also shown in fig.15. The vertical width of the shaded bands represents the experimental errors.

The theoretical curve in fig.15 has been calculated from a formula given by Bleaney and Trenam (1954) which gives the susceptibility χ for powdered samples with a trigonal crystalline field when $g = 2$ and $S = 5/2$. Here $\chi = \gamma \chi_i$, where χ_i is the susceptibility of an ideal paramagnetic substance obeying Curie's law and, for the case of FMA,

$$\gamma = \frac{\left[\left(25 - \frac{5kT}{D}\right)e^{-\frac{6D}{kT}} + \left(19 + \frac{16kT}{D}\right) + \left(9 - \frac{11kT}{D}\right)e^{-\frac{2D}{kT}}\right]}{35\left[e^{-6D/kT} + 1 + e^{-2D/kT}\right]}$$

$T^* - T$ is then given by the value of $T(\frac{1}{\gamma} - 1)$ which may be calculated at a number of chosen temperatures between 0.1°K and 1°K.

The experimental results of Cooke, Meyer and Wolf differ from

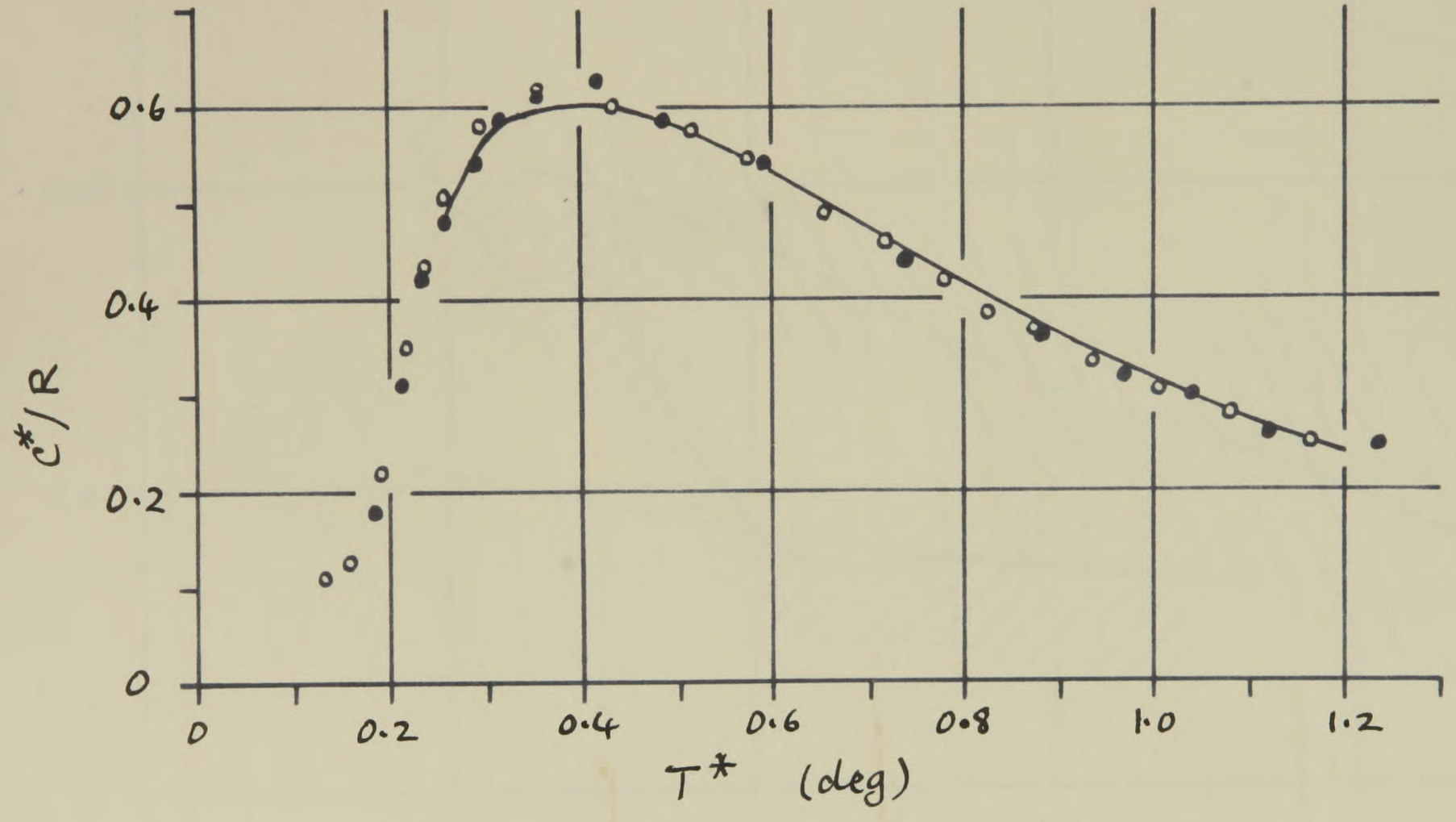

Figure 14 Specific heat of FMA; •○ present results;
_____ results of Cooke, Meyer and Wolf.

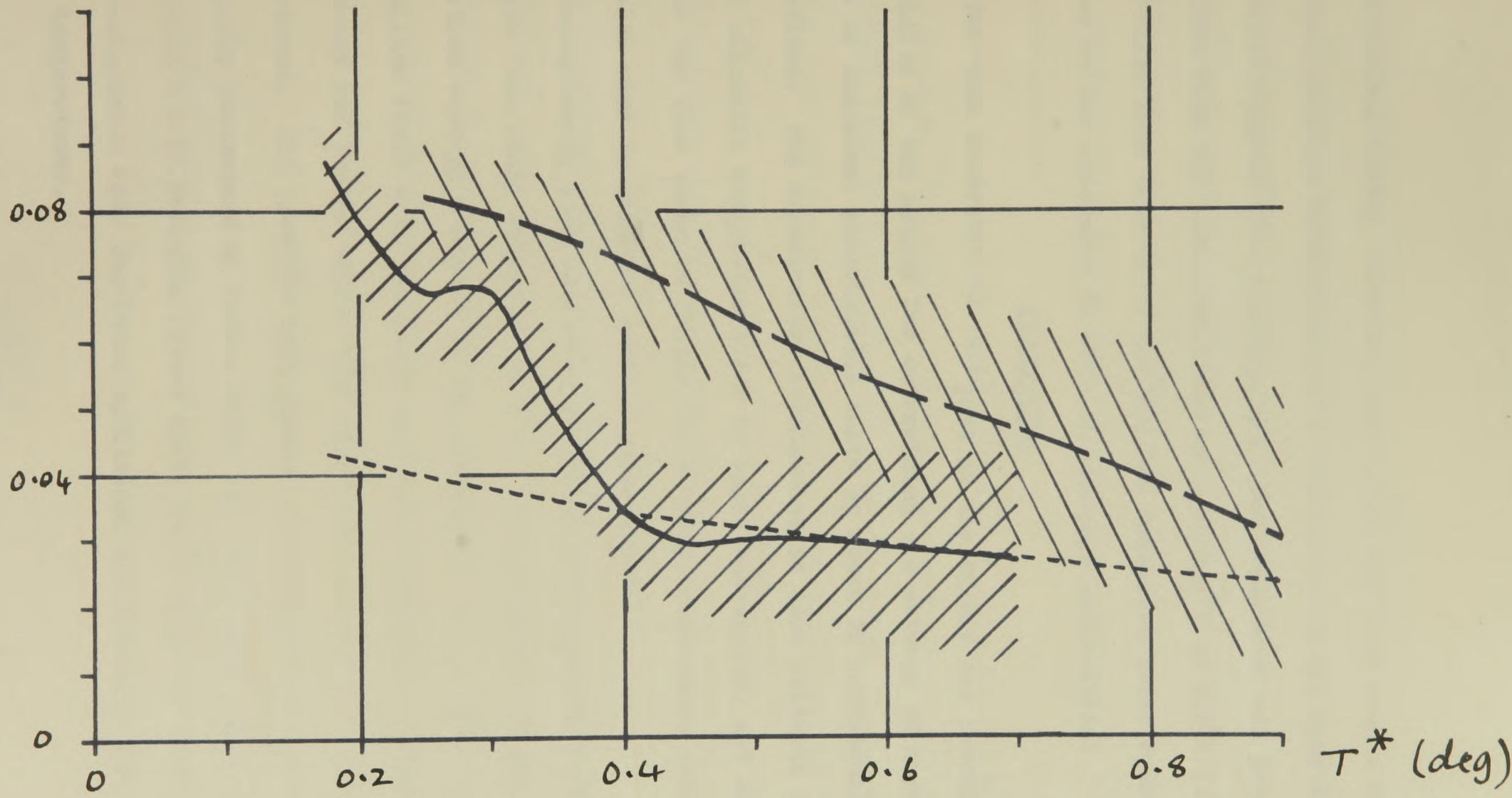

Figure 15. T^*-T as a function of T^* for FMA.

——— present results.

— — — results of Cooke, Mayer and Wolf.

- - - - - - Curve calculated from the Stark Splittings.

the theoretical curve. However, they point out that even a small additional exchange interaction, not noticeable in the specific heat, might explain this discrepancy. The results of the present work agree with the theoretical values from 0.4°K to 0.7°K (though they deviate from them below 0.4°K), and therefore leave open the question of the existence of such an exchange interaction.

CONCLUSION

The work described in this part of the thesis has proved the feasibility of the method for determining the entropy of magnetization of non-ideal paramagnetic salts by means of isothermal demagnetizations. The experimental arrangement is also suitable for making adiabatic demagnetizations in rapid succession, and this reduces the time taken to obtain the entropy-temperature relation for salts used in magnetic cooling experiments.

Measurements have been made on ferric methylammonium alum which deviates from ideal behaviour at 1°K. It was found that the magnetization entropy computed on the assumption of a purely trigonal crystalline field with the Stark splitting parameter determined by Bleaney and Trenam agreed with experiment within the errors of measurement. The specific heat values are in agreement with those previously determined by Cooke, Meyer and Wolf. The experimentally determined $T - T^*$ relation agrees above 0.4°K with the theoretical curve calculated from the Stark splittings but deviates from it at lower temperatures.

Further applications

Having seen the details of the work on FMA, we turn in this section to a discussion of other possible applications of the isothermal demagnetization method of measuring the magnetic entropy. We shall consider uses for other paramagnetic salts, for paramagnetic alloys which may be used for magnetic cooling, and for the study of superparamagnetism.

A cooling salt for which measurements of the magnetization entropy would be interesting is gadolinium sulphate, $Gd_2(SO_4)_3.8H_2O$. The specific heat is large below 1°K, and the energy levels of the Gd^{3+} ion which consist of four doublets, have an overall splitting of k x 1.18°K in a diluted salt (Bogle and Heine, 1954). The T-T* relation has been determined experimentally by Van Dijk (1946) down to 0.22°K. He measured (1) the specific heat $C_o^* = dQ/dT^*$ in zero field below 1°K, (2) the specific heat $C_H = dQ/dT_H$ in a fixed applied field H above 1°K, and (3) the temperatures T_o^* below 1°K obtained by adiabatic demagnetizations from the field H and various temperatures T_H above 1°K. The absolute temperature T_o corresponding to T* was then given by

$$T_o = T_H \frac{C_o^*}{C_H} \frac{dT_o^*}{dT_H} .$$

This method is similar in principle to our method using isothermal demagnetizations, the entropy in Van Dijk's experiments being

determined from the measurements of C_H. It can be shown from Van Dijk's data that the deviations of $\Delta S/R$ in gadolinium sulphate from the ideal values for $J = 7/2$ could be determined by our method. For example at $1.3^{\circ}K$ in a field of 10.25 kG this deviation is 0.091, which is roughly the same as for FMA. We note also that the entropy could be calculated in a similar way to that described in Chapter Three.

A direct determination of the magnetization entropy for gadolinium sulphate would be essentially a repeat of the earlier work. But the isothermal demagnetization method may have slight advantages over that using specific heat measurements in a magnetic field because, since all the measurements are made at a lower and a constant temperature, the thermal isolation is improved and the heat leak to the surroundings (also at the same temperature) is minimised. However, since the introduction of the concentric sphere method using cerium magnesium nitrate, and of calibrated carbon thermometers, entropy measurements are less useful for determining absolute temperatures below $1^{\circ}K$.

On the other han d the method does provide a simple way of measuring the effective spin S' of a paramagnetic substance from the total magnetic entropy $\Delta S/R = \ln(2S' + 1)$. It could also be used to study the effects of magnetic dilution on Stark splittings of the type occuring in cerium ethyl sulphate (Bogle, Cooke, and

Whitley, 1951) or in ferric rubidium alum (see Kurti, 1957) when the microwave resonance lines are too broad for measurement. In this case, however, the method would need considerable refinement.

Let us now consider possible applications for magnetization entropy measurements in metallic samples. Since at present the theory of metals is still incomplete, we cannot calculate the details of the magnetic behaviour with certainty, and experimental measurements are necessary. For example entropy measurements would be useful in the case of paramagnetic alloys suitable for magnetic cooling. The advantages of such coolants over the more usual salts are that they are more stable chemically, and their thermal conductivity is higher. On the other hand not very low temperatures have been reached so far.

Nelson and Legvold (1961) found some magnetic cooling in alloys of 0.6% and 1.0% holmium in yttrium, but it was too small for practical use. The lowest temperature reached was 0.75°K by demagnetizing the 1% Ho sample from a field of 11.4 kG at 1.25°K. The entropy removed during isothermal magnetization calculated from the magnetization curves was found to be much less than that expected for "ideal" behaviour.

Parks and Little (1961) obtained more success with alloys of 0.82%-9.6% erbium in thorium. Temperatures of ~0.1°K were obtained by adiabatic demagnetizations from about 8 kG at 0.73°K. Presumably the final temperatures were measured with a carbon thermometer.

Measurements of the magnetization would be especially useful if these paramagnetic alloys became generally used for magnetic cooling because so far theoretical calculations are not reliable. It should be noted that one would have to take precautions against eddy-current heating in these experiments.

Finally, we mention that determinations of magnetization entropy might be used in the study of superparamagnetism. This phenomenon occurs when clusters of atoms in single ferromagnetic domains exhibit a behaviour analogous to that of ordinary paramagnetic atoms (see Bean and Livingston, 1959). Such behaviour has been shown to occur, for example, in the case of fine particles of iron suspended in mercury, and with small particles of cobalt precipitated out of solid solution in a Co_2Cu_{98} alloy. It is also believed to be the cause of anomalies in the low temperature specific heats of some transition metal alloys (Cheng, Wei, and Beck, 1960. Guthrie, Friedberg, and Goldman, 1959), and in TiFe as discussed in detail in Part Three of this thesis (page 149).

Consider N clusters each with n atoms bearing a mean spin of $\bar{S}$. (In reality n is not the same for every cluster, but a distribution of cluster sizes exists, and this complicates the simple theory presented here) The magnetic moment μ of each cluster is given by $\mu = g\beta n\bar{S}$, and the susceptibility χ of the N clusters is then

$$\chi = \frac{N\mu^2}{3kT} = \frac{N(g\beta n\bar{S})^2}{3kT} \quad \ldots (1)$$

The saturation magnetization M_s is given by

$$M_s = Ng\beta n\bar{S}. \quad \ldots (2)$$

Measurements of χ and M_s then determine N and $gn\bar{S}$. Usually $g\bar{S}$ is assumed to be known. If, for example, in the case of iron particles $g\bar{S}$ is taken to be 2.2, measurements of χ may be used to determine the particle size from the value of n.

However, the total magnetization entropy, ΔS_m is given by

$$\Delta S_m = Nk \ln(2n\bar{S}+1) \quad \ldots (3)$$

and so if N is known $n\bar{S}$, and hence g, may be determined experimentally. As mentioned earlier, precautions agai nst eddy-current heating would have to be taken in isothermal demagnetization experiments for measuring ΔS_m in alloys. It would be interesting to compare the entropies obtained in this way with those found under the specific heat anomalies at low temperatures. One would be able to separate the entropy of superparamagnetism from the lattice and electronic contributions if the superparamagnetism could be destroyed by quenching the samples from a high temperature. The results of Part Three show that the specific heat measurements would have to be made over a range of temperatures extending below $1^{\circ}K$.

PART TWO

HYPERFINE COUPLING IN FERROMAGNETIC MATERIALS

CHAPTER ONE

HYPERFINE COUPLING IN TRANSITION METALS

Introduction

The magnetic moment of a nucleus interacts with the spins and orbits of the surrounding electrons. In free atoms and ions the effect gives rise to hyperfine structure in optical spectra. In solids the interaction is also seen as hyperfine structure in the microwave absorption spectra of paramagnetic salts (see Bleaney and Stevens, 1953). This interaction may be described by the spin Hamiltonian $\mathcal{H} = AS_z I_z + B(S_x I_x + S_y I_y)$, of Abragam and Pryce (1951). S_x, S_y, S_z, denote the components of the effective electron spin, and I_x, I_y, I_z, denote the components of the nuclear spin. A and B are parameters describing the magnitude of the hyperfine splitting of the energy levels in a field of axial symmetry about the z-direction. In ferromagnetic materials however the hyperfine structure cannot be observed because the microwave resonance lines are too broad (see Bagguley and Owen, 1957), and other experimental methods have to be used. The ferromagnetic electrons produce an effective magnetic field H_{eff} at the nuclei usually of the order 10^2 to 10^3 kG. This field, which has an orienting effect on the nucleus, may be measured at low temperatures from the anisotropy

of gamma-ray emmission from aligned radioactive nuclei, and from a Schottky anomaly in the specific heat. The effective field H_{eff} may also be determined by nuclear resonance, and from Mössbauer experiments.

An account is given in this part of the thesis of some measurements of H_{eff} at the cobalt nuclei in iron-cobalt alloys determined from heat capacity measurements between $0.4^{\circ}K$ and $1.2^{\circ}K$. The experiments also give the contribution to the heat capacity due to the conduction electrons in these alloys, and from this an indication of the density of electronic states at the Fermi surface.

The transition metals

The electronic structure of the 3d-transition metals is not fully understood. A review of the existing theories has recently been published by Herring (1960). A brief summary will now be given of those ideas which are useful for understanding the results of the present experiments.

The free atoms of iron, cobalt, nickel, and copper each have an inner core of eighteen electrons in the closed-shell argon configuration. The outer electrons exist in 3d and 4s states.

	Fe	Co	Ni	Cu
Free atom	$(3d)^6(4s)^2$;	$(3d)^7(4s)^2$;	$(3d)^8(4s)^2$;	$(3d)^{10}(4s)^1$
Crystal structure	bcc	hcp	fcc	fcc

In the metallic crystals the eighteen inner electrons remain

in the argon configuration. The 4s electrons, which have well spread out wave functions and hence large interactions between neighbours, occupy a wide energy band. The 3d electrons are more localized near the nuclei and exist in a narrow band. The 4s and 3d bands overlap as sketched in fig.1. The 3d band holds ten electrons per atom, and the 4s band holds two electrons per atom. Hence the number of energy levels in the band per unit energy range is greater in the 3d band than in the 4s band. In these metals the density of states is a complicated function of energy. In the crystal the 4s electrons may be pictured as moving freely through the lattice as Bloch waves, while the 3d electrons are partly bound to individual nuclei and partly itinerant. The cohesion arises partly from the coulomb attraction of the lattice of positive ions to the common system of negative electrons, and partly from 3d bonding orbitals.

The origin of the positive exchange interaction which ferromagnetically couples the 3d-electron spins of neighbouring atoms in metallic iron, cobalt, and nickel is uncertain. Possible causes for such an exchange coupling are: the motion of electrons from one atom to another, direct exchange between the spins of neighbouring atom, or exchange via conduction electron polarization. The exchange interaction splits the 3d band into two sub-bands of opposite spin orientation, 3d $\uparrow$ and 3d $\downarrow$, separated in energy by the exchange

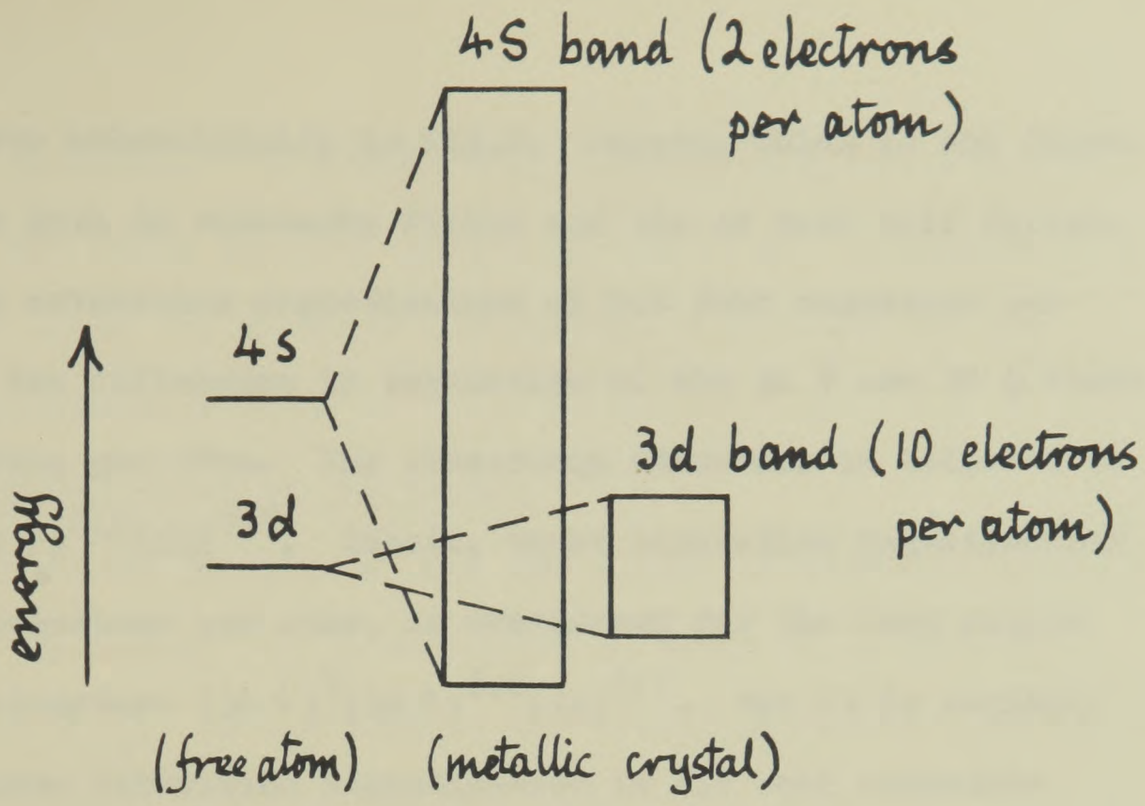

Figure 1 Sketch of the energy bands in transition metals.

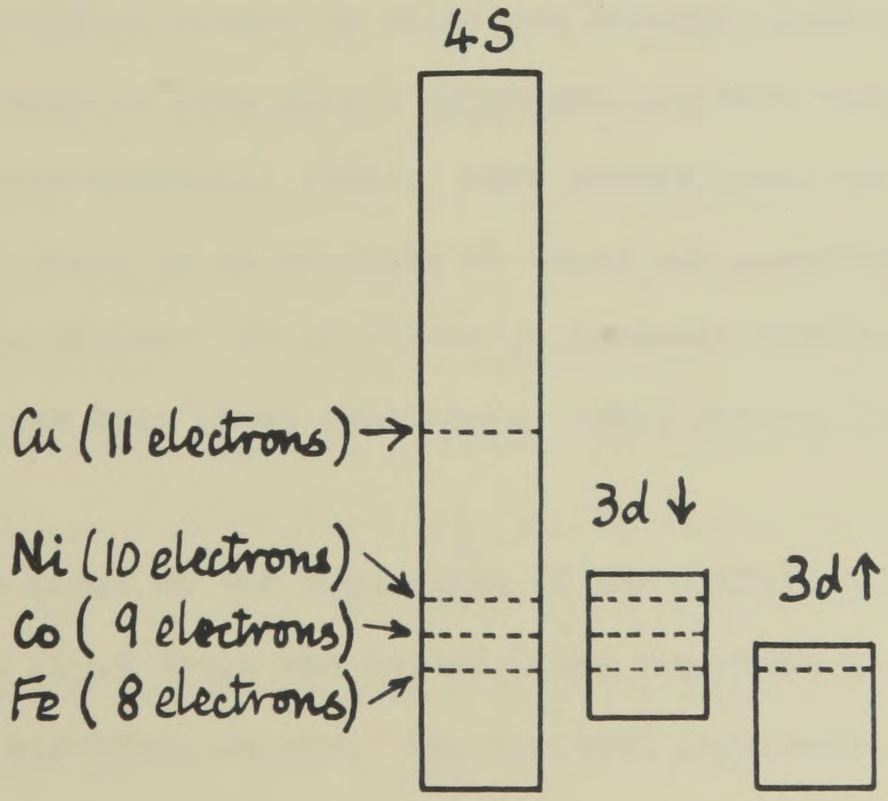

Figure 2 Sketch of band populations in transition metals.

energy as shown schematically is fig.2. Copper, which is not ferromagnetic, has both 3d sub-bands filled and the 4s band half filled. Nickel, has a saturation magnetization of 0.6 Bohr magnetons per atom. Hence the difference in population of the 3d ↑ and 3d ↓ bands is 0.6 electrons per atom. The electronic structure is believed to be $(3d\downarrow)^5(3d\uparrow)^{4.4}(4s)^{0.6}$. Cobalt, whose saturation magnetization is 1.7 Bohr magnetons per atom, is considered for the same reason to have the structure $(3d\downarrow)^5(3d\uparrow)^{3.3}(4s)^{0.7}$. But it is unlikely that iron, whose saturation magnetization is 2.2 Bohr magnetons per atom, has the structure $(3d\downarrow)^5(3d\uparrow)^{2.8}(4s)^{0.2}$. There are too few electrons in the 4s band for stable cohesion, and more probably neither of the two 3d sub-bands is completely full. X-ray studies of transition metals by Weiss and DeMarco (1958) gave rise to the theory that in iron only 2 electrons per atom occupied 3d states (Lomer and Marshall, 1958). More recent X-ray measurements have indicated that, to an accuracy of about one electron per atom, the number of electrons in 3d states in metallic iron is not different from that for free atoms (Batterman, 1959; Komura, Tomiie, and Nathans 1959).

The above ideas on the population of the different bands are illustrated in fig.2 where the dotted lines represent the Fermi levels of the different metals. The electron structures of alloys may be represented by Fermi levels intermediate between those for

the metallic elements. One should remember here that the relative positions of the bands and the density of states as a function of energy differ among the elements and alloys, especially for the different crystal structures.

Effective magnetic field at the nuclei

Marshall (1958) has proved that the effect of the ferromagnetic electrons at the nuclei may be described in terms of an effective magnetic field H_{eff}. He has studied the contributions to this field and his ideas may be recalled briefly here. The field at a nucleus is given by $H_{eff} = H_{loc} + H_c + H_a$, where H_{loc} is the local field, H_c is due to the 4s conduction electrons, and H_a is due to the localized electrons on the same atom.

The local field H_{loc} is the sum of the external field, the demagnetizing field, the Lorentz internal field, and a small additional internal field which vanishes for cubic structures and is negligible in hexagonal cobalt. The field H_c due to contact interaction with the 4s electrons is a positive contribution having two parts - that due to conduction electron polarization (which for cobalt Marshall estimated as roughly 40 kG), and that due to mixing of the 4s wave functions into the 3d band. The field H_a in cobalt was estimated by Marshall on the assumption that 70% of the atoms have a $(3d)^8$ ^3F configuration and 30% have a $(3d)^9$ ^2D configuration. This gives the correct saturation magnetisation of 1.7 Bohr magnetons per atom.

The hyperfine coupling for each configuration is described by the Abragam-pryce spin Hamiltonian (mentioned earlier), namely $\mathcal{H} = AS_z I_z$, where z is the direction of the ferromagnetic spins. The effective field H_a is given by $-A\bar{S}/g_N \beta_N$, where g_N is the nuclear g-factor and β_N is the nuclear magneton. H_a is the sum of four parts. The first part H_{a1} is a negative contribution due to the polarisation of the inner 3s and 2s electrons by the 3d electrons. This polarization, though slight, has an appreciable effect because of the large contact interaction of the s-electrons with the nucleus. Marshall gave for the free atom of cobalt $H_{a1} = -128$ kG which, though probably the same in the metal, might differ considerably from this value. The other three parts of H_a, which depend on the crystal symmetry, are the dipole-dipole magnetic interactions between nuclear and electron spins (H_{a2}), the magnetic interaction between the nucleus and the unquenched part of the orbital moment (H_{a3}), and the cross effect of the dipole-dipole nuclear-electron spin interaction and the spin-orbit coupling (H_{a4}). Marshall estimated that for cubic alloys H_{a2} (or more strictly the root mean square value of H_{a2}) is small, $H_{a3} \simeq 54$ kG, and H_{a4} is zero; while for hexagonal cobalt $H_{a2} \simeq 81$ kG, $H_{a3} \simeq 83$ kG, and H_{a4} is small.

EXPERIMENTAL DETERMINATIONS OF H_{eff}

Gamma-ray anisotropy

H_{eff} may be measured experimentally in cobalt metal and alloys by its orienting effect on the gamma-emitting Co^{60} nucleus (Alekseevsky, Shchegolev, and Zavaritsky; see Khutsishvili, 1956. Grace, Johnson, Kurti, Scurlock, and Taylor, 1955, 1959). A sample of the alloy to be studied with some of the Co^{59} nuclei replaced by Co^{60} is placed in a demagnetization cryostat in thermal contact with a paramagnetic salt, and is cooled to a temperature below $0.1^{\circ}K$. Then the ferromagnetic domains are made parallel by the application of a small magnetic field (~1 kG). Since the electron spins are parallel throughout a domain H_{eff} has the same direction for all the nuclei in the sample. At these temperatures kT is close to the energy separation between different orientations of the nuclei relative to H_{eff}, and partial nuclear polarization occurs. The nuclei reach thermal equilibrium with the surroundings in a short time via the interaction with the conduction electrons. The amount of polarization is determined from the anisotropy of the gamma-rays emitted from the Co^{60} nuclei. In practice the quantity

$$\epsilon = 1 - W(0)/W(\pi/2)$$

is measured, where $W(0)$ and $W(\pi/2)$ are the gamma-ray intensities parallel and perpendicular to the domain orientations. The effective field at the nucleus is then obtained when ϵ is not too large from

the expression

$$\epsilon = \text{Constant}\left(\frac{\mu_n H_{eff}}{I\,kT}\right)^2$$

where μ_n is the nuclear magnetic moment, I is the nuclear spin and the constant depends in a known way on the decay scheme. The above equation shows that the sign of H_{eff}, that is its direction relative to the domain magnetization, is not determined.

Heat capacity

There are two observable contributions to the heat capacity of iron-cobalt alloys in the temperature range $0.4^{\circ}K$ to $1.2^{\circ}K$ - the tail of the nuclear Schottky anomaly, and the heat capacity of the conduction electrons. The lattice and spin-wave contributions are negligible. The spin-wave contribution is given for body-centred cubic ferromagnets, as used in the experiments described later, by the expression

$$C = \frac{0.113}{2} Nk\left(\frac{kT}{2JS}\right)^{3/2},$$

where J is the exchange energy and S is the spin (see for example: Van Kranendonk and Van Vleck, 1958). By substituting J = 205k (see Kittel, Solid State Physics, 2nd Ed. p. 407) and S = 1 for iron we obtain $C/R \simeq 0.56T^{3/2}$ millijoules mol^{-1} deg^{-1}. This is small compared with the other contributions below $1^{\circ}K$ as the results given later show.

The Schottky anomaly is caused by the low temperature orientation of the nuclear spins in the magnetic field H_{eff}. Nuclei of spin I in the field have 2I + 1 orientations separated in energy by $g_N \beta_N H_{eff}$, where g_N is the nuclear g-factor, and β_N is the nuclear magneton. The maximum in the heat capacity occurs when $kT \sim g_N \beta_N H_{eff}$. When kT is large compared with $g_N \beta_N H_{eff}$ the tail of the anomaly is given by

$$\frac{C}{R} = \frac{1}{3} I(I+1)\left(\frac{g_N \beta_N H_{eff}}{kT}\right)^2 + O\left(\frac{g_N \beta_N H_{eff}}{kT}\right)^4 + \cdots$$

or

$$\frac{C}{R} = \frac{(I+1)}{3I}\left(\frac{\mu_n H_{eff}}{kT}\right)^2 = \frac{\alpha}{T^2}$$

since $\mu_n = g_N I \beta_N$, where μ_n is the nuclear magnetic moment. These expressions may easily be verified for high temperatures by substituting the 2I + 1 energy levels into the following expression for the specific heat derived from the partition function.

$$\frac{C}{R} = \frac{\sum_i \left(\frac{E_i}{kT}\right)^2 e^{-E_i/kT}}{\sum_i e^{-E_i/kT}} - \left(\frac{\sum_i \left(\frac{E_i}{kT}\right) e^{-E_i/kT}}{\sum_i e^{-E_i/kT}}\right)^2 .$$

Like the gamma-ray anisotropy experiments, the heat capacity measurements do not give the sign of H_{eff}.

Early measurements of the low temperature heat capacity showed that $H_{eff} \simeq 200$ kG in cobalt metal (Heer and Erickson, 1957; and Arp, Kurti, and Petersen, 1957). Since the Co^{59} nucleus has a spin of 7/2 and a magnetic moment μ_n of 4.583 nuclear magnetons (Freeman,

Murray, and Richards, 1957) we see from the above expressions for the heat capacity that the maximum in the anomaly occurs at $\sim 10^{-2}\ ^{\circ}K$ and the contribution from $0.4^{\circ}K$ to $1.2^{\circ}K$ is given approximately by $C \simeq 5\ T^{-2}$ millijoules $mol^{-1}\ deg^{-1}$. Similar results have been obtained in the present work at these temperatures for the iron-cobalt alloys as given in detail later.

The heat capacity of the conduction electrons, which is proportional to T at low temperatures, is given by $C = \frac{1}{3}\pi^2 k^2 N(E_F)T = \gamma T$, if $kT \ll E_F$, where E_F is the Fermi energy, and $N(E_F)$ is the number of electronic states per unit energy range at the Fermi surface. The known values of γ for iron, cobalt, nickel, and copper are as follows -

Fe	Co	Ni	Cu	
5.0	5.0	7.3	0.74	millijoules $mol^{-1}\ deg^{-2}$.

They are consistent with the ideas mentioned earlier that for copper the Fermi surface lies above the 3d band in the 4s band where there is a low density of states, while for iron, cobalt, and nickel the Fermi surface lies in the 3d band where the density of states is high. Determinations of the electronic heat capacity for a series of alloys having the same crystal structure give the density of states at the Fermi surface $N(E_F)$ as a function of outer electron concentration (see Cheng, Wei, and Beck, 1960 for the bcc alloys of 3d transition elements).

To make heat capacity measurements below $1^{\circ}K$ a sample of the metal or alloy bearing an electrical resistance heater, a carbon thermometer, and a crystal of cerium magnesium nitrate, is placed in a demagnetization cryostat. It is cooled below $1^{\circ}K$ by an adiabatic demagnetization of the cerium magnesium nitrate. This is a good coolant because it has a sufficiently large entropy of magnetization to cool the sample, while having a negligible heat capacity from $0.3^{\circ}K$ to $1^{\circ}K$. The heat capacity is found by introducing heat electrically in steps and noting the temperature rise each step on the carbon thermometer.

The total heat capacity in the temperature range of the measurements has the form $C = \frac{\alpha}{T^2} + \gamma T$, where α/T^2 is due to the hyperfine coupling and γT is due to the conduction electrons. The values of α and γ are found from the straight line obtained by plotting CT^2 as a function of T^3. The effective field at the cobalt nuclei H_{eff} and the density of electronic states at the Fermi surface $N(E_F)$ may then be calculated.

Nuclear resonance

In ferromagnetic metals, since the paramagnetic resonance line widths are large and the radio-frequency penetration is low, one expects only a very small nuclear resonance absorption. Gossard and Portis (1959) have however reported a strong nuclear resonance in cobalt at room temperature. The absorption is probably enhanced

by domain oscillations following the r.f. field. The value of H_{eff} obtained was close to that found in gamma-ray anisotropy and in heat capacity experiments. But similar results have not been obtained for the whole series of iron-cobalt alloys. The nuclear resonance method provides the most accurate determinations of H_{eff} when it can be used.

Mössbauer experiments

Mössbauer (1958) discovered that nuclear resonance absorption of gamma-rays may take place in crystalline solids. The nuclei are strongly bound to the crystal lattice, and virtually no energy is lost by recoil in the emitting and absorbing processes. The lines are so sharp ($\Delta E \sim \mu$ eV, $E \sim$ keV) that if a relative velocity of a few cm/sec exists between the source and absorber, the Doppler shift modifies or destroys the resonance. The line shape may be studied experimentally as a function of the relative velocity. This method has been used to measure the value of H_{eff} at Fe^{57} nuclei in ferromagnetic iron by the nuclear Zeeman effect. A special feature of this type of experiment is that the sign of H_{eff} may be determined.

Some results for iron-cobalt alloys

The measurements of H_{eff} at the cobalt nuclei in iron-cobalt alloys prior to the present experiments must be outlined to explain the reasons for the present experiments.

Measurements were made at Oxford by Baldock, Scurlock, and Sowter of H_{eff} in iron-cobalt alloys by the gamma-ray anisotropy method (private communication). Their results are plotted on the diagram in fig.3. They indicate that the value of H_{eff} is constant in the bcc alloys and probably changes at the boundary between the bcc and fcc structures, a result suggested by the theory of Mott and Stevens (1957). Fig.3 also shows values of H_{eff} obtained at Berkeley by Arp, Edmonds, and Petersen (1959) from low temperature heat capacity measurements. These results were kindly sent to Oxford by Arp before publication. Unlike the Oxford results, they suggest that the value of H_{eff} is a linear function of alloy composition. The 30% Fe - 70% Co alloy used at Oxford was in the disordered state, while the 59% Co - 41% Fe alloy used at Berkeley was believed to be in the ordered state.

The heat capacity measurements described in this thesis were made initially to examine the large discrepancy between the Oxford and Berkeley results for alloys in the middle of the range of compositions, and to find out whether or not the value of H_{eff} in an iron-cobalt sample depends strongly on the degree of order. A disordered 47.5% Co - 52.5% Fe sample was kindly prepared at Harwell by Mr. A.E. LeClaire. The value of H_{eff} for this sample was determined from the heat capacity measurements. The sample was then annealed at Harwell, and H_{eff} was determined for the ordered state. The

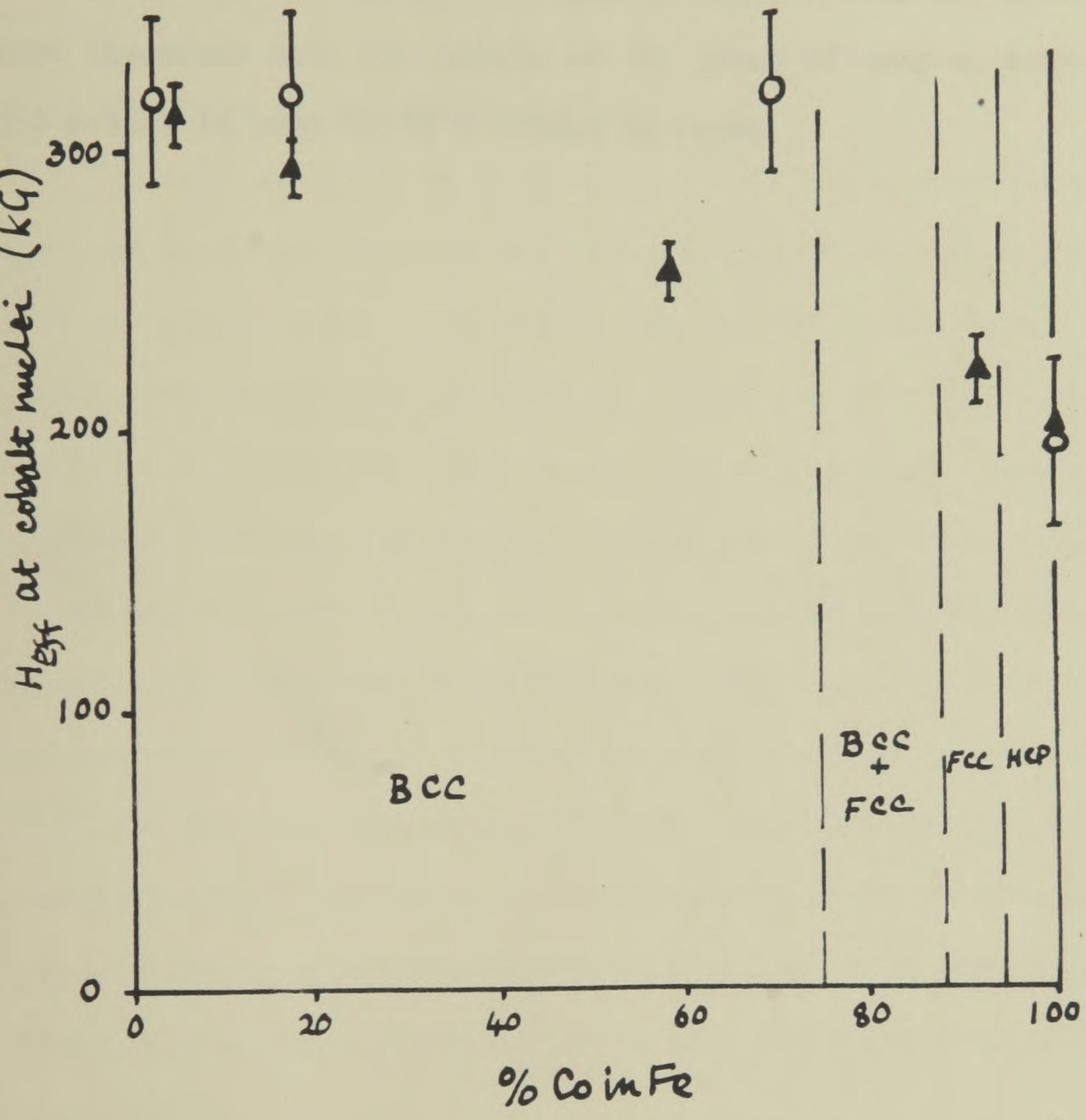

Figure 3 Values of H_{eff} at the Co nuclei in Fe-Co alloys.

o Oxford nuclear orientation results.

▲ Berkeley heat capacity results.

same value of H_{eff} (293 kG) was found in both cases. This is lower than what one would expect from the Oxford results, and higher than what one would expect from the Berkeley results. Further measurements were therefore made for alloys in the range of compositions from 30% cobalt in iron to 70 % cobalt in iron.

CHAPTER TWO

APPARATUS AND ASSEMBLY OF SAMPLES

A modification to the vacuum jacket

The same cryostat as that described in Part One was used for the heat capacity measurements. Eight electrical connections leading into the vacuum space were needed for accurate measurements on the carbon thermometer and the heater. A new cap was therefore made for the bottom of the vacuum case. Two copper-glass seals, each with four platinum leads taken through the glass, were soldered to the cap as shown in fig.4. Bismuth-cadmium solder was used between the copper and the brass cap. This alloy is non-superconducting above 0.8°K and it melts at 140°C. A superconducting solder would prevent one from using this cap for experiments in which susceptibility measurements on paramagnetic salts are made. Hard solder which is non-superconducting could not used because the temperature needed to melt it would have destroyed the seals.

Cooling salt

Most of the alloy samples used weighed about 15 gm. The approximate contributions to the heat capacity of a 15 gm sample of 50 % Fe - 50% Co alloy are shown in fig.5. The electronic heat capacity and the hyperfine Schottky anomaly are the only appreciable

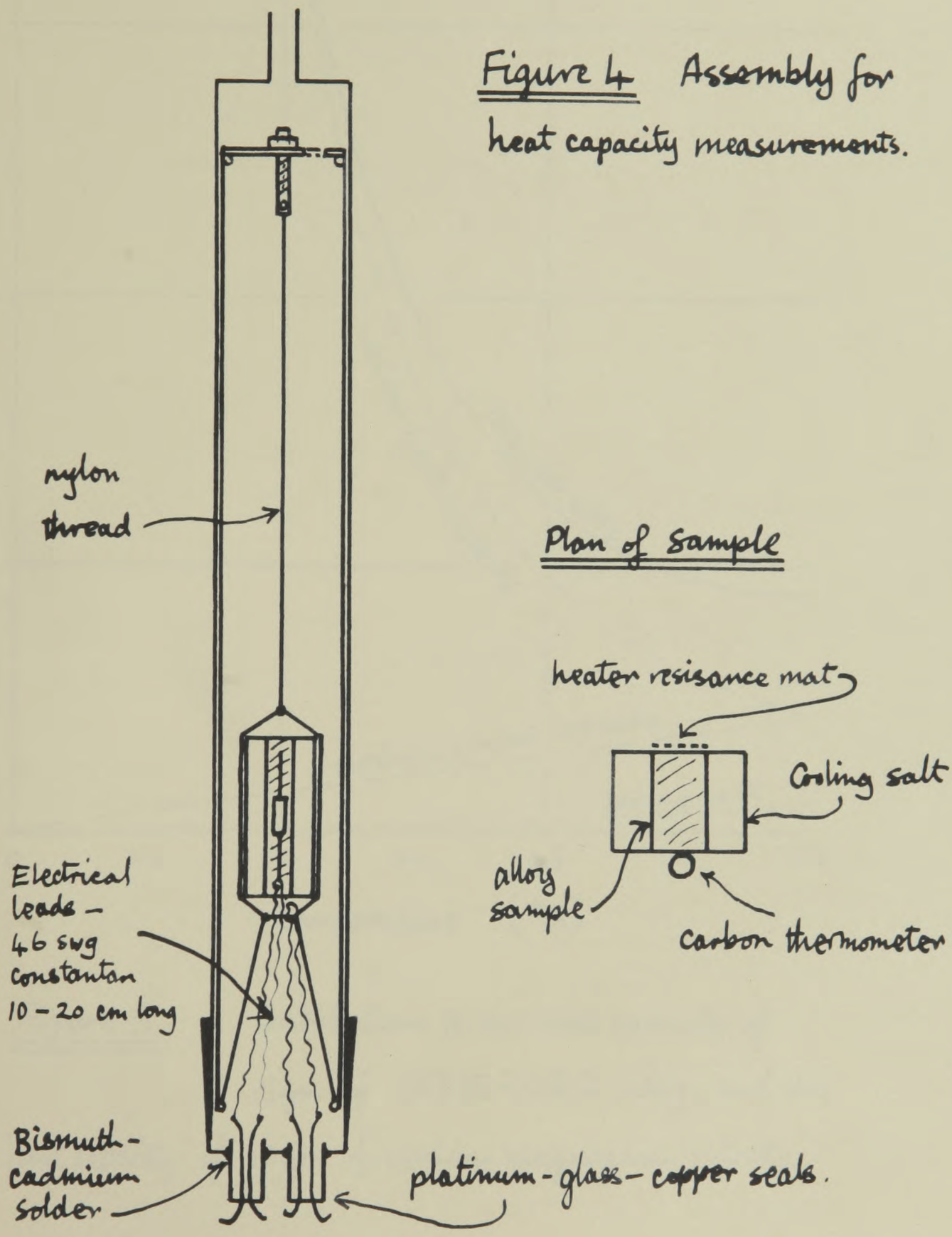

Figure 4 Assembly for heat capacity measurements.

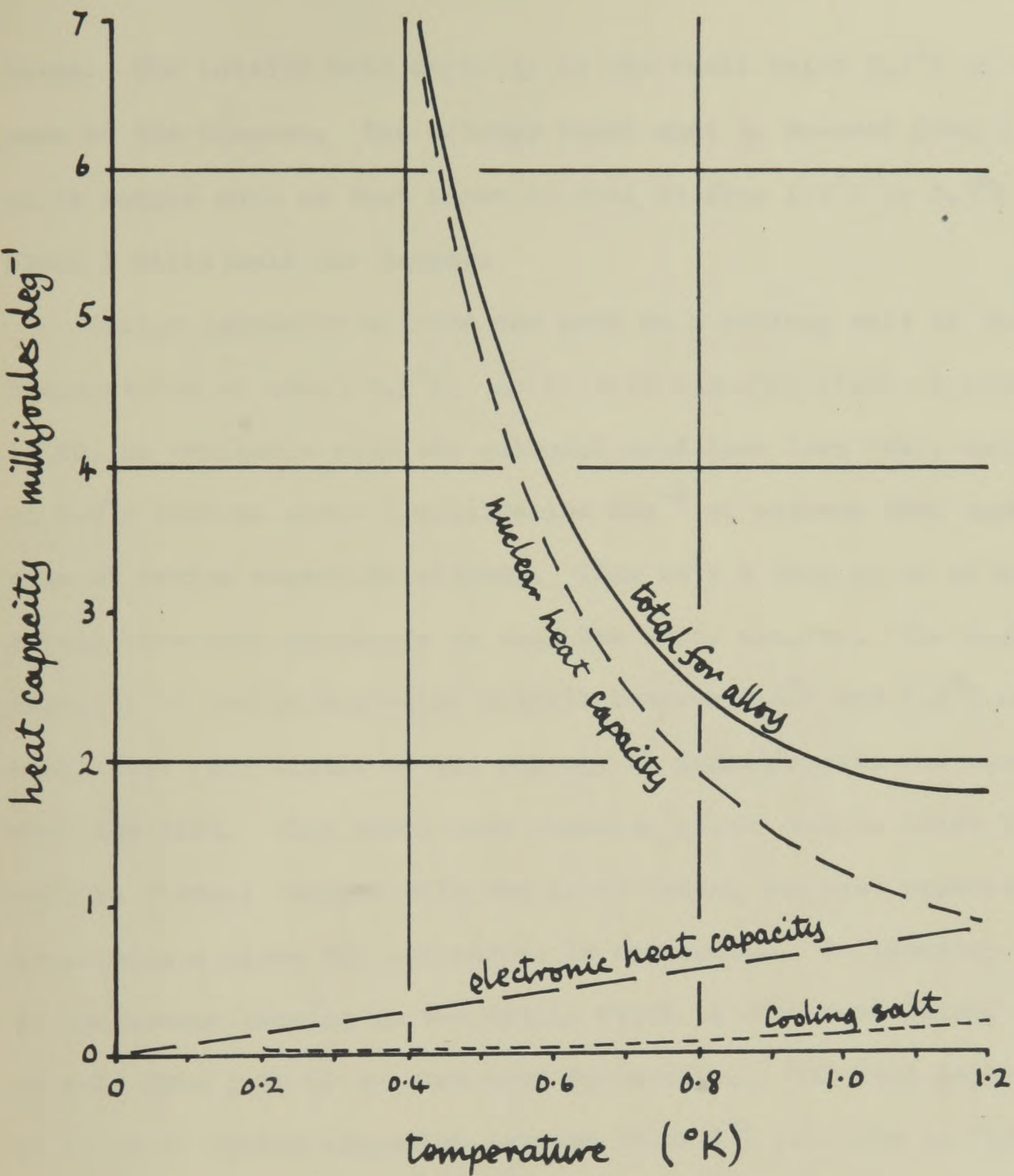

Figure 5 Contributions to the heat capacity of 15gm of 50% Fe-50% Co alloy, and the heat capacity of 10gm of cerium magnesium nitrate.

terms. The lattice heat capacity is too small below 1.2°K to be seen on the diagram. The entropy which must be removed from a 15 gm alloy sample such as that shown to cool it from 1.2°K to 0.3°K is about 1 millijoule per degree.

Cerium magnesium nitrate was used as a cooling salt to reach temperatures of about 0.3°K. An initial magnetic field of about 13 kG, as available with the solenoid used (see Part One), applied at 1.2°K removes about 5 millijoules deg^{-1} of entropy from each gram of cerium magnesium nitrate. Thus only a gram or so of salt should have been necessary to cool the alloy samples. The heat capacity of cerium magnesium nitrate between 0.2°K and 1.2°K is so small that very little of the entropy of magnetization was used to cool the salt. This small heat capacity allows one to leave the salt in thermal contact with the alloy during the heat capacity measurements since the correction is negligible. In practice owing to hysteresis heating in the metal, which is discussed later, amounts of salt from 4 to 10 gm were used for cooling. The heat capacity of 10 gm of cerium magnesium nitrate below 1°K is shown in fig.5. Since the cerium magnesium nitrate has marked magnetic anisotropy it was not used in the powdered form. Single crystals up to 5 cm across were grown from solution, cut with a fretsaw and shaped with sandpaper. A sketch of the crystal shape is shown in fig.6(a), and the splitting factors $g_{\parallel}$ and $g_{\perp}$ are indicated. Diagram 6(b)

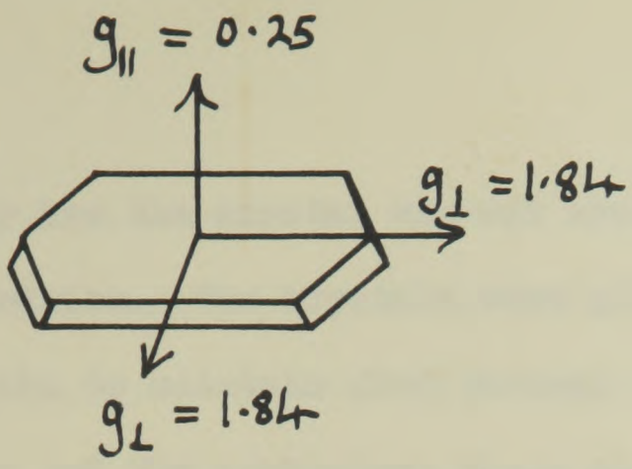

Figure 6(a) cerium magnesium nitrate.

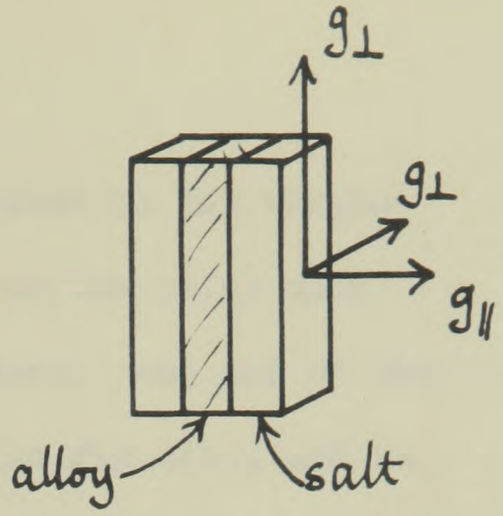

Figure 6(b)

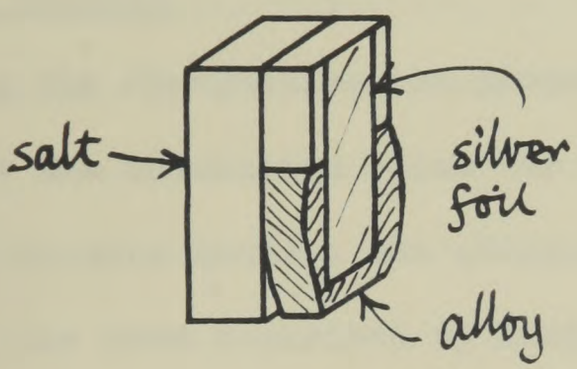

Figure 6(c)

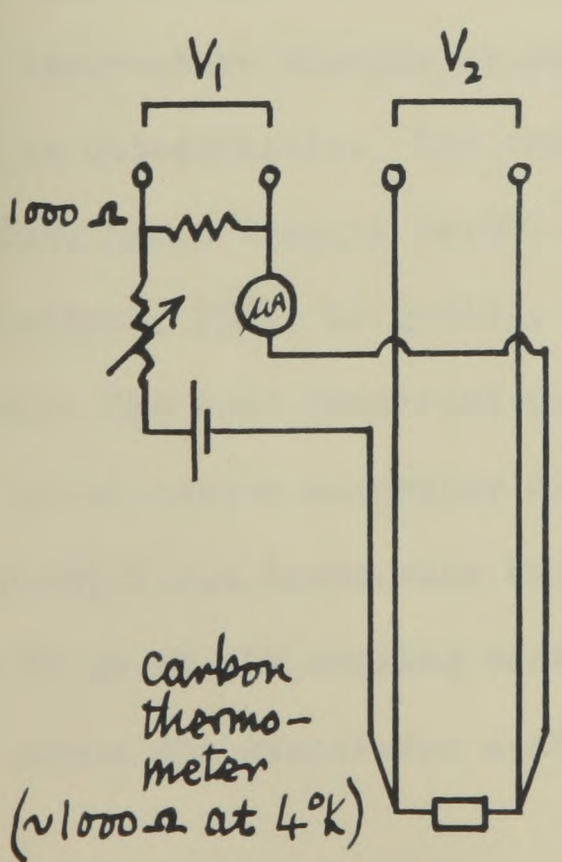

Figure 7(a)

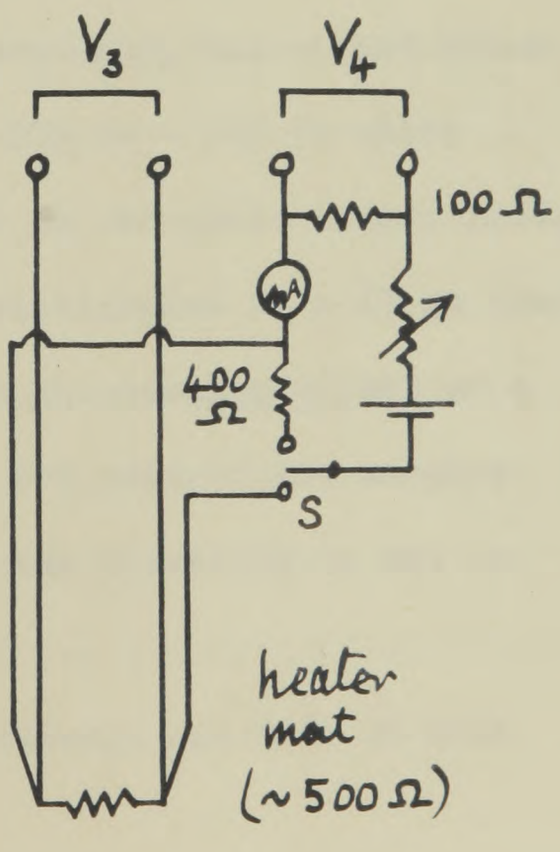

Figure 7(b)

shows clearly how the crystal was cut and mounted on the sample to make a sandwich. The crystals were glued to the alloy with GE 7031 varnish to maintain good thermal contact. Not all of the alloy samples had the convenient shape shown in fig.6(b), and in these cases the arrangement was modified. Sometimes thin silver foil (of negligible heat capacity below 1°K) was used to improve thermal contact between the salt and alloy sample as shown in fig.6(c).

Hysteresis heating

During the demagnetization process, when the applied field falls below the saturation value for the ferromagnetic alloys, hysteresis heating hinders the attainment of very low temperatures. The effect has been described by Kurti and Safrata (1958). It was observed in the present experiments in field strengths below about 1 kG. Although the hysteresis loss in a single cycle produces negligible temperature changes at room temperatures, the effect below 1°K may be catastrophic. For example, a 50% Fe - 50% Co alloy (Permendur) has a loss of 12,000 ergs per cc per cycle (Amer. Inst. Phys. Handbook, 1957, p. 5-216), or 2.4 millijoules in a 15 gm sample. In practice the heat developed may offset the cooling effect of a gram or so of cerium magnesium nitrate. For some of the samples which showed large hysteresis heating it was necessary to use as much as 10 gm of the cooling salt.

To avoid the hysteresis heating an attempt was made to make

heat capacity measurements in residual fields of from $1\frac{1}{2}$ to $2\frac{1}{2}$ kG. This practice was abandoned for several reasons. The heat capacity of the cerium nitrate was no longer negligible in the magnetic field; the effect of the field on the carbon thermometer below $1^{\circ}K$ was unknown; and ripple in the supply to the solenoid caused additional heating in the sample.

Carbon thermometer

For a carbon resistance thermometer a $\frac{1}{2}$ watt Old Speer 470 ohm resistor similar to that mentioned in Part One was used. Most of the outside coating was carefully ground away. Silver foil was wrapped round the resistor and glued on with GE 7031 varnish. The foil was glued to the alloy sample as shown in fig.4. The resistance of the thermometer was determined by current and voltage measurements with the circuit shown in fig.7(a). The voltages V_1 and V_2 were measured with a Tinsley potentiometer and a sensitive galvanometer. Since the resistance of R_1 ($\simeq 2\ M\Omega$) was large compared with that of the carbon thermometer ($\sim 1000\Omega$ at $3^{\circ}K$ and $\sim 4000\Omega$ at $0.3^{\circ}K$) the measuring current of $0.8\ \mu A$ was practically constant throughout each experiment, while the voltage V_2 across the resistor indicated the temperature of the sample. The carbon thermometer was calibrated for each experimental run against the helium vapour pressure scale (T_{55E}) at four or five points between $4^{\circ}K$ and $1.2^{\circ}K$, and the following calibration formula was used -

$$T = A\log_{10}R/(\log_{10}R - B)^2,$$

where R is the resistance of the carbon thermometer at the temperature T, and A and B are constants. A and B were found from the straight line obtained by plotting log R against $\sqrt{\log R/T}$. The two constants were observed to vary by a few percents between experimental runs. The calibration formula was then used at temperatures between $1^{\circ}K$ and $0.4^{\circ}K$ where most of the heat capacity measurements were made. A separate experiment was made to examine the validity of this step, and small corrections to the values of A and B were found for use at the lower temperatures.

To calibrate the carbon thermometer below $1^{\circ}K$ it was thermally attached to an elipsoidal pill of chrome methylammonium alum as shown in fig.8. The magnetic temperature T* of the chrome methylammonium alum pill, and the resistance of the carbon thermometer were both calibrated against the helium vapour pressure scale between $4^{\circ}K$ and $1.2^{\circ}K$. The assembly was then cooled to a number of different temperatures between $0.9^{\circ}K$ and $0.3^{\circ}K$ by adiabatic demagnetization. At each temperature the resistance of the carbon thermometer and the value of T* was noted. The absolute temperature T was obtained from the known T - T* relation for chrome methylammonium alum (Ambler and Hudson, 1957). The results of one experiment are shown in fig.(9 where the resistance of the thermometer is plotted as a function of absolute temperature. These measurements may be compared with

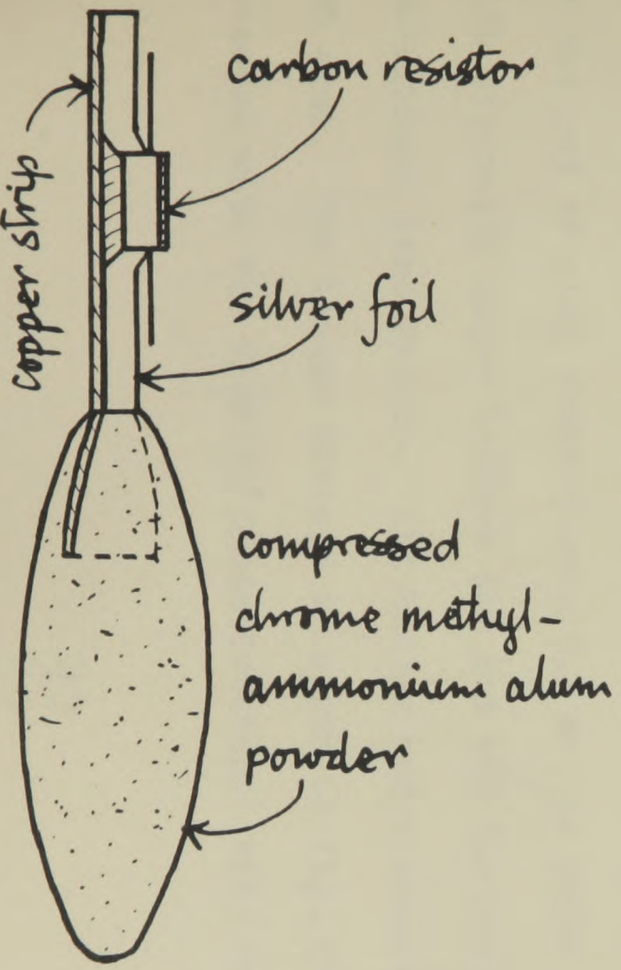

Figure 8

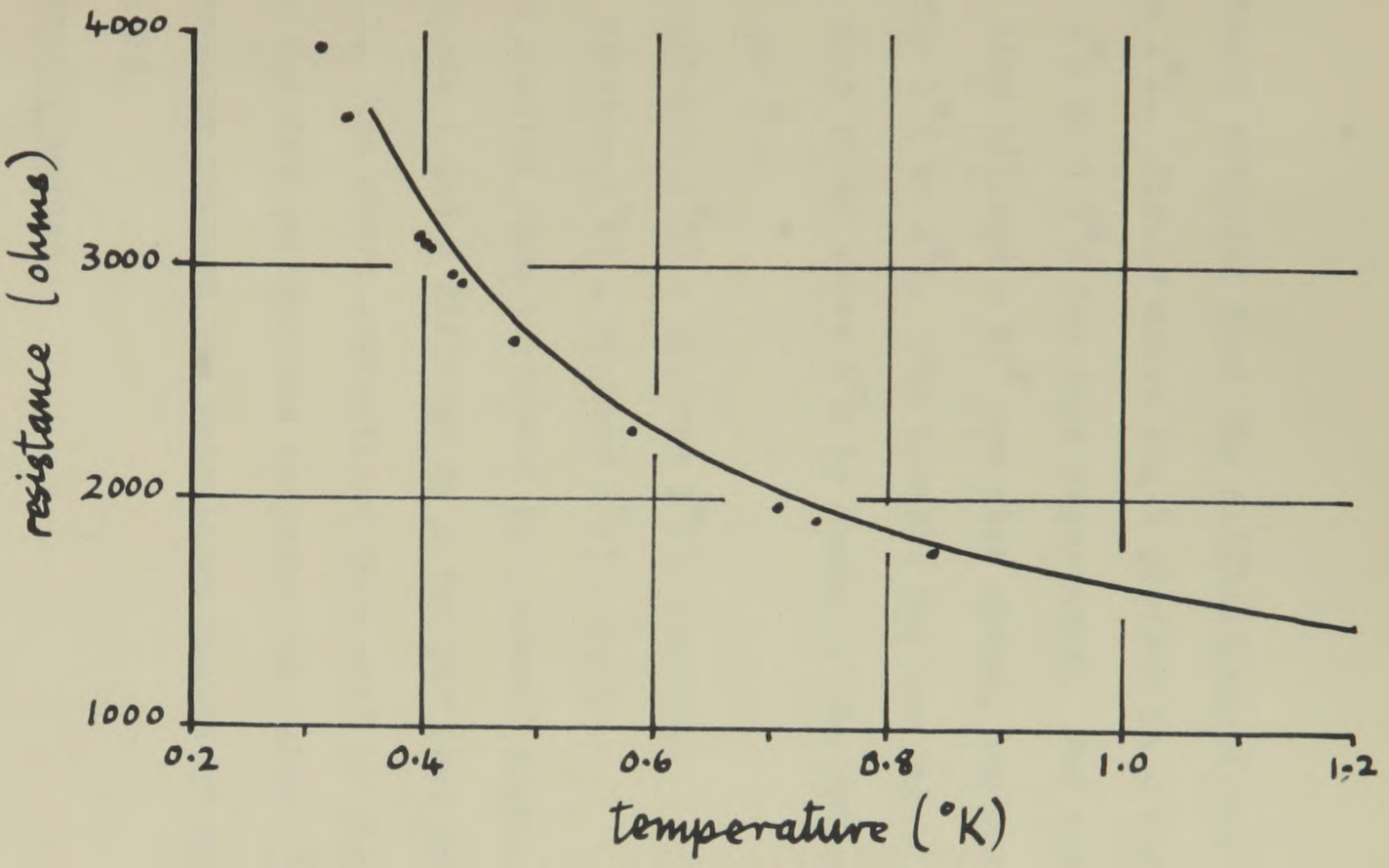

Figure 9 Carbon thermometer calibration below 1°K.
—— extrapolation of curve
obtained between 1·2°K
and 4°K.

the curve obtained from the calibration of the carbon resistor above 1°K. Fig.10 shows log R plotted as a function of $\sqrt{\log R/T}$ from 4°K to 0.3°K for this experiment. Two calibration formulae $T = A \log R/(\log R - B)^2$ are also shown, one for 0.5°K to 1°K and one for 1°K to 4°K. The formula for use below 1°K could be obtained from that found above 1°K by means of the following corrections to A and B -

A(below 1°K) = A(above 1°K) - 0.0049;

B(below 1°K) = B(above 1°K) + 0.014.

These results were confirmed in a second experiment, in which the constants A and B differed by a few per cent from those shown in fig.10. The above corrections were used in the heat capacity experiments for determining the temperatures below 1°K. The use of these corrections reduced the calculated values of the heat capacity by about 1%.

Electrical heater

The electrical heater was made of "Silko" constantan resistance mat (manufactured by the CIBA Company, Basle, Switzerland). A strip of the mat of size about 3 cm x 0.3 cm was glued to the alloy sample with cigarette paper between the mat and the sample for electrical insulation (see fig.4). The heater had a resistance of about 500 ohms. The heater circuit is shown in fig. 7(b); V_3 and V_4 were measured with the Tinsley potentiometer. With this circuit accurate

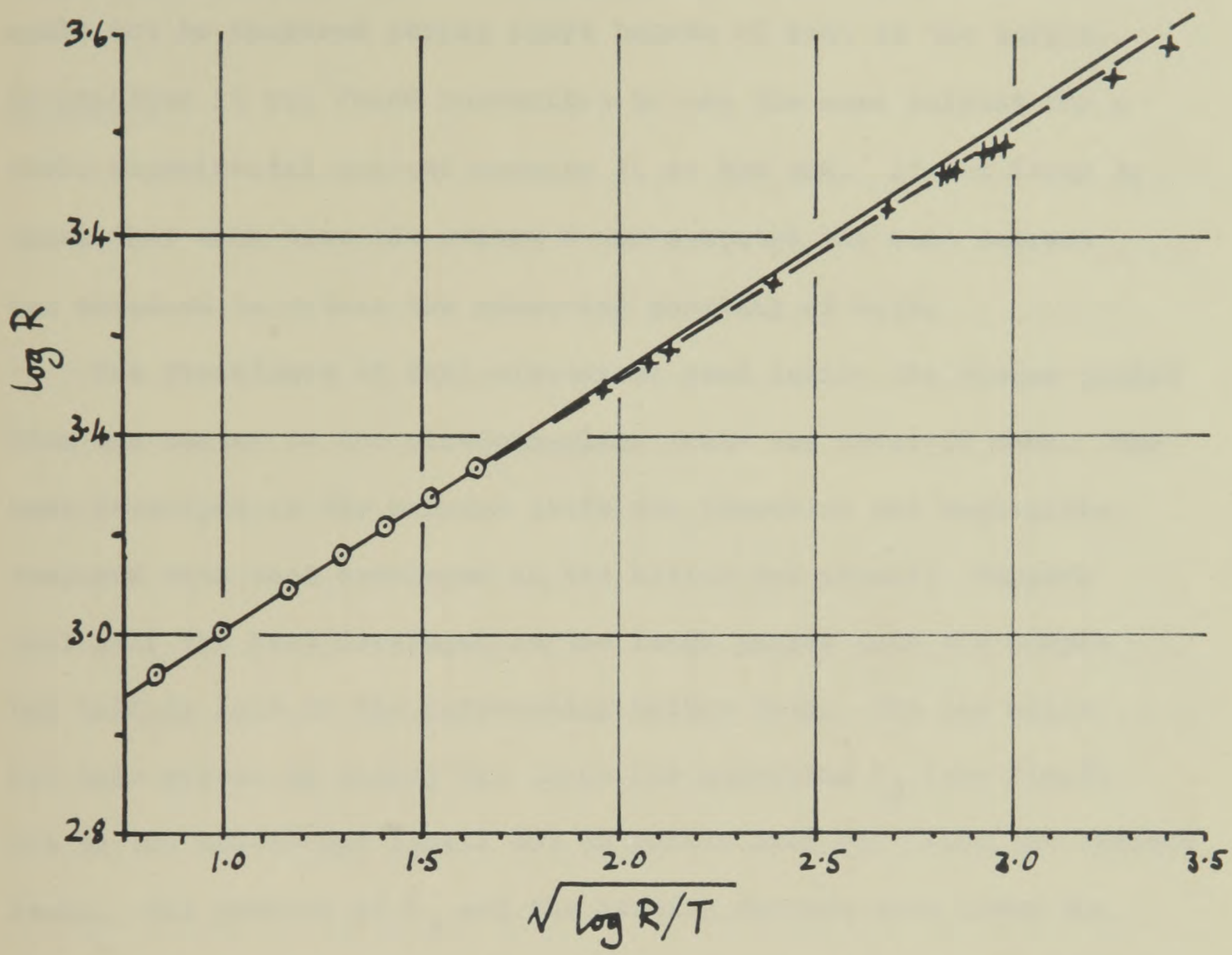

Figure 10 Carbon thermometer calibration.

From 4°K to 1°K $$T = \frac{0.0673 \log R}{(\log R - 2.743)^2}$$

From 1°K to 0.4°K $$T = \frac{\overset{0.0624}{\cancel{0.0674}} \log R}{(\log R - 2.757)^2}$$

values were obtained for the heater current from V_4, which, however, could not be measured during short bursts of heat to the sample. In practice it was found convenient to use the same current for a whole experimental run and measure it at the end. It was found by trial that each time the switch S was operated the same current was obtained to within the measuring accuracy of 0.1%.

The resistance of each electrical lead inside the vacuum jacket from the heater to the platinum-glass seals was about 20 ohms. The heat developed in the current leads was therefore not negligible compared with that developed in the heater mat itself. Suppose that half the heat developed in the leads passes into the sample and half is lost to the surrounding helium bath. One may allow for this effect by taking the leads for measuring V_3 (see fig.7) not to the heater mat itself but to points half way along the current leads. The product of V_3 and the heating current then gives the correct heating power for the sample. This device was used in the present experiments. Logan, Clement, and Jeffers (1957) have discussed this point and described a similar arrangement. The voltage leads in their experiments were connected so as to measure the potential across the heater and that part of one current lead which was inside the evacuated jacket.

EXPERIMENTS

Procedure

We shall now outline the procedure followed during the experiments. The carbon thermometer was first calibrated from $4^{\circ}K$ to $1.2^{\circ}K$ against the helium vapour pressure scale as already described. A magnetic field of about 12 kG was then applied to the cooling salt and alloy sample at $1.15^{\circ}K$ (the lowest temperature of the helium bath). When equilibrium between the sample and the helium bath had been reached the exchange gas maintaining thermal contact between the sample and the helium bath was pumped away. After about ten minutes' pumping the temperature of the sample was observed in most of the experiments to rise slowly above $1.15^{\circ}K$. This was attributed to eddy current heating in the sample caused by ripple in the solenoid power supply. An unsuccessful attempt was made to cure the trouble by shielding the sample with a copper cylinder placed in the hydrogen bath. It was found practicable however to cool the assembly below $1^{\circ}K$ by adiabatic demagnetisation after pumping out exchange gas for about fifteen minutes. In this apparatus half an hour's pumping is needed to get the best thermal insulation at low temperatures. In these experiments fifteen minutes' pumping provided satisfactory insulation, while not allowing the sample to reach temperatures much above $1.2^{\circ}K$ before demagnetization.

During the demagnetization the cooling of the sample was watched on the carbon thermometer. The magnetic field was reduced sufficiently slowly for the alloy sample and the cooling salt to remain in equilibrium with each other. The process took about ten minutes. The lowest temperature reached in a field of about 1 kG was usually about $0.2^{\circ}K$. As the field was reduced further the hysteresis heating, already discussed, caused the temperature of the sample to rise to about $0.4^{\circ}K$. Very slow and careful reduction of the field was necessary at this stage, since any sudden change would cause the sample to warm up appreciably, even to temperatures above $1^{\circ}K$. It should be noted that the figures given here are those for a typical case, and were found to vary from one sample to another.

The heat capacity C of the sample was then found from $0.4^{\circ}K$ to $1.2^{\circ}K$ in the usual way by electrical heating in steps from the formula $C = \Delta Q / \Delta T$, where ΔT is the temperature rise produced by the addition of a quantity of heat ΔQ. The value of V_2 (see fig.7) was read every 30 seconds to find the temperature drift rate. The heater was then switched on for a known time (usually 60 or 120 seconds) and after the heat had been switched off the readings of V_2 were resumed. The quantity of heat ΔQ was so chosen that the temperature rise ΔT was about $0.05^{\circ}K$, a value which could be determined with sufficient accuracy while not being to large. At the end of the run the carbon thermometer current, the heater voltage, and the heater

current were determined by measuring V_1, V_3, and V_4 respectively. The sample was then cooled again to 0.4°K and more heat capacity measurements were made. In many of the experiments the sample was cooled five or six times to make enough measurements.

Calculation of results

The standard method for calculating the heat capacity from the readings when the rate of change of temperature due to heat leaks is small compared with that due to the electrical heating is as follows. The temperature T of the sample is plotted as a function of time for the periods before, during, and after the introduction of heat. The drift lines before and after the heating are then extrapolated to the centre of the heating period. The difference in temperature $T_2 - T_1$, between the drift lines at this time gives the temperature rise ΔT of the sample caused by the known heat Δq, while the average $\frac{1}{2}(T_1 + T_2)$ gives the temperature of the heat capacity measurement.

In the present experiments this method was followed with one exception. V_2, the potential across the carbon thermometer, was plotted in place of the temperature as a function of time. The values of V_2 on the extrapolated drift lines at the centre of the heating period were then used to obtain T_1 and T_2 from the thermometer calibration formula $T = A\log R/(\log R - B)^2$. This procedure avoided the necessity of calculating the temperature for every reading in the

whole mass of data taken down. Fig.11 shows as a typical example the data for one of the heat capacity measurements.

As already explained the heat capacity of each sample between 0.4°K and 1°K was fitted to a formula of the type $C = \alpha/T^2 + \gamma T$ by plotting CT^2 as a function of T^3. The effective magnetic field H_{eff} at the cobalt nuclei was obtained from the value of α as explained in Chapter One. The iron makes no contribution to this nuclear term because the naturally occuring isotope Fe^{56} has no magnetic moment. For the cobalt nucleus

$$H_{eff} = \frac{k}{\mu_n}\sqrt{\frac{3I\alpha}{I+1}},$$

where k is Boltzman's constant, μ_n is the magnetic moment of the Co^{59} nucleus = 4.583 nuclear magnetons (Freeman, Murray, and Richards, 1957), I is the nuclear spin quantum number = 7/2, and α is the experimentally measured value of CT^2 per gram atom of cobalt. If α is expressed in units of millijoules deg.gm-atom^{-1} of cobalt this formula takes the practical form

$$H_{eff} = \sqrt{\alpha \times 10^6} \quad kG,$$

which was used for calculating the effective field in each experiment.

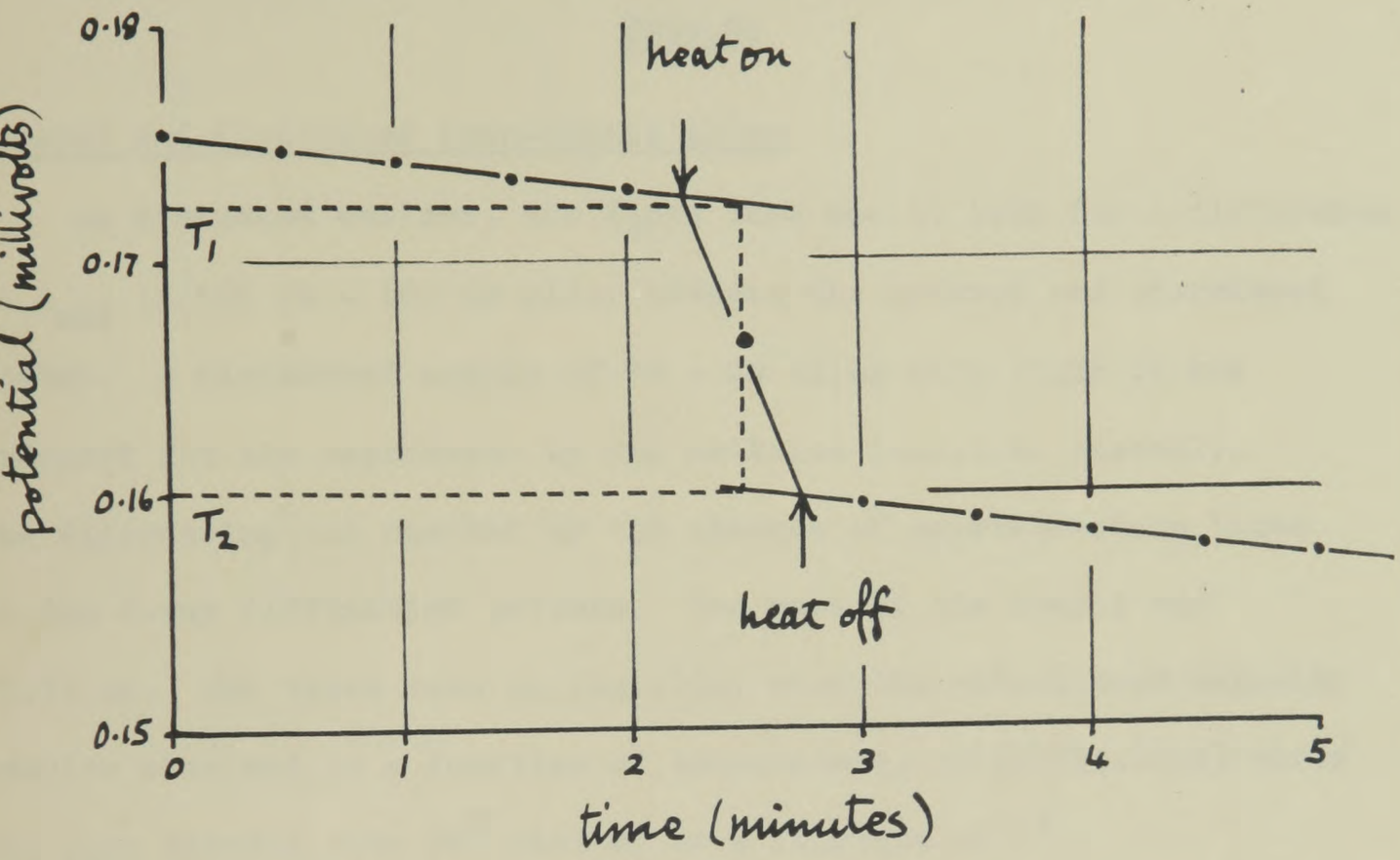

Data: 14·053 gm of 30% Co – 70% Fe alloy

heating power: 0.453×10^{-5} watts

$T_1 = 0.541\,^{\circ}K$ $T_2 = 0.598\,^{\circ}K$

heat capacity = 2·38 millijoules.deg^{-1}

Figure 11 A typical heat capacity measurement.

CHAPTER THREE

RESULTS

Ordered and disordered iron-cobalt alloy

As discussed earlier, the first task was to look for a difference in H_{eff} in 50% Fe - 50% Co alloy between the ordered and disordered states. A disordered sample of Fe - Co alloy with 47.5% Co was prepared for the experiment by Mr. LeClaire (A.E.R.E. Harwell). The disordering was checked by the absence of superstructure lines in the X-ray diffraction pattern. The mass of the sample was 15.72 gm. The black dots in fig.12(a) show the actual heat capacity results obtained as a function of temperature, while fig.12(b) shows the same results with CT^2 plotted as a function of T^3.

When these measurements had been made the sample was brought into the ordered state by Mr. LeClaire by cooling it slowly (15 deg/hr) from a temperature above the order-disorder transition (730°C). The ordering was checked by X-ray diffraction. The specific heat measurements were then repeated. The results are shown by the open circles in figures 12(a) and 12(b). The heat capacity C of the sample in both the disordered and in the ordered states may be represented from 0.5°K to 1°K by the equation

$$C = \frac{4.08(\pm 0.22)}{T^2} + 2.19(\pm 0.26)T, \text{ millijoules.mol}^{-1}.\text{deg}^{-1},$$

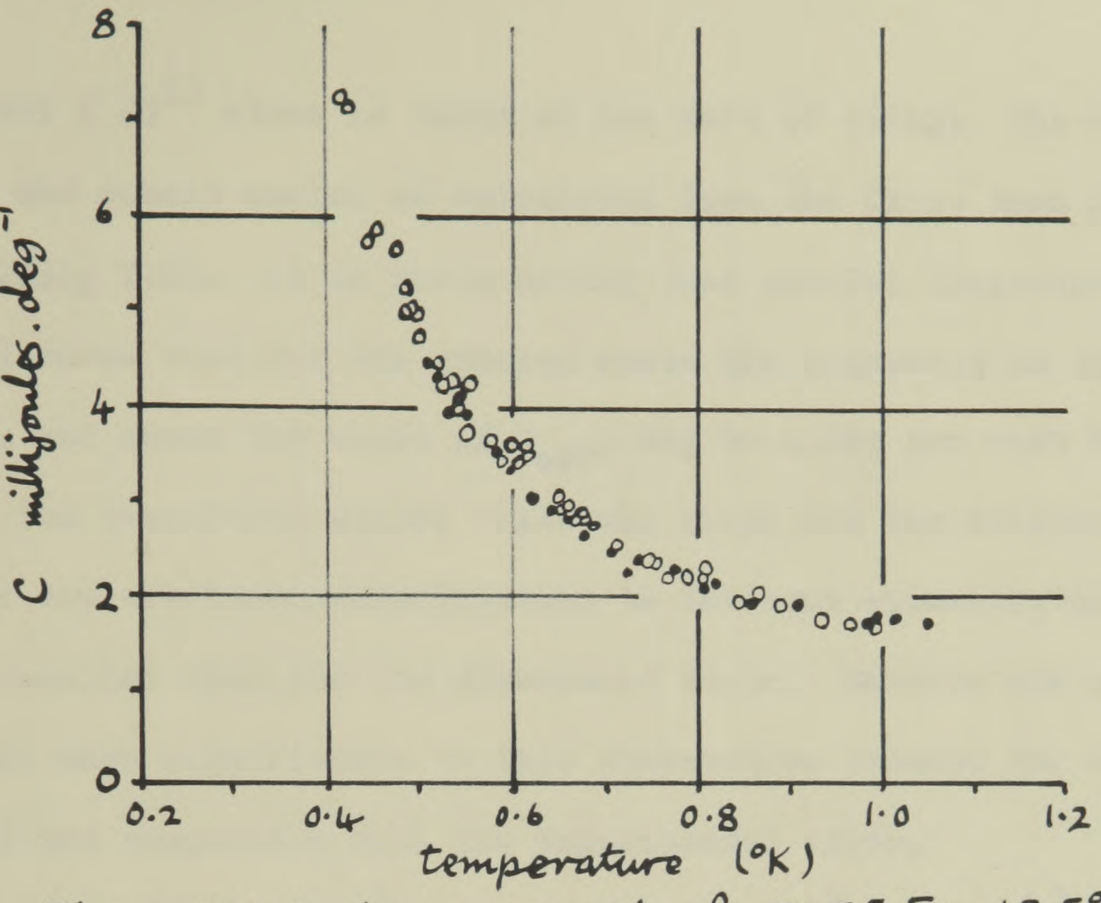

Figure 12(a) heat capacity of 52·5% Fe - 47·5% Co.

• disordered state o ordered state mass: 15·72 gm

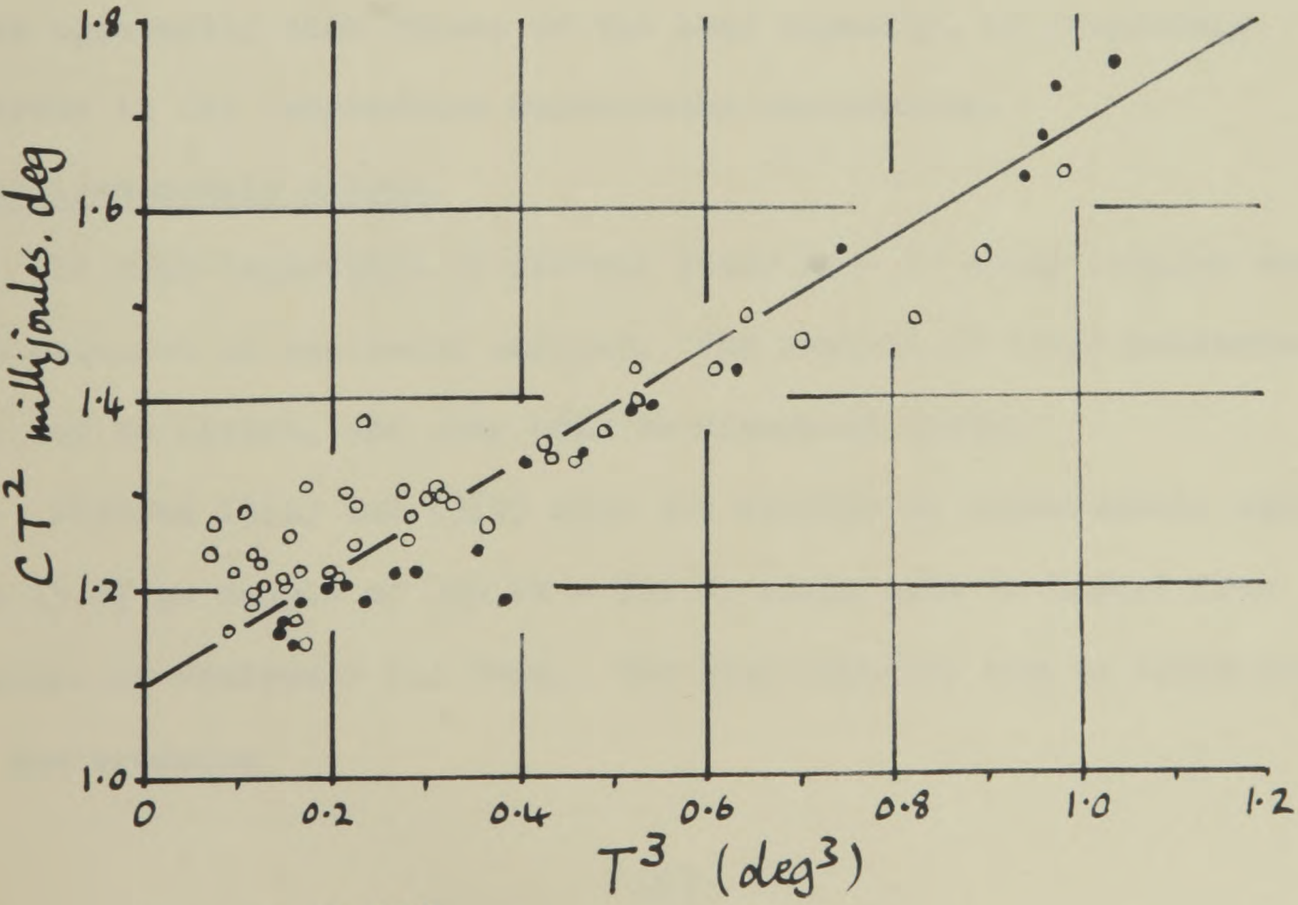

Figure 12(b)

where 6.025×10^{23} atoms is taken as one mole of alloy. The magnetic field at the cobalt nuclei as calculated from the first term is $H_{eff} = 293(\pm 7)$kG. It is worth noting that careful inspection of fig.12(b) shows that for the ordered state the intercept on the CT^2 axis, and hence the value of H_{eff}, may be a few per cent higher than for the disordered state; while the slope for the ordered state, and hence the electronic contribution to the heat capacity, may be slightly smaller than for the disordered state. However one cannot attach too much significance to this observation because the variations suggested are comparable with the experimental error.

The high values of CT^2 on fig.12(b) below $T^3 = 0.3$ deg^3 may indicate that helium absorbed on the sample at the lowest temperatures was being desorbed during the heating period. This effect, which gives apparantly high values of the heat capacity, is frequently observed in low temperature calorimetry experiments.

Other iron-cobalt alloys

The heat capacities of several other Fe - Co alloy samples were then measured as mentioned earlier. The results of these measurements will now be listed, and they will be discussed later.

Figures 13(a) and 13(b) show the results of measurements made on a 15.67 gm sample of 30% Fe - 70% Co alloy sent to Oxford from Illinois by Professor P.A Beck. The heat capacity may be represented by the equation

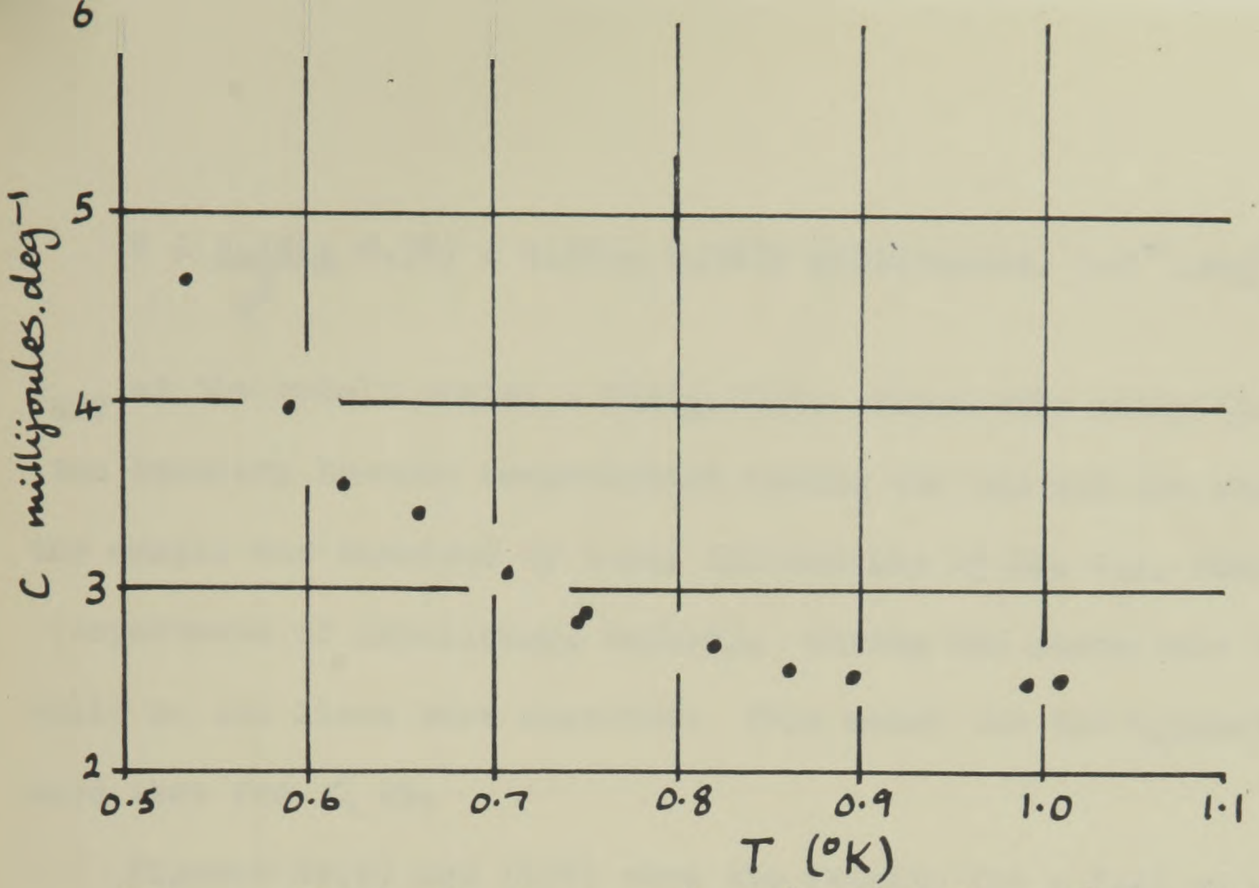

Figure 13(a) heat capacity of 30% Fe - 60% Co (15·67 gm)

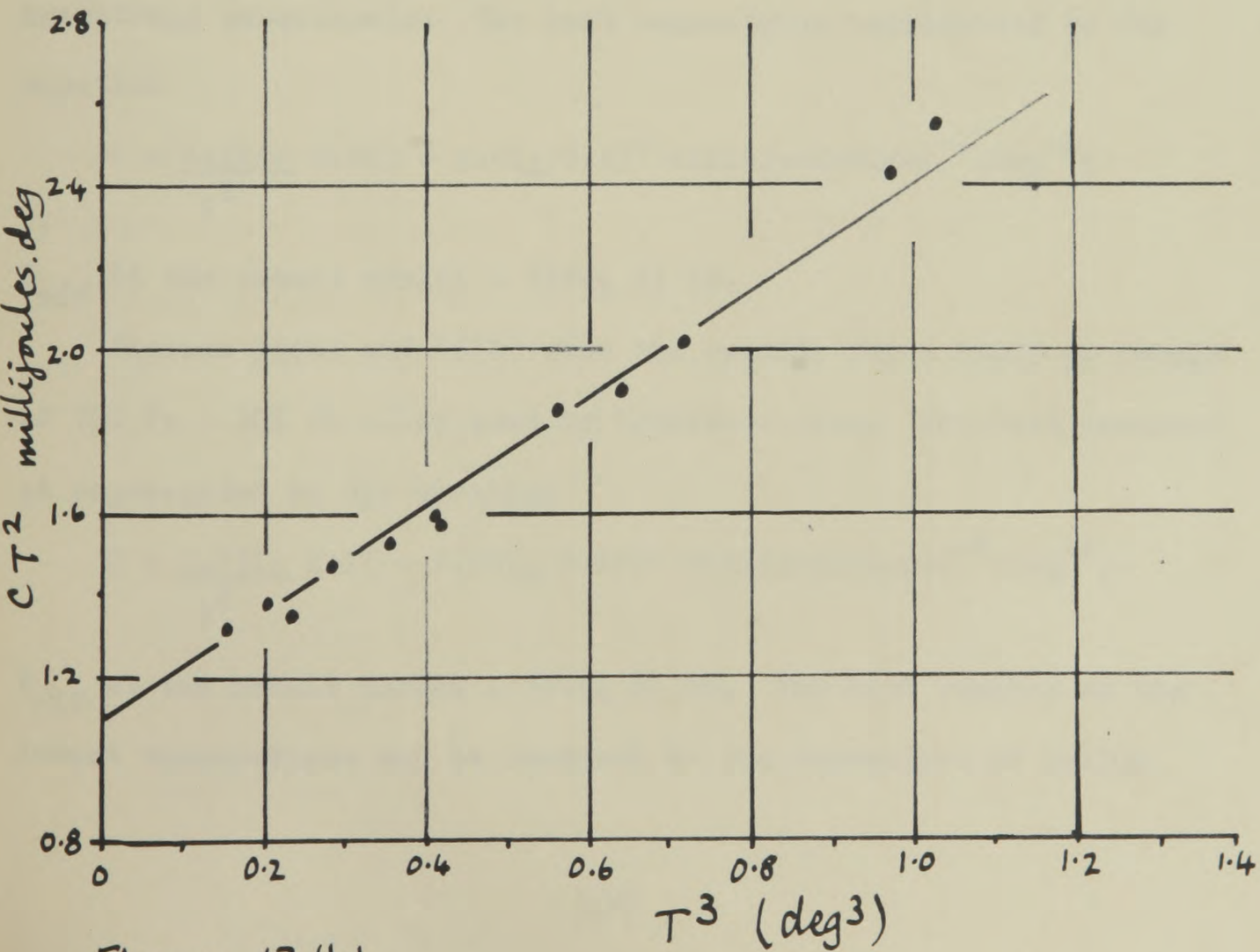

Figure 13 (b)

$$C = \frac{4.16(\pm\ 0.38)}{T^2} + 4.91(\pm\ 0.38)T \text{ millijoules. mol}^{-1}.\text{deg}^{-1};$$

H_{eff} at the cobalt nuclei = 244(± 7)kG. Since this alloy lies near the boundary between compositions having the bcc and fcc structure, the sample was examined by X-ray diffraction by Dr. J.W. Christian (Department of Metallurgy, Oxford). Strong bcc lines were found, while no fcc lines were observed. This means for the apparatus used that fcc $< 2\%$.

Figures 14(a) and 14(b) show the results for a 7.23 gm sample of 30.7% Fe - 69.3% Co alloy lent by Dr. D.M.S. Bagguley, the actual sample used by Baldock, Scurlock, and Sowter for their gamma-ray anisotropy experiments. The heat capacity is represented by the equation

$$C = \frac{4.21(\pm\ 0.24)}{T^2} + 5.4(\pm\ 0.4)T \text{ millijoules.mol}^{-1}.\text{deg}^{-1};$$

H_{eff} at the cobalt nuclei = 246(± 6) kG.

Figures 15(a) and 15(b) show the results for a 14.05 gm sample of 70% Fe - 30% Co alloy sent by Professor Beck. The heat capacity is represented by the equation

$$C = \frac{2.73(\pm\ 0.2)}{T^2} + 2.06(\pm\ 0.12)T \text{ millijoules.mol}^{-1}.\text{deg}^{-1};$$

H_{eff} at the cobalt nuclei = 301(± 8) kG. The high results at the lowest temperatures may be produced by the desorption of helium

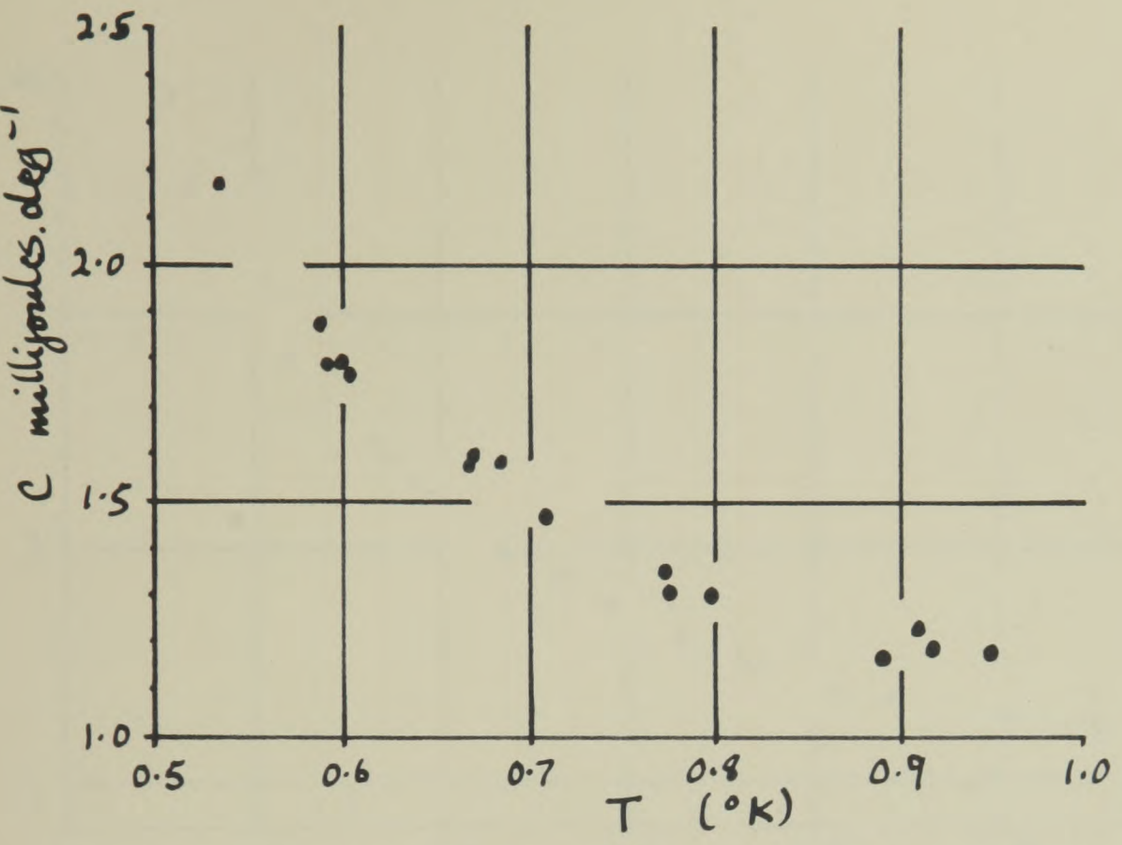

Figure 14(a) heat capacity of 30.7%Fe–69.3%Co.
mass: 7.23 gm.

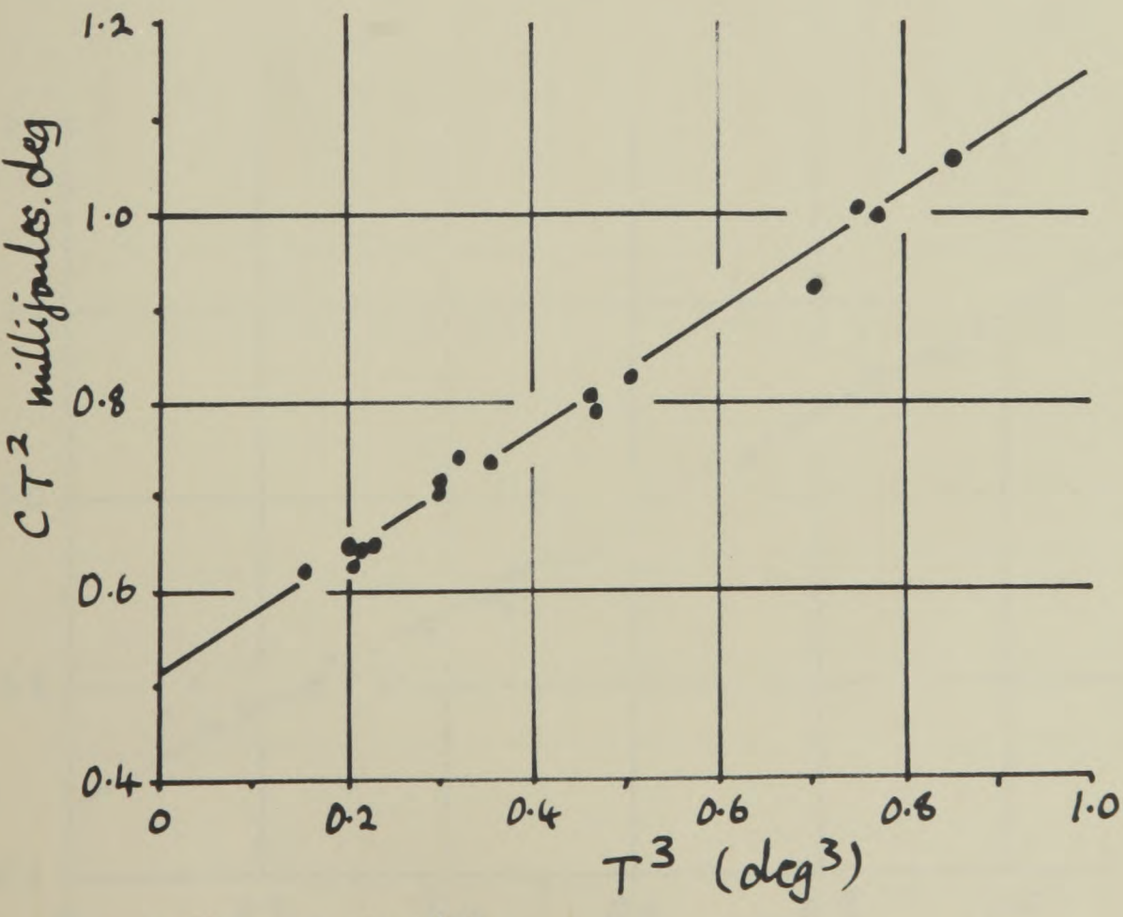

Figure 14(b)

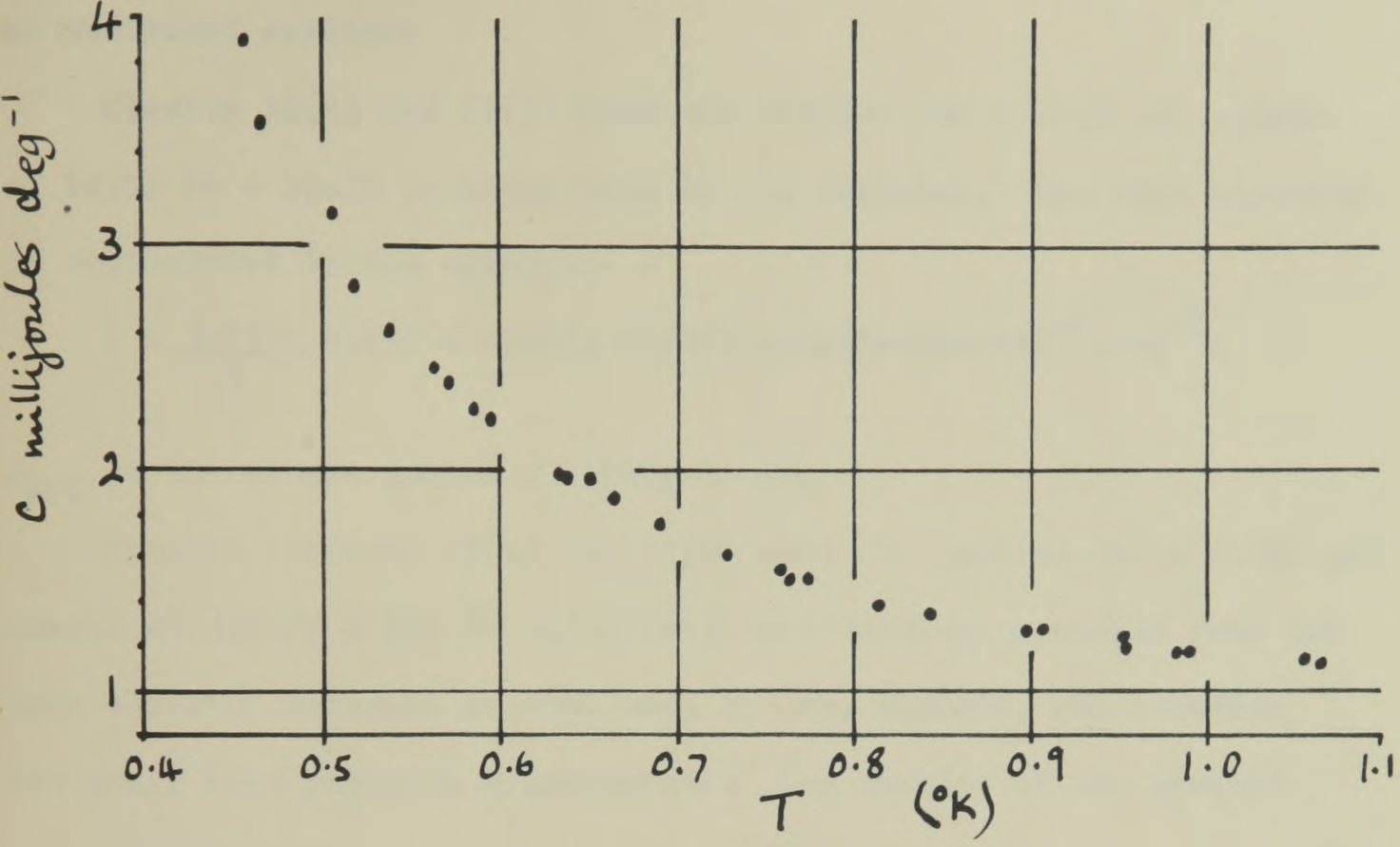

Figure 15(a) heat capacity of 70%Fe - 30%Co. (14.05 gm)

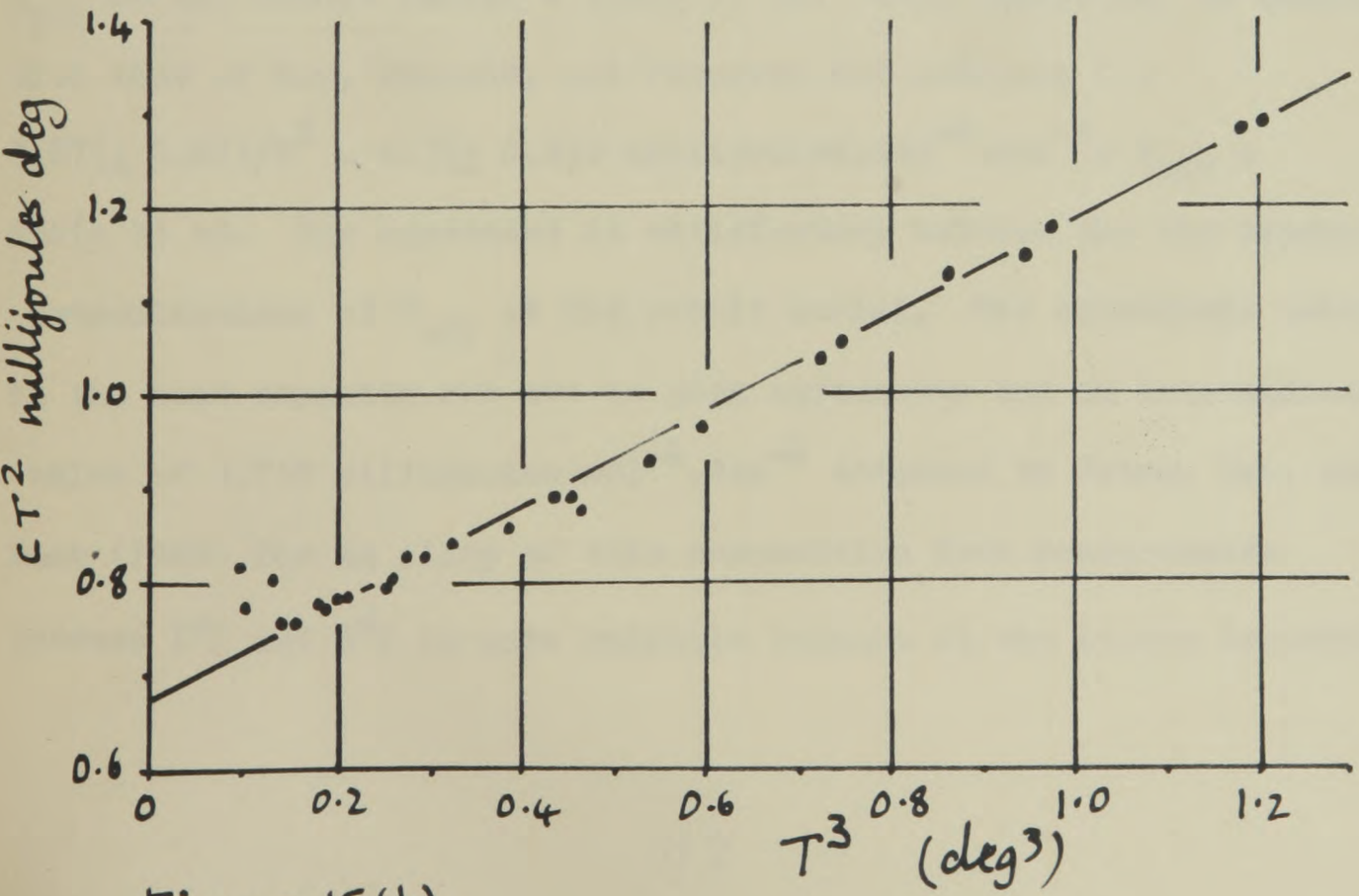

Figure 15(b)

as mentioned earlier.

Figures 16(a) and 16(b) show the results for a 10.53 gm sample of 60.5% Fe - 39.5% Co alloy lent by Dr. Bagguley. The heat capacity is represented by the equation

$$C = \frac{3.53(\pm\ 0.27)}{T^2} + 2.07(\pm\ 0.72)T \text{ millijoules.mol}^{-1}\text{.deg}^{-1};$$

H_{eff} at the cobalt nuclei = 298($\pm$ 8) kG.

Finally, figures 17(a) and 17(b) show the results for a 14.31 gm sample of 41% Fe - 59% Co alloy sent from Berkdey, a sample from the same block of material as that used by Arp, Edmonds, and Petersen for their heat capacity measurements. The results of the present measurements are represented by the equation

$$C = \frac{3.94(\pm\ 0.28)}{T^2} + 3.09(\pm\ 0.28)T \text{ millijoules.mol}^{-1}\text{.deg}^{-1};$$

H_{eff} at the cobalt nuclei = 259($\pm$ 7) kG. This result may be compared with that of Arp, Edmonds, and Petersen who obtained $C = 3.87(\pm\ 0.07)/T^2 + 4.3(\pm\ 0.2)T$ millijoules.deg^{-1}.mol^{-1}; H_{eff} = 256($\pm$ 3) kG. The agreement is satisfactory between the two separate determinations of H_{eff} at the cobalt nuclei. The electronic terms in the heat capacity are not in good agreement; but an intermediate value of 3.73T millijoules.mol^{-1}.deg^{-1} obtained by Cheng, Wei, and Beck (1960) for an alloy of this composition from measurements between 1°K and 4°K is more reliable because at the higher temperatures

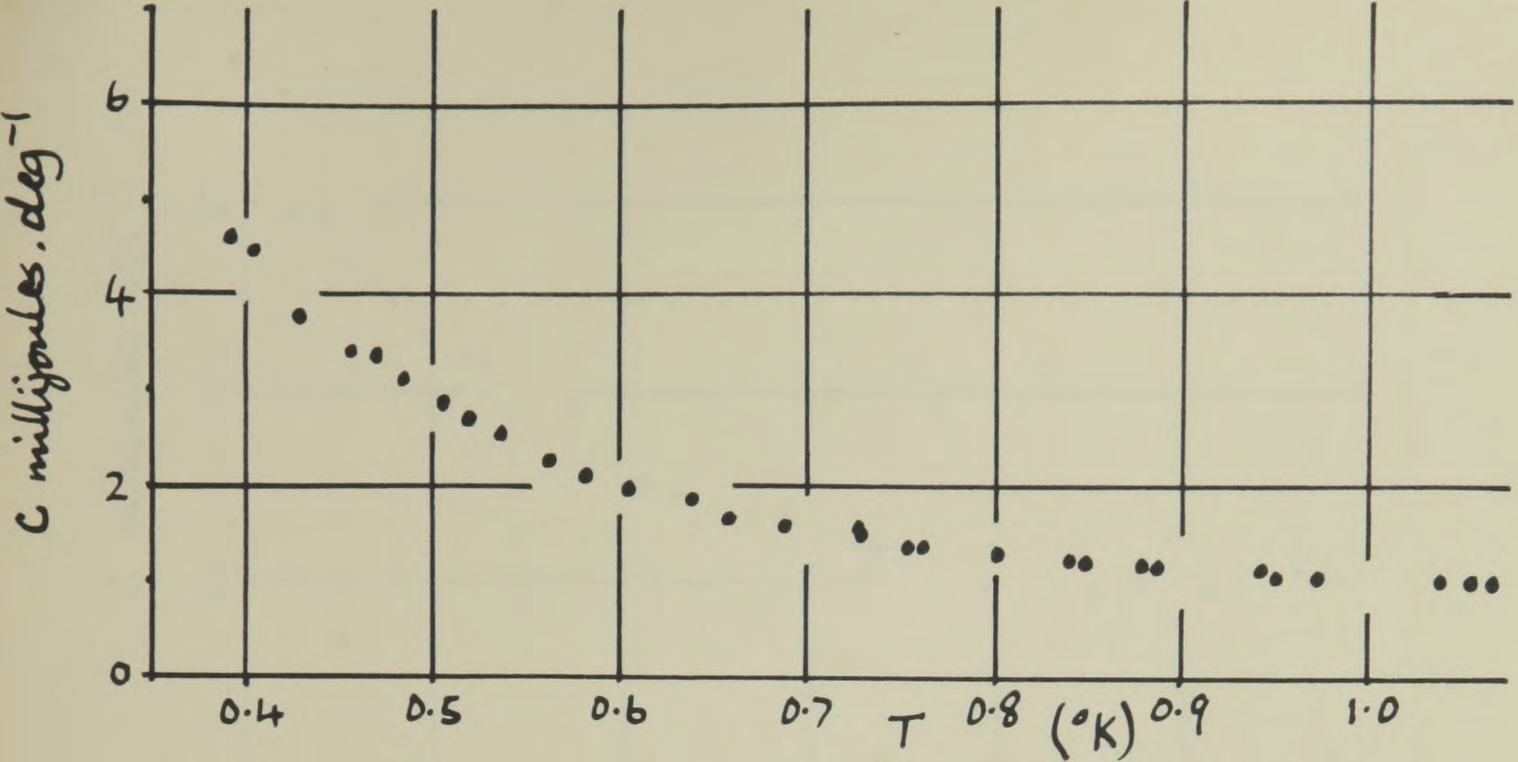

Figure 16(a) heat capacity of 60.5% Fe – 39.5% Co (10.53 gm)

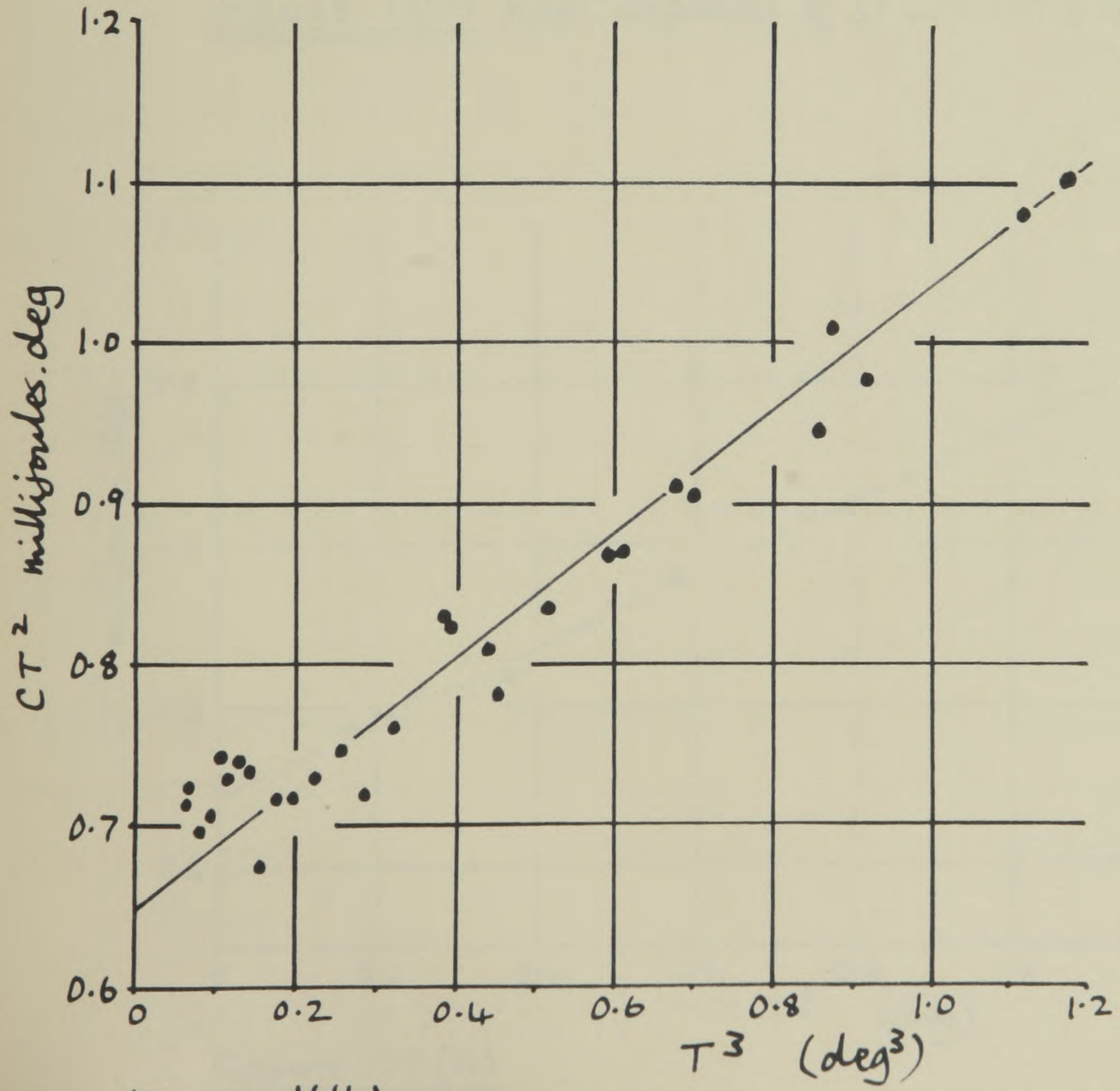

Figure 16(b)

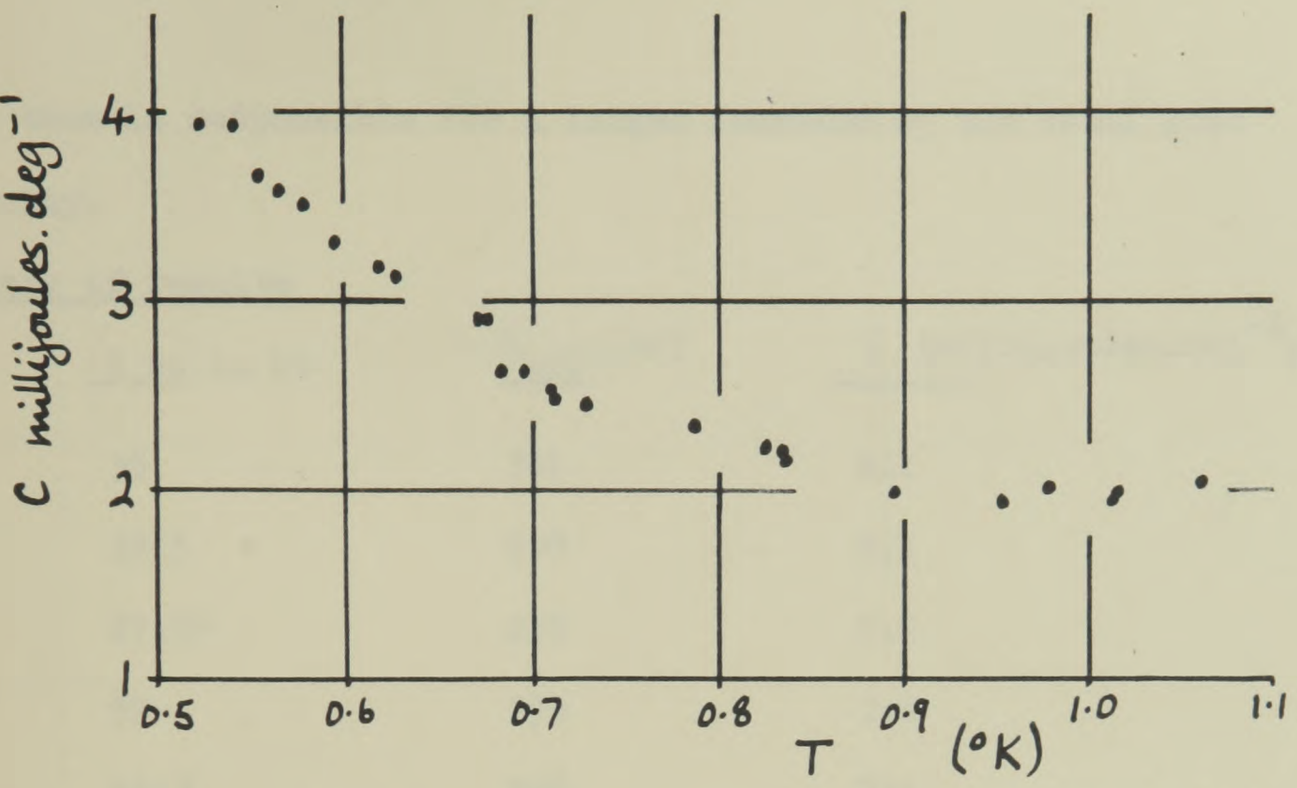

Figure 17(a) heat capacity of 41% Fe – 59% Co (14·31 gm)

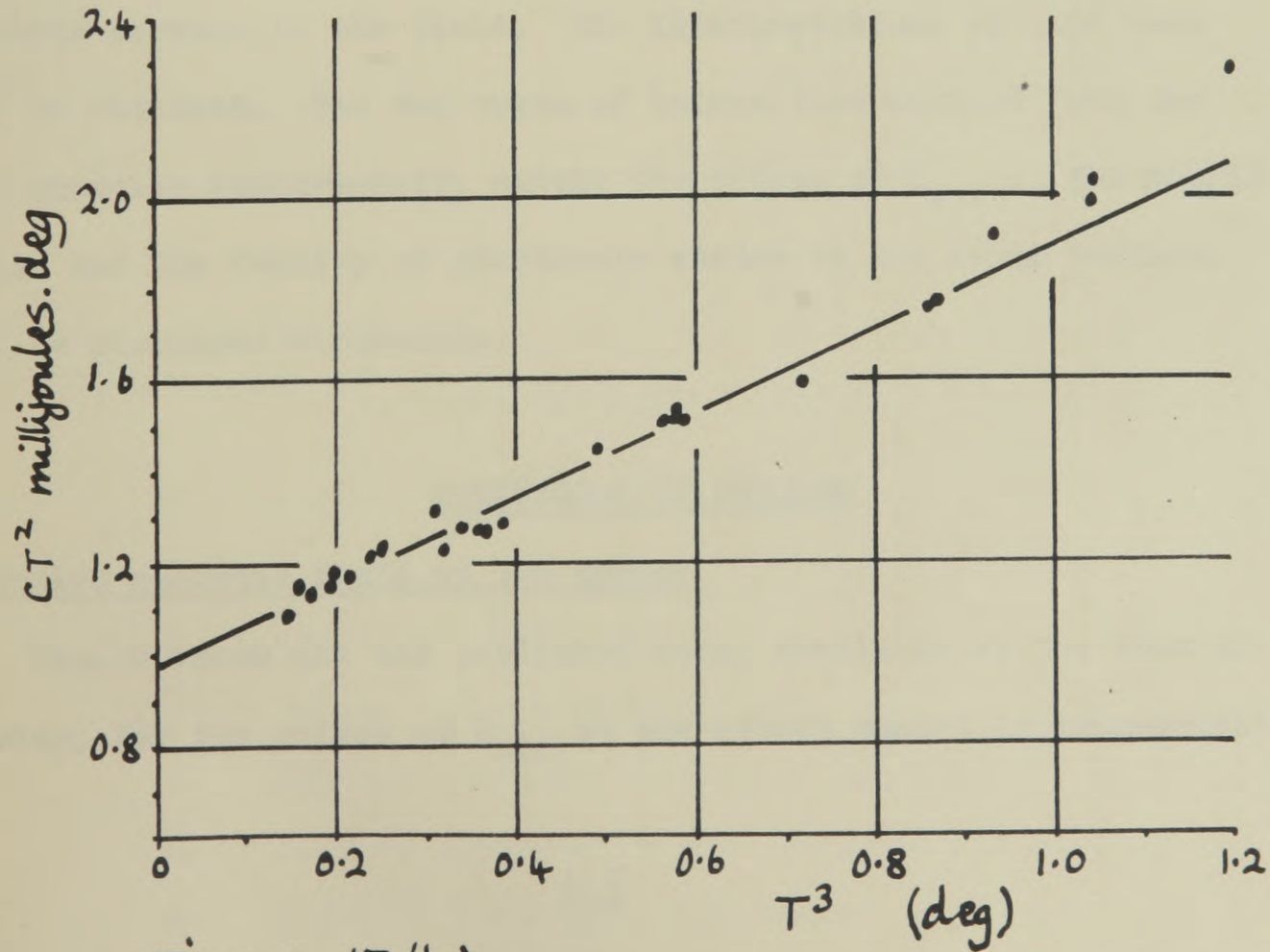

Figure 17 (b)

this term is responsible for a larger fraction of the total heat capacity.

Summary of results

% Co in Fe	H_{eff} (kG)	γ (millijoules.mol^{-1}.deg^{-2})
30	301	2.1
39.5	298	2.1
47.5*	293	2.2
59	259	3.1
69.3	246	5.4
70	244	4.9

* Ordered and disordered.

These results will be discussed below and compared with those of other workers in the field. The interpretations of this work will be outlined. The two types of information derived from the heat capacity measurements, namely the values of H_{eff} at the cobalt nuclei and the density of electronic states at the Fermi surface, will be discussed separately.

DISCUSSION OF RESULTS

Effective magnetic field at the nuclei

Fig.18 shows all the published data, available at the time of writing, for the values of H_{eff} at the cobalt nuclei in iron-cobalt

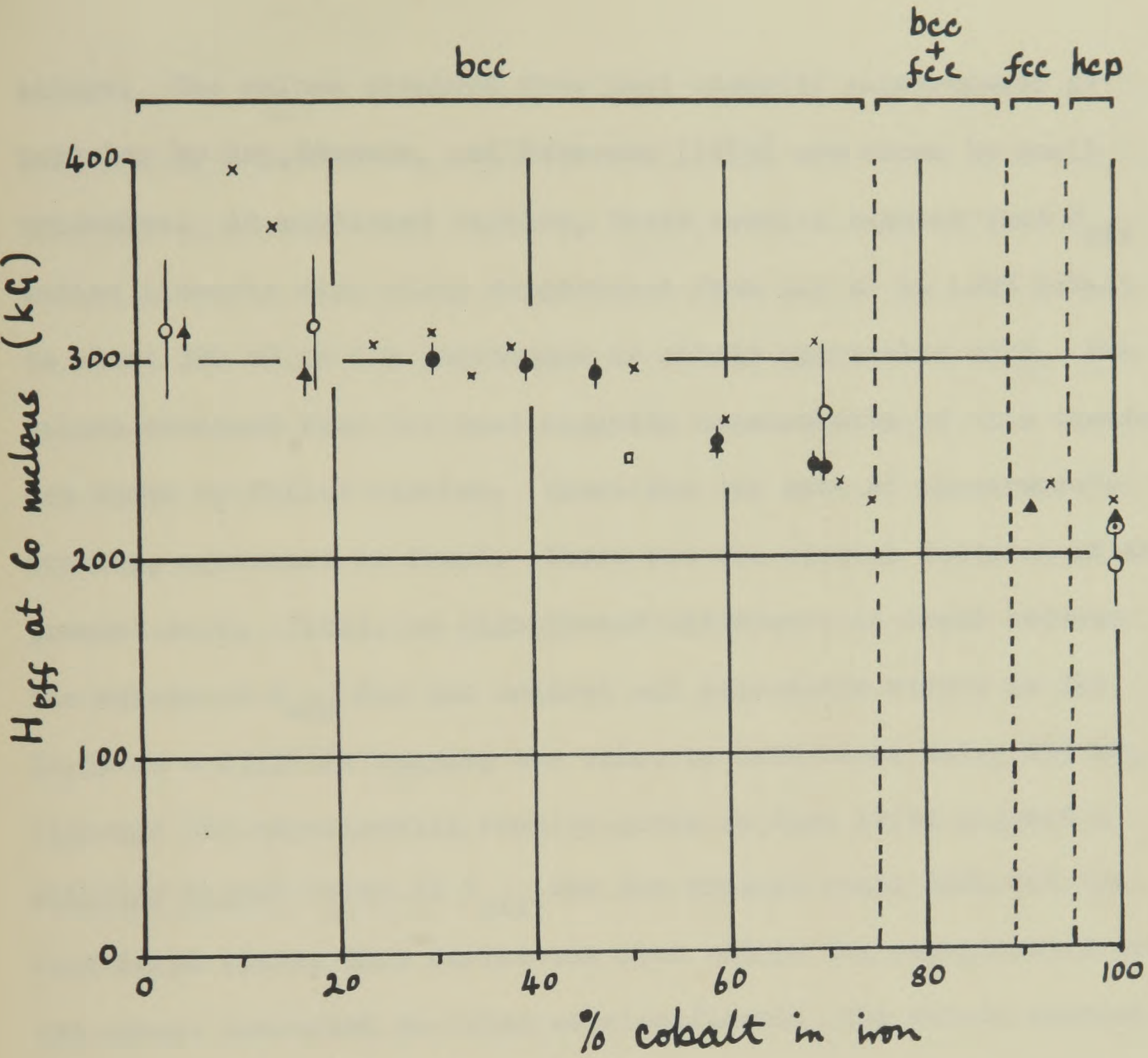

Figure 18 Values of H_{eff} at the cobalt nucleus in iron-cobalt alloys.

- ● present results (heat capacity)
- ▲ Berkeley (heat capacity)
- x Illinois (heat capacity)
- o Oxford (nuclear γ-ray anisotropy)
- □ U.S.S.R (nuclear γ-ray anisotropy)
- ⊙ Berkeley (nuclear resonance)

alloys. The values obtained from heat capacity measurements at Berkeley by Arp, Edmonds, and Petersen (1959) are shown by small triangles. As mentioned earlier, these results suggest that H_{eff} varies linearly with alloy composition from 219 kG in 100% cobalt to about 320 kG as the percentage of cobalt approaches zero. The values obtained from the heat capacity measurements of this thesis are shown by filled circles. Where the two sets of measurements overlap, agreement is found. There are two special features of the present work. First, no significant difference is found between the values of H_{eff} for the ordered and disordered states in the 52.5% Co - 47.5% Fe sample, the value in both cases being 293 kG. Although the experimental results given in fig. 12(b) suggest a slightly higher value of H_{eff} for the ordered state than for the disordered state, this difference lies within the experimental error and cannot therefore be taken as significant. The second special feature of this work is that the results between 30% cobalt and 60% cobalt in iron show that H_{eff} at the cobalt nuclei in these alloys is not a simple linear function of cobalt concentration. The Berkeley and Oxford results taken together show a maximum of about 300 kG near 30% cobalt in iron, that is near the maximum in the Slater-Pauling curve of saturation magnetization as a function of alloy composition (see for example: Kittel "Solid State Physics", 2nd ed., page 336). As mentioned later, Johnson has suggested that

the value of H_{eff} at the cobalt nuclei might decrease with decreasing cobalt concentration from 30% Co to 0% Co in Fe. This idea conflicts with the relatively high value of H_{eff} at the cobalt nuclei found at Berkeley for 5% cobalt in iron. But it should be remembered that for very low cobalt concentrations the determination of H_{eff} by heat capacity measurements is not easy. The contribution of the nuclear Schottky anomaly to the total heat capacity of the sample is small. Heat capacity measurements for a 10% cobalt in iron sample might throw some light on this problem by doubling the nuclear contribution to the heat capacity while still maintaining a low cobalt concentration.

The values of H_{eff} deduced from the heat capacity measurements made at Illinois by Cheng, Wei, and Beck(1960) are also shown in fig. 18 by small crosses. Their experiments were designed primarily to measure the electronic contribution to the heat capacity and were therefore done at temperatures above $1^{\circ}K$. Since here the nuclear contribution is small the values of H_{eff} obtained are not accurate. However their results are mostly in agreement with the results of this thesis, especially in the region from 30% cobalt to 60% cobalt in iron.

Fig.3 in Chapter One shows the values of H_{eff} at the cobalt nuclei deduced from the earlier gamma-ray anisotropy experiments

done at Oxford by Baldock, Scurlock, and Sowter (private communication). Baldock, Turrell, and Stone (see Baldock, 1960) repeated some of the measurements and the new results are plotted in fig.18. The new value of H_{eff} for the 70% Co - 30% Fe sample, 260 ± 10 kG, is in better agreement with that found from the present heat capacity measurements (246 ± 6 kG). It is probable that experimental difficulties make the values of H_{eff} obtained from the gamma-ray experiments less accurate than those obtained from heat capacity measurements.

A measurement of H_{eff} by the gamma-ray anisotropy method has been made in the U.S.S.R. by Samoilov, Sklyarevskii, and Stepanov (1959) for a 50% Co - 50% Fe alloy. This result of 250 kG has also been plotted in fig.18. It is low compared with the other measurements, but unfortunately an estimate of the accuracy is not given in the Russian paper.

Fig.18 shows also the value of H_{eff} at the nuclei in pure cobalt obtained by Gossard and Portis (1959) using the nuclear resonance method. In their experiments powdered face-centered cubic Co^{59} metal was used, and the value of H_{eff} was found to be 213.4 kG. The heat capacity measurements of Arp, Edmonds, and Petersen give a value of 219(± 4) kG for H_{eff} in hexagonal cobalt. H_{eff} in the cubic phase is therefore about 6 kG less than in the hexagonal phase.

The Mössbauer experiments mentioned in Chapter One have given important results in the study of hyperfine interactions in ferro-

magnetic iron metal and alloys. A detailed examination of the hyperfine Zeeman splitting in Fe^{57} by Hanna, Heberle, Littlejohn, Perlow, Preston, and Vincent (1960 a) gave 333 kG for the value of H_{eff} at the iron nuclei in the ferromagnetic metal. The same group (Hanna et al., 1960 b) later determined the sense of H_{eff} relative to the sample magnetization by observing the change in the Zeeman splittings on the application of an external field. Contrary to expectation, H_{eff} was found to be negative, that is in the opposite direction to the domain magnetization. This means that the contribution to H_{eff} at the nuclei from inner electron polarization, which Marshall called H_{al} (see Chapter One), must completely dominate the other contributions.

Mössbauer experiments have been made by Nagle, Frauenfelder, Taylor, Cochran, and Matthias (1960) to measure the temperature dependence of the effective field in Fe^{57} at low temperatures. They showed that the relative effective field $H(T)/H(297^{\circ}K)$ followed the same curve as the relative saturation magnetization $\sigma(T)/\sigma(297^{\circ}K)$ of iron. The effective field H_{eff} is therefore proportional to the saturation magnetization.

Heer (1960) has observed that the effective field at the nuclei in the 3d-transition ferromagnetic materials is given approximately by the expression $H_{eff} = 125\ \mu_{eff}$, where the atomic moment μ_{eff} is taken from the Slater-Pauling curve.

C.E.Johnson working at Harwell has determined from Mössbauer

experiments the values of H_{eff} at the iron nuclei in iron-cobalt alloys containing Fe^{57} (private discussion). His results are sketched in fig.19(a). The values of H_{eff} at the cobalt nuclei, obtained from the heat capacity measurements of Arp, Edmonds, and Petersen (1959), and from the results of the present thesis (see fig.18) are sketched again in fig.19(b). Johnson has used these two sets of results to confirm the observation that H_{eff} is proportional to the saturation magnetization. Having calculated the ratios between H_{eff} and μ_{eff} for the pure metals, iron and cobalt, and having assumed that the ratio between μ_{eff} and H_{eff} is constant for each kind of atom in the alloy, he calculated the mean saturation magnetization per atom $\bar{\mu}$ for the whole range of alloys, as sketched in fig.19(c). He found close agreement with the Slater-Pauling curve of saturation magnetizations. Johnson noticed that better agreement with the Slater-Pauling curve is obtained if one assumes that H_{eff} at the cobalt nuclei decreases as one passes from 30% to 0% cobalt in iron. This is indicated by the dotted line in fig.19(b). Johnson also remarked that his experiments suggest a value of H_{eff} at the iron nuclei which is a few per cent higher for the ordered state than for the disordered state. This shift of H_{eff} by ordering is similar to that at the cobalt nuclei hinted at, but not proved, by the present heat capacity measurements on the 52.5% Fe -47.5% Co sample (see fig.12).

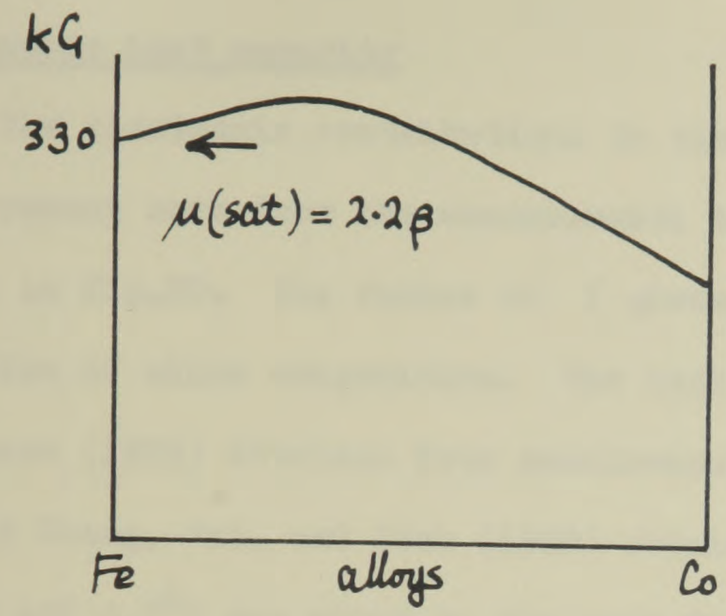

Figure 19(a) H_{eff} at Fe^{57} nuclei from Mössbauer experiments. (Johnson)

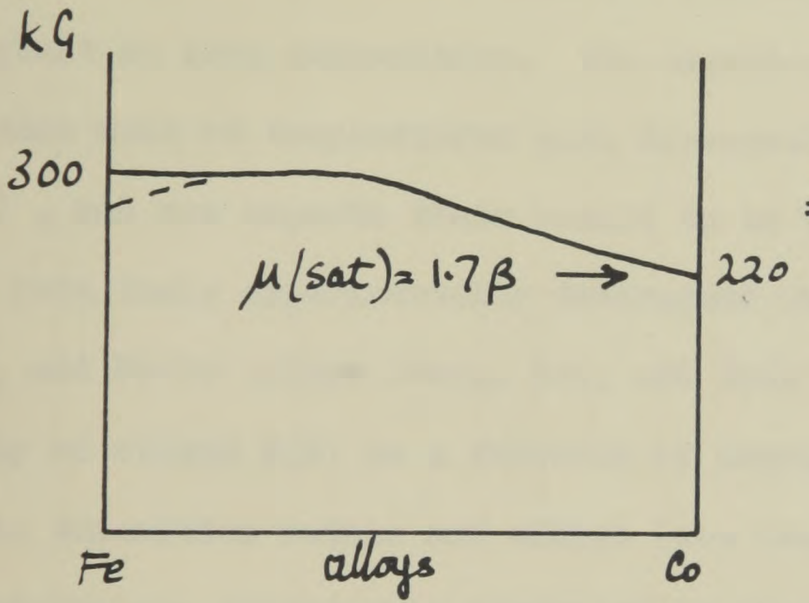

Figure 19(b) H_{eff} at Co^{59} nuclei from heat capacity experiments. (Berkeley and Oxford)

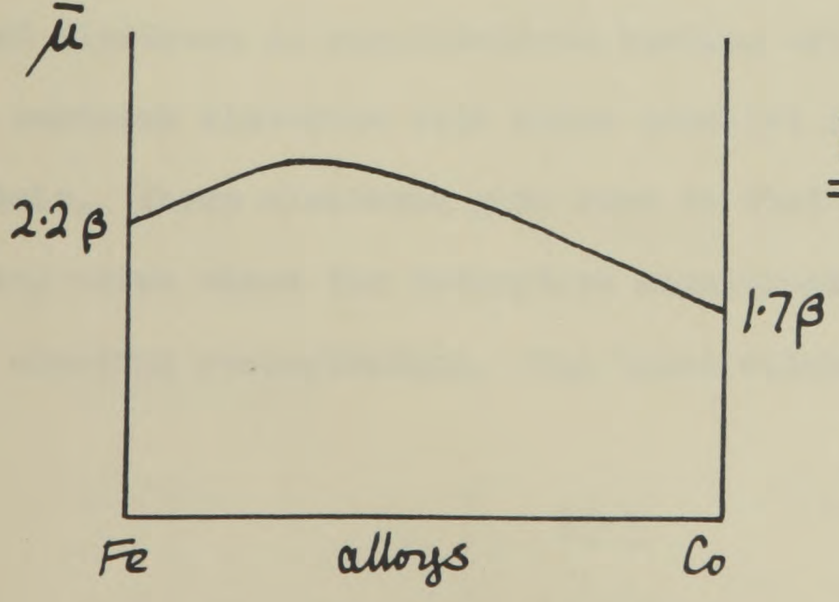

Figure 19(c) mean saturation magnetization (atomic moment) calculated from the above two curves. (Johnson)

Electronic heat capacity

The electronic contributions to the heat capacity obtained in the present work from the measurements between 0.4°K and 1.2°K are shown in fig.20. The values of γ given earlier are plotted as a function of alloy composition. The results of Arp, Edmonds, and Petersen (1959) obtained from measurements between 0.3°K and 0.7°K, and of Cheng, Wei, and Beck (1960) obtained from measurements between 1.4°K and 4.2°K are shown on the same diagram. In the pure body-centred cubic region good agreement among the results is found except for the 60% cobalt in iron composition. The experiments of Cheng, Wei, and Beck were made at temperatures more favourable for the determination of γ, and one expects their result to be the most reliable.

From their experimentally determined values of γ in V-Cr, Cr-Fe, and Fe-Co alloys Cheng, Wei, and Beck have derived a curve of density of states N(E) as a function of energy for the 3d band of the bcc transition metals and alloys (see Chapter One of this thesis). The results are tentatively described by the authors as arising from three slightly overlapping 3d sub-bands. The first sub-band contains paired electrons in non-localized bonding orbitals. The second sub-band contains electrons with spins parallel in localized atomic orbitals. These electrons give rise to that part of the Slater-Pauling curve where the saturation magnetization increases with increasing electron concentration. The third sub-band, contains electrons

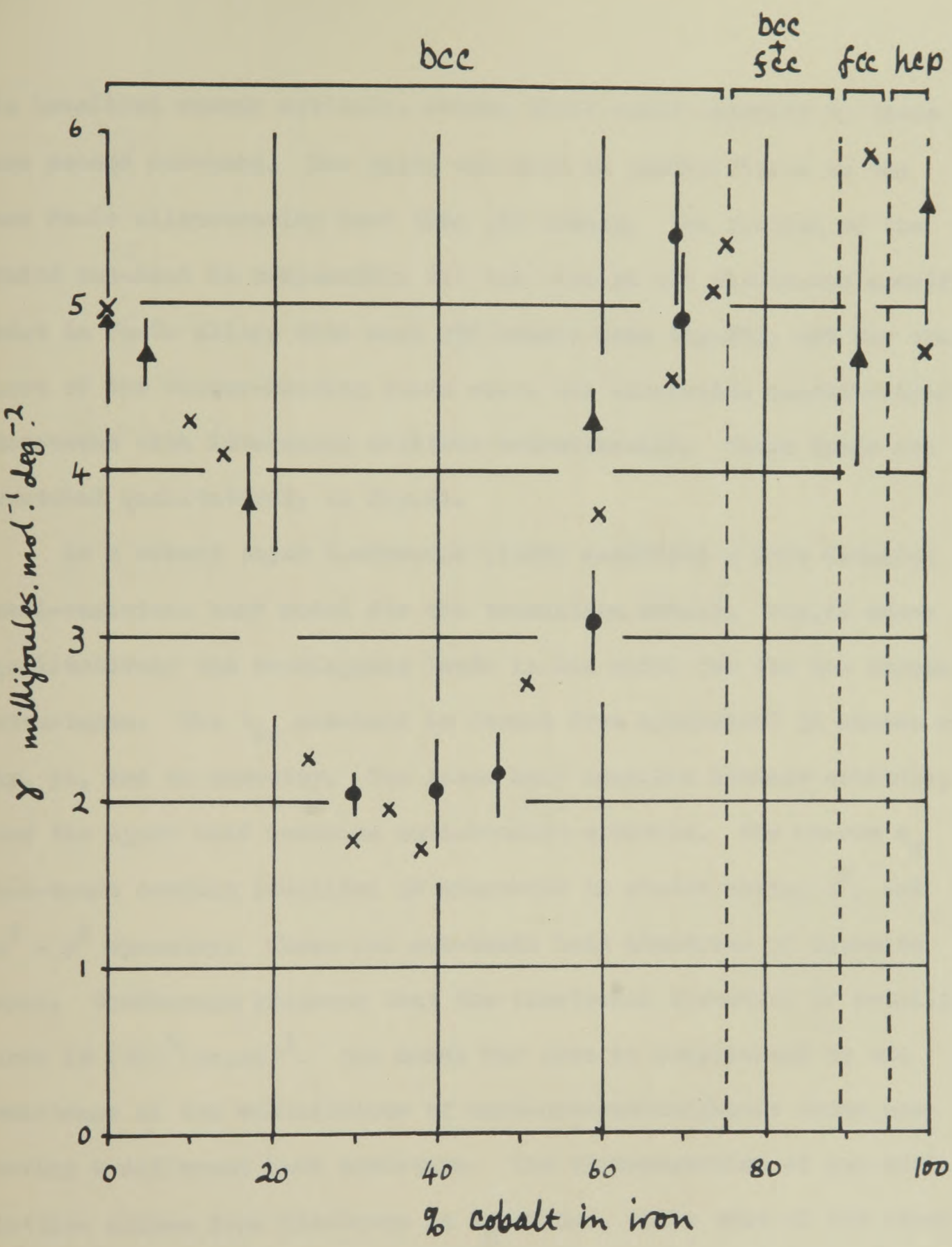

Figure 20 Electronic heat capacity of iron-cobalt alloys.

- ● present results.
- x Cheng, Wei, and Beck.
- ▲ Arp, Edmonds, and Petersen.

in localized atomic orbitals, having their spins opposite to those in the second sub-band. The third sub-band is partly filled in the bcc Fe-Co alloysshaving more than 35% cobalt. The filling of the third sub-band is responsible for the rise in the electronic specific heat in Fe-Co alloys with more 35% cobalt (see fig.20), and for that part of the Slater-Pauling curve where the saturation magnetization decreases with increasing electron concentration. These bands are sketched qualitatively in fig.21.

In a recent paper Goodenough (1960) described a more detailed semi-empirical band model for the transition metals. Fig,22 shows qualitatively the overlapping bands in his model for the bcc crystal structures. The t_{2g} sub-band is formed from hybridized 3d states of xy, yz, and zx symmetry. The lower half contains bonding orbitals, and the upper half contains anti-bonding orbitals. The narrow e_g sub-bands contain localized 3d electrons in states having z^2, and $x^2 - y^2$ symmetry. These two sub-bands hold electrons of opposite spin. Goodenough proposes that the electronic structure of metallic iron is $(3d)^5(4s,4p)^3$. His model for iron is complicated by the existence of two sub-lattices of next-nearest-neighbour atoms each having a different band structure. The ferromagnetism of one sub-lattice arises from electrons in e_g states, while that of the other sub-lattice arises from holes in the t_{2g} band. In the iron-cobalt

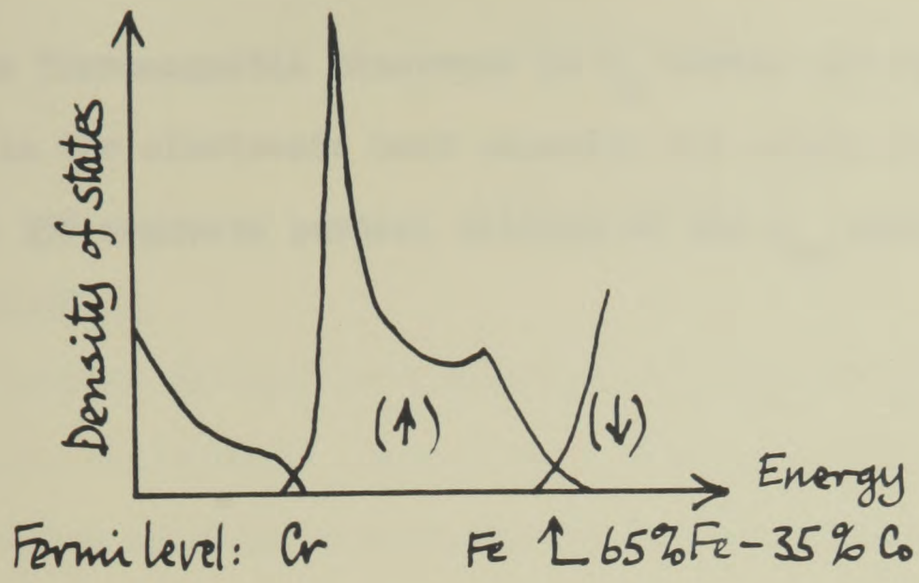

Figure 21 3d sub-bands in bcc transition alloys (Cheng, Wei, and Beck)

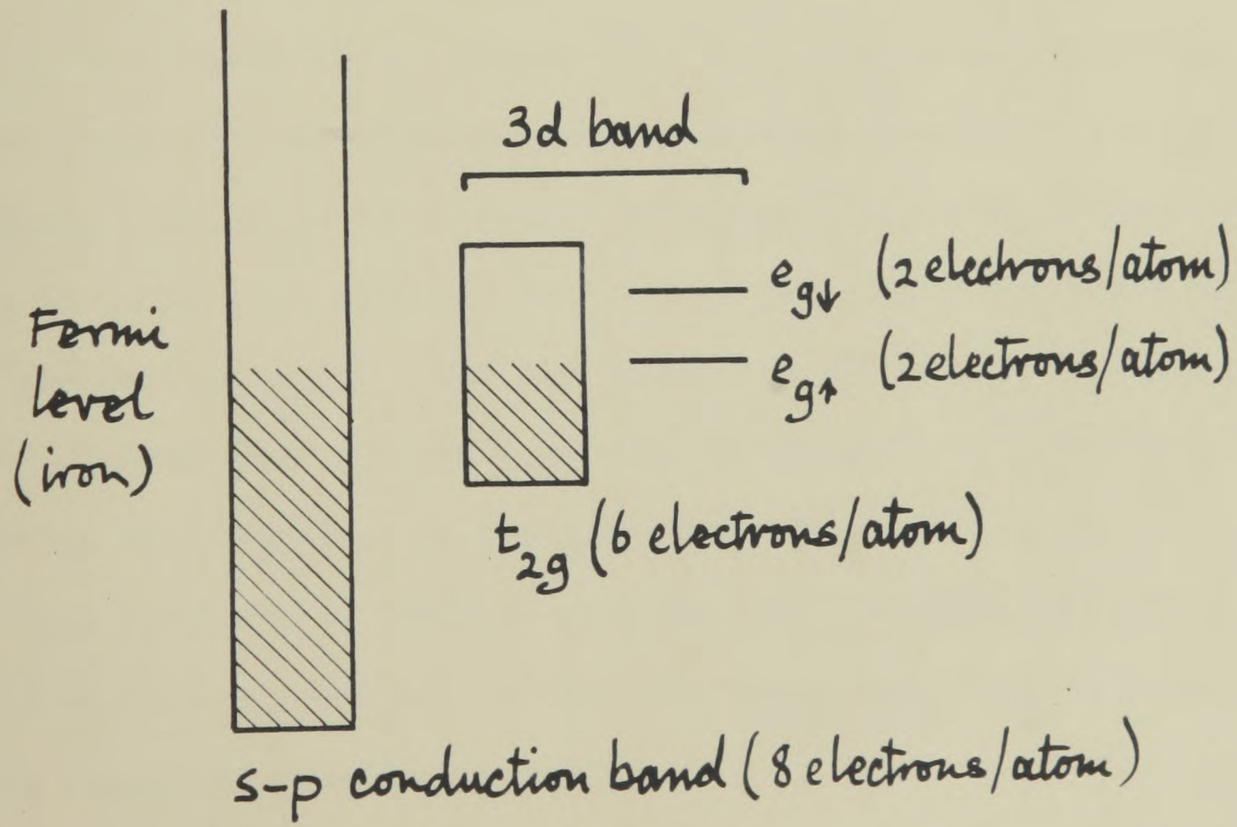

Figure 22 Band structure of bcc 3d-metals. (Goodenough)

alloys ferromagnetic electrons in e_g states are favoured. The sharp rise in the electronic heat capacity for cobalt concentrations above 35% suggests partial filling of the $e_{g\downarrow}$ sub-band.

CHAPTER FOUR

URANIUM HYDRIDE

Introduction

Uranium hydride is a compound of definite composition. It conducts electricity like a metal. The arrangement of uranium atoms in uranium hydride is unrelated to that in uranium metal and is almost lacking in metal-metal bonds.

The structure, determined by X-ray diffraction and by neutron diffraction, and described by Rundle (1947, 1951), is cubic with side 6.631 A. In beta uranium hydride there are eight uranium atoms per unit cell at positions (a) 000, $\frac{1}{2}\frac{1}{2}\frac{1}{2}$ and (c) $\frac{1}{4}\frac{1}{2}0$, $0\frac{1}{4}\frac{1}{2}$, $\frac{1}{2}0\frac{1}{4}$, $\frac{3}{4}\frac{1}{2}0$, $0\frac{3}{4}\frac{1}{2}$, $\frac{1}{2}0\frac{3}{4}$, as illustrated in figure 23. This arrangement is quite different from that of uranium metal. Alpha-uranium has a complex orthorhombic structure which may be considered as a deformed hcp lattice in which each atom has four neighbours nearer the other eight (Jacob and Warren, 1937). The hydrogen atoms in uranium hydride lie in distorted tetrahedra, and are equidistant from four uranium atoms at 2.32 A. The two types of uranium atoms, labelled (a) and (c) above, each have twelve nearest hydrogen atoms at this distance. It would confuse the diagram to show the positions of the hydrogen atoms in figure 23 (see Rundle, 1951).

The ferromagnetic transition in uranium hydride near 170°K

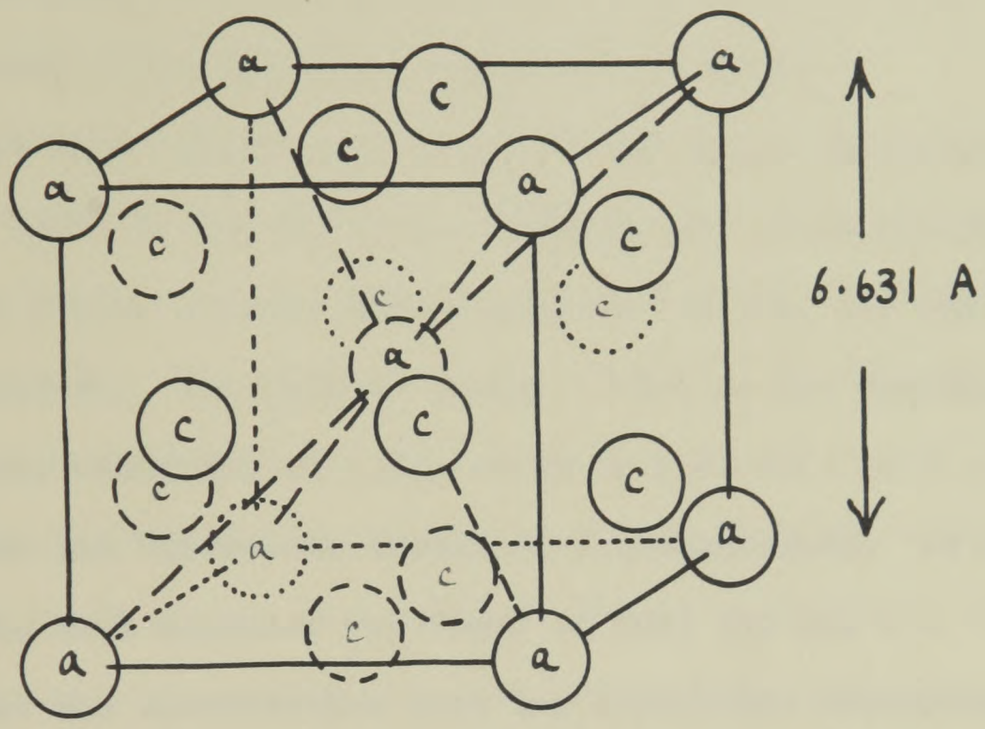

Figure 23 Positions of uranium atoms in UH_3 showing two types of atoms (a) and (c).

was discovered by Trzebiatowski, Silwa, and Stalinski (1952, 1954). The magnetic properties have been studied by Gruen (1955), Lin and Kaufman (1956), and Henry (1958). The saturation magnetization is 1.2 Bohr magnetons per atom of uranium. It arises from the spins of electrons whose orbital angular momentum is quenched.

The heat capacity of beta uranium hydride has been measured from 5°K to 350°K by Flotow, Lohr, Abraham, and Osborne (1959). They found a lambda anomaly with a peak at 170.7°K, the ferromagnetic Curie temperature. The entropy change $\Delta S/R$ in the ferromagnetic transition was estimated at 0.51, which is less than $\ln 2 = 0.693$ expected from the Heisenberg theory of ferromagnetism. At low temperatures the heat capacity was found to obey the law $C = \gamma T + aT^3$, where γT is the contribution from the conduction electrons, and aT^3 is the lattice contribution. From 10°K to 15°K the results fitted the relation $C = 33T + 0.21T^3$ millijoules.deg^{-1}.mol^{-1}, but these figures were not well established at lower temperatures. The value of the electronic heat capacity is high compared with that of uranium metal (11 T millijoules. deg^{-1}.mol^{-1}, Smith and Wolcott, 1955).

Uranium hydride is normally prepared by passing hydrogen gas at 1 atm pressure and 200°C - 300°C over uranium metal. When the hydride is formed it breaks up into a fine powder. This powder oxidises violently in air at room temperature and must therefore be handled in an inert atmosphere. Dr. A. Küssner (University of Münster)

using a new method has prepared uranium hydride in solid lumps weighing a few grams. These lumps are stable in air, and have a metallic appearance.

With these samples it is possible to measure the heat capacity of uranium hydride at temperatures below 1°K by the method described earlier in Chapter Two. If there is an appreciable effective magnetic field at the hydrogen nuclei in uranium hydride associated with the ferromagnetism, there should be a Schottky anomaly in the heat capacity below 1°K. No contributions to such an anomaly are expected from the uranium nuclei because U^{238} has zero spin and U^{235} (magnetic moment ~ 0.51 nm) is not sufficiently abundant in natural uranium. Some heat capacity measurements on uranium hydride made from 0.5°K to 5°K to look for an anomaly due to the hydrogen nuclei are described in the present chapter.

In addition, measurements of the electrical conductivity of a solid lump of uranium hydride have been made in the Clarendon Laboratory by M.B.Goitein and M.G.Richards. Their results in the region of the ferromagnetic transition temperature will be quoted later (private discussion, 1960)

Heat capacity measurements above 1°K

The sample of uranium hydride used for the present heat capacity measurements was kindly supplied by Dr. Küsener. It consisted of 4.57 gm of the material in two solid lumps, roughly cylindrical in shape. The large lump had a length of about 2 cm and a diameter of about $\frac{1}{2}$ cm. The two were mounted in the vacuum space of the cryostat with a heater resistance

mat, a carbon thermometer, and 2.16 gm of cerium magnesium nitrate for cooling. Thermal contact between the cooling salt was made via silver foil glued with GE 7031 varnish.

Attempts to cool the sample with this arrangement to temperatures below 1°K failed because of strong hysteresis heating in magnetic fields below 1.3 kG. The heat evolved during each magnetization was estimated at ½ millijoule for this sample. Heat capacity measurements were, however, made between 1.2°K and 5°K before the assembly in the vacuum space was changed. Measurements at these temperatures were not easy for the following reasons. The carbon thermometer sensitivity was poor above 1°K, a large correction for the heat capacity of the cooling salt was necessary, and the heat insulation was not good for making heat capacity measurements on such a small sample. To reduce the effect of the heat leak one might warm up the helium bath during the measurements in order to maintain a small difference in temperature between the bath and the sample. The helium dewar of the present apparatus unfortunately does not hold enough liquid for more than one cooling from 4.2°K to 1.2°K. Since several runs between 1.2°K and 5°K were necessary to get enough data, the liquid helium bath was kept at its lowest temperature throughout the experiment.

The open circles in figure 24 show the results for the heat capacity of the uranium hydride sample plus the cerium magnesium nitrate as a function of temperature between 1°K and 5°K. (The results shown below 1.2°K will be described later). The heat capacity of the cerium magnesium ni-

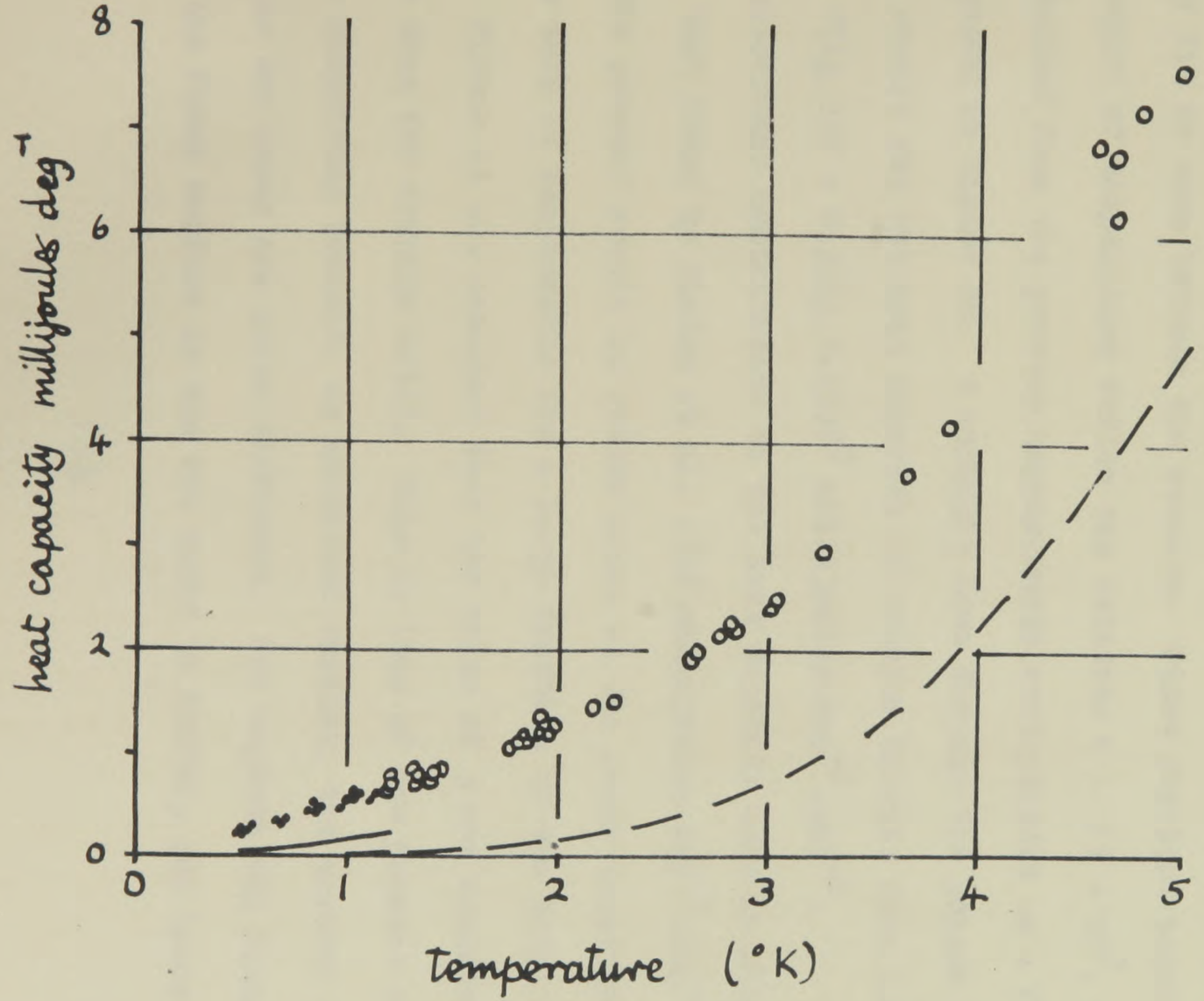

Figure 24. Heat capacity.

o 4·57gm UH_3 + 2·16gm salt

• 4·57gm UH_3 + 15·8 gm salt

– – – 2 gm of salt

——— 15 gm of salt

trate calculated from data published by Bailey (1959) is also shown. The heat capacity of the uranium hydride alone is shown in figure 25 as a function of temperature from 1.2°K to 5°K. The measurements of Flotow, Lohr, Abraham, and Osborne (1959) below 15°K are also shown for comparison with the present results. The results of the present work are not accurate above about 3°K because of the difficulties mentioned above, while the results of Flotow et al. are probably inaccurate at their lowest temperatures because of the adsorption and desorption of helium exchange gas on the sample. If these reservations are borne in mind a satisfactory fit is seen between the results. Since the heat capacities in this region of temperature follow the relation $C = \gamma T + aT^3$, values of C/T obtained from the present measurements were plotted as a function of T^2 as shown in figure 26. A straight line through the points gave the following result for the heat capacity of uranium hydride from 1.2°K to 5°K: $C = 27(\pm 3)T + 0.33(\pm 0.15)T^3$ millijoules.deg^{-1}.mol^{-1}.

The electronic contribution to the heat capacity here is slightly less than that found by Flotow et al. (33T millijoules.deg^{-1}.mol^{-1}.). Probably the present result is better since at the lower temperatures the electronic term is responsible for a large fraction of the total heat capacity. Flotow et al. remarked that the value of γ for uranium hydride was higher than for uranium metal. This is true of the present results and is not surprising because, as mentioned earlier, the crystal structures in the two cases are quite different. One expects the density of states at the Fermi surface in the two cases to differ, and hence give

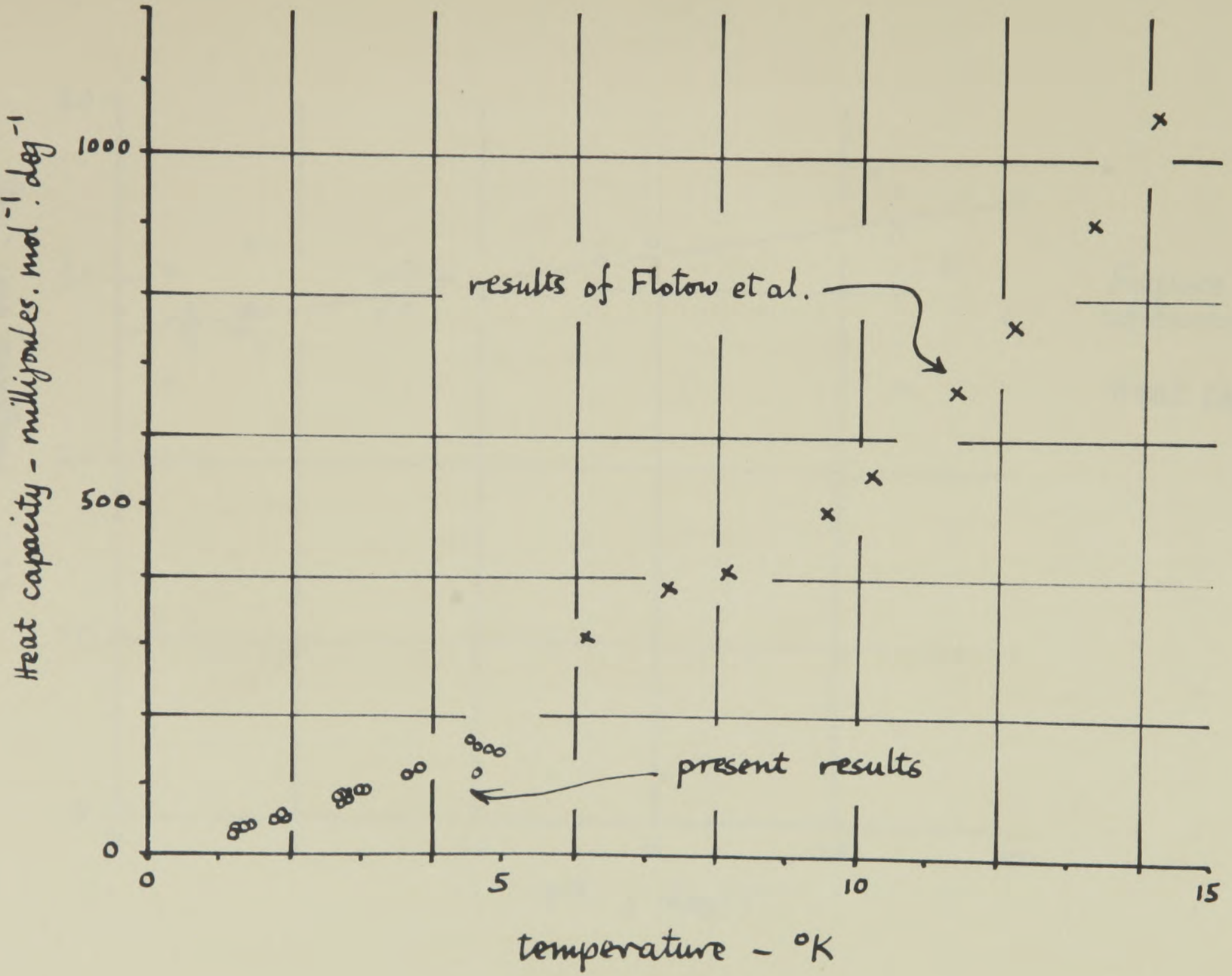

Figure 25

Heat capacity of UH_3

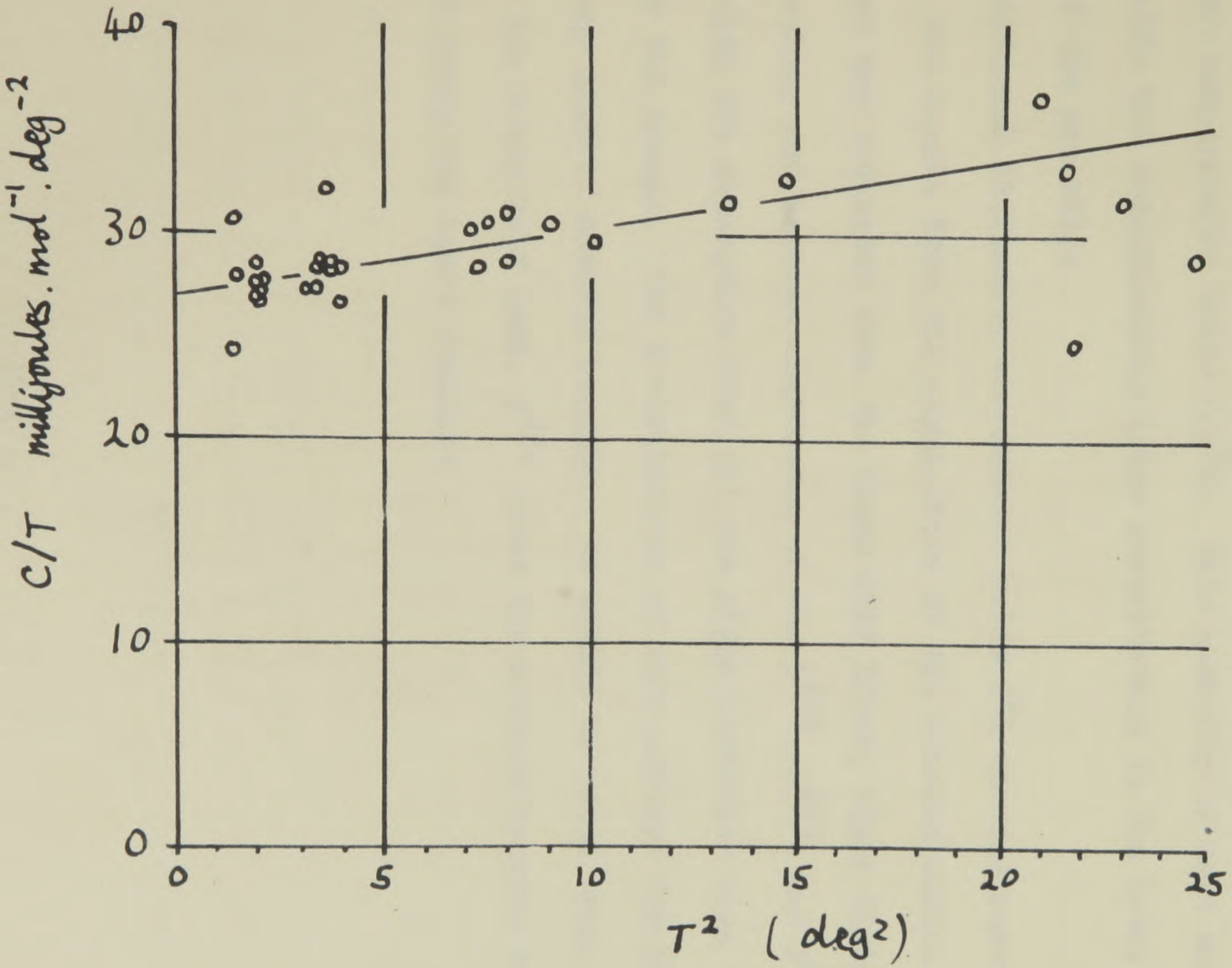

Figure 26

Heat capacity of UH_3

rise to different values of γ. Finally we note that the present measurements give only a rough value for the lattice heat capacity, which is relatively small at liquid helium temperatures.

Heat capacity measurements below 1°K

When the experiments described above had been completed, the amount of cooling salt thermally attached to the uranium hydride was increased from 2.16 gm to 15.8 gm to offset the hysteresis heating, and to reach temperatures below 0.5°K. This quantity of salt made an unavoidable but uncomfortably large contribution to the total heat capacity of the assembly.

An additional difficulty encountered below 1°K was radioactive heating in the sample from the alpha-decay of the uranium nuclei. This heating was estimated from the known half lives, alpha disintegration energies, and natural abundances of the U^{234}, U^{235}, and U^{238} isotopes, with the assumption that all the alpha particles were absorbed by the sample. The contributions of each isotope are given below for one gram of natural uranium. It should be noted that, because of its short half life, U^{234} gives the largest heating effect in spite of being the least abundant.

Isotope	natural abundance	Half life (yrs)	disintegration energy(MeV)	heating effect (erg/sec)
U^{234}	0.0058 %	2.48×10^5	4.76	0.095
U^{235}	0.71 %	7.1×10^8	4.4, 4.58	0.004
U^{238}	99.3 ~~0.993~~ %	4.5×10^9	4.2	0.079
			total:	0.178

For the present sample the radioactive heating was estimated at 0.8 erg/sec. The experimentally observed warming up rate at 0.6°K was about 0.06 deg/min. The total heat input to the sample, estimated from this figure and from the heat capacity results given later, was about 3 erg/sec. This indicates a heat leak from the helium bath to the sample of 2.2 erg/sec, a figure which is somewhat larger than usual with this apparatus. On account of the fast warming up rate, short bursts of heat of about 10 sec were used to measure the heat capacity of the sample below 1.2°K.

The results are shown by the black dots in figures 24 and 27. The heat capacity of the 15.8 gm of cerium magnesium nitrate is also indicated in figure 24. Although the unfavourable conditions made the results inaccurate, they show clearly that there is no Schottky anomaly visible from the measurements, and that the heat capacity is proportional to the temperature between 0.5°K and 1.2°K. Figure 27 shows the values of CT^2 plotted as a function of T^3 for the heat capacity results below 1.2°K shown in figure24. An upper limit for the effective field H_{eff} at the hydrogen nuclei in uranium

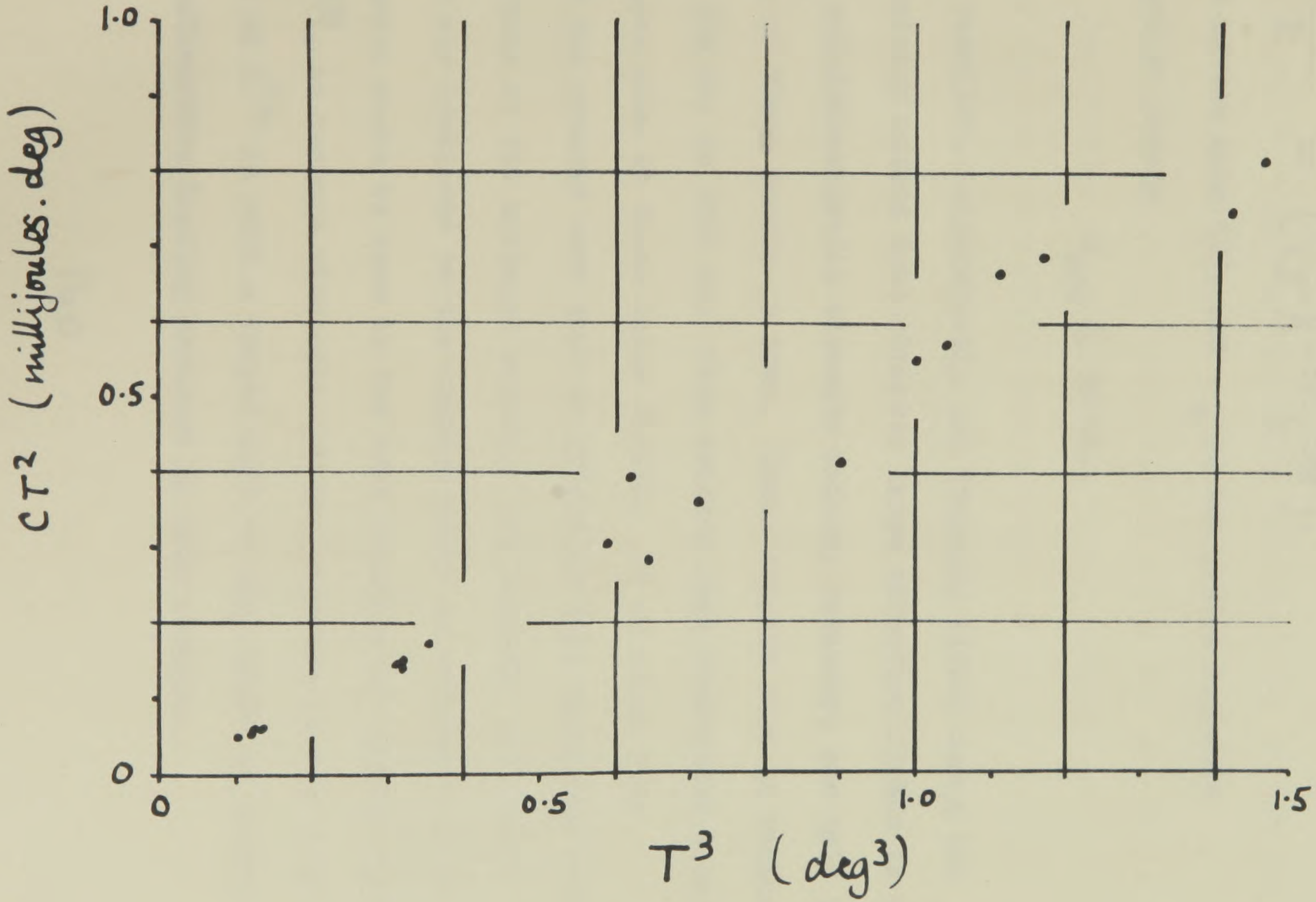

Figure 27

Heat capacity of UH_3 below 1·2°K.

Values shown are for 4·57gm of UH_3 + 15gm of salt.

hydride compatible with the results has been found from the maximum possible intercept ΔCT^2 on the CT^2 axis of a straight line through the points. Here $\Delta CT^2(\max) \simeq 0.005$ millijoules.deg. Since the sample containes 0.019 moles, and since

$$\frac{\Delta CT^2}{R} = \left(\frac{I+1}{3I}\right)\left(\frac{\mu_n H_{eff}}{k}\right)^2,$$

where I is the proton spin ($\frac{1}{2}$), and μ_n is the proton magnetic moment (2.79 nm) we obtain

$$H_{eff} \leqslant 30 \text{ kG}.$$

Discussion

Recently Samoilov, Sklyarevskii, and Stepanov (1960) using the gamma-ray anisotropy method have observed large effective fields on the nuclei of the non-ferromagnetic elements indium, antimony, and gold in weak solutions of these metals in iron. Their results were as follows: In 250 kG, Sb 280 kG, Au 1000 kG. They assumed that conduction electron polarization gave rise to these large fields. It is clear from the results of the present work that no effect of this magnitude occurs in uranium hydride at the hydrogen nuclei. If, however, the ferromagnetic spins are localized on the uranium atoms an effective field at the uranium nuclei might be seen in the heat capacity of uranium hydride enriched in U^{235}, an isotope with spin 7/2 and magnetic moment -0.51 nm. The proportion of U^{234} in such a sample must be kept small on account of the large radioactive heating produced by this isotope.

APPENDIX

Electrical resistivity of uranium hydride

Some recent measurements of the electrical resistivity of uranium hydride made by M.B Goitein and M.C Richards in the Clarendon Laboratory are reported in this section (private discussion, 1960). A constant current was maintained through the longer of the two pieces of solid uranium hydride which were used for the heat capacity measurements described earlier. The potential across the sample, which is then proportional to the resistivity, was measured as a function of temperature between the boiling point of liquid oxygen and room temperature. The curve obtained near the ferromagnetic Curie point (~ 170°K) is given in figure 28. Absolute values of the resistivity ρ estimated by Goitein and Richards are given below. There is an uncertainty of 30% in these figures due to the irregular shape of the sample, but the relative values are probably correct to the accuracy quoted.

T °K	ρ ohm.cm.
241	1.64×10^{-4}
167	1.37×10^{-4}
93	0.82×10^{-4}

We see that the resistivity of uranium hydride has the same order of magnitude as that found in metals. But it is greater than that of uranium metal, whose resistivity is 0.29×10^{-4} ohm.cm. at

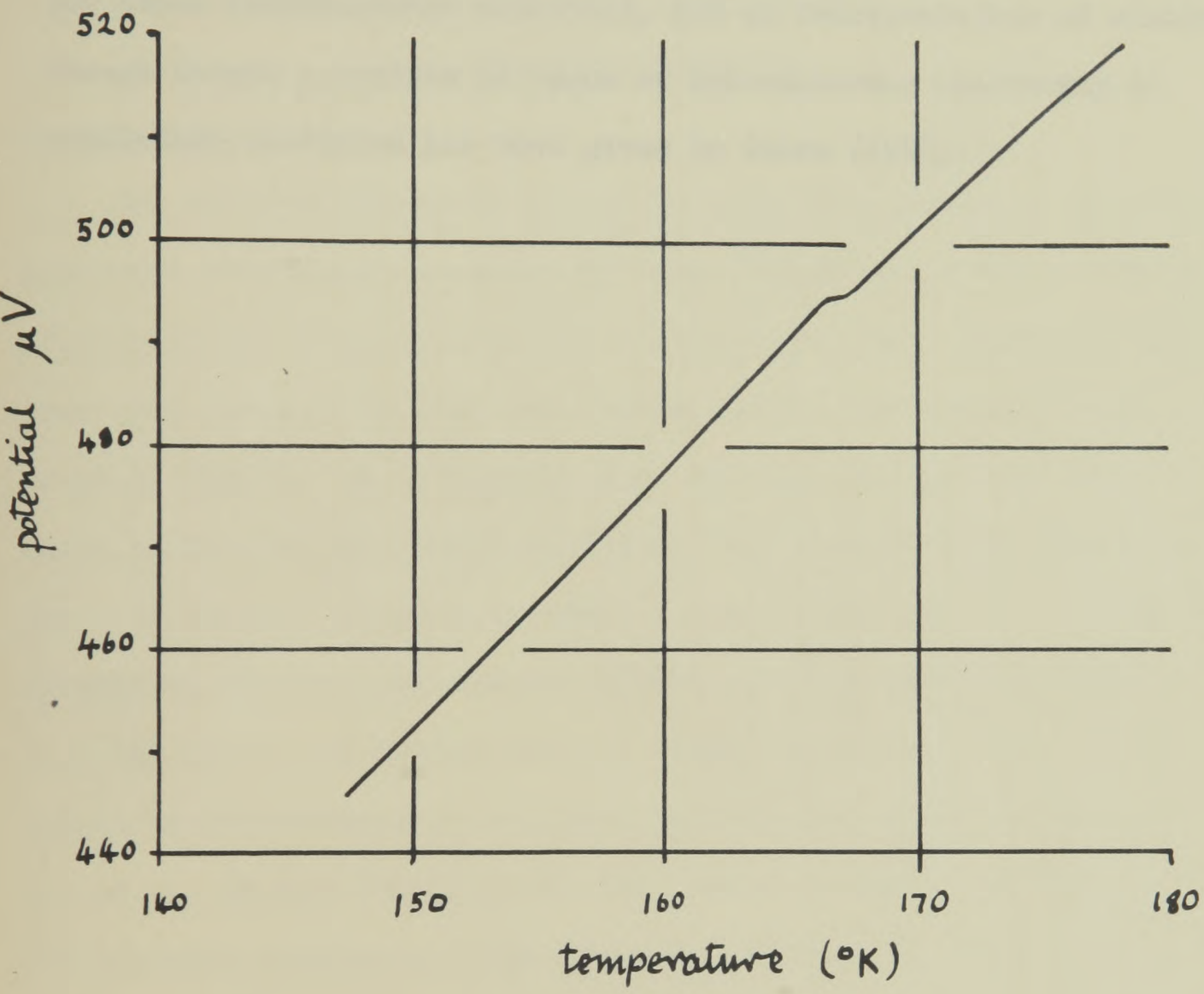

Figure 28 Electrical resistivity of UH_3 (after Goltein and Richards). The potential across a sample for constant current is given as a function of temperature.

273°K. Figure 28 shows a slight anomaly in the resistivity near the Curie point. A review of experimentally observed resistivities for other ferromagnetic materials, and an interpretation of similar though larger anomalies in terms of spin-disorder scattering of conduction electrons has been given by Coles (1958).

CHAPTER FIVE

THE INTERPRETATION OF HFC RESULTS IN FERROMAGNETIC MATERIALS

Introduction

The electron structure of the 3d transition metals is frequently discussed with models in which the outer electrons of the constituent atoms populate d-like states and a conduction band. Models of this type were proposed by Mott and Stevens (1957), and by Lomer and Marshall (1958). In particular that of Lomer and Marshall was based on results from X-ray scattering experiments which gave only two d-electrons per atom in metallic iron (Weiss and deMarco, 1958). Batterman, Chipman, and deMarco (1961) have now concluded however that the atomic scattering factors cannot be used to determine the number of 3d electrons in metallic iron because of the spreading out of the 3d wave functions in the metal. Recently another model for the band structure of the transition metals and their alloys has been described by Goodenough (1960). In this chapter we shall use Goodenough's model, which successfully describes many properties of the transition metals, especially those of the first long period. We should remember that these models are empirical in nature and do not rest on a firm theoretical basis, but they do provide a plausible picture of the electrons in the metals and alloys which

serves as a background for experimental work, and which is likely to improve as more data become available.

Goodenough's model is based on three postulates: (1) localized and collective 3d electrons may be simultaneously present; (2) localized 3d electrons obey Hund's rule and may therefore introduce an atomic moment; and (3) if nearest neighbour antiferromagnetic order can be propagated throughout the lattice, and if the overlapping orbitals are half or less filled, the collective electrons may be stabilized by bonding band formation. It is also concluded that if these orbitals are more than half filled a net ferromagnetism of the "extra" electrons is possible. When nearest neighbour antiferromagnetic order cannot be propagated throughout the lattice the electrons form a conventional metallic band, which may be spontaneously magnetized if an atomic moment from localized electrons is also present. The actual configurations proposed will be given later as required.

In this chapter we shall take the experimental results of this thesis in combination with other published work on hyperfine coupling in the 3d transition metals and alloys and try to find an interpretation of them with the help of Goodenough's model. We shall discuss the two main contributions to H_{eff} at the atomic nuclei - that from the conduction electrons H_c and that from electrons on the same atom H_a (see page 77).

The main results are as follows : The hyperfine fields on impurity gold and tin atoms in the ferromagnetic metals differ greatly so it is not easy to estimate H_c for the matrix atoms from them in a simple way. But since no fields have been observed at vanadium nuclei in a ferromagnetic V-Fe alloy and at copper nuclei in ferromagnetic Ni-Cu alloys, H_c is probably not large.

The relatively large negative hyperfine fields on magnetic atoms in the bcc alloys are considered to be caused mainly* by localized e_g electrons and by antibonding t_{2g} electrons. If this is so initial additions of cobalt and nickel to iron are shown to contribute electrons to the t_{2g} states on iron, but for more than 50% cobalt in the Fe-Co alloys the added electrons go onto the cobalt atoms.

In the fcc alloys the effective field on iron seems to arise mainly* from localized e_g electrons with another contribution from t_{2g} electrons in a metallic band. This latter contribution depends on the average atomic moment, and causes H_{eff} on iron nuclei in the Fe-Ni and Ni-Cu systems to fall slightly as the electron concentration is increased.

The discussions which follow show that, although at present there is no exact theory of the electronic structure of the transition metals, and of the hyperfine fields, the experimental results can be partly understood in terms of Goodenough's model. It should be

* via inner s-electron polarization

emphasized, however, that the ideas proposed in this chapter are tentative and may well need modification as more experimental and theoretical results become known. Finally we mention that as this chapter was being written an article by Watson and Freeman (1961b) appeared which gives a discussion of the origin of the effective fields in magnetic materials but there is no discussion for the case of alloys as presented here.

The conduction electrons

We shall find it convenient to consider first the field H_c produced by the conduction electrons. The part due to conduction electron polarization is given by

$$H = -\frac{8\pi}{3}\beta|\psi(0)|^2 np, \qquad \ldots (1)$$

where β is the Bohr magneton, n is the number of conduction electrons per atom, and p is their polarization. $|\psi(0)|^2$ is the probability density at the nucleus of an s-conduction electron near the Fermi surface.

There is a further positive contribution due to the mixing of 4s functions into the 3d band. Anderson and Clogston (1961) have stated that there is also an antiferromagnetic contribution to the conduction electron polarization caused by this mixing. This almost exactly cancels the ferromagnetic polarization due to mixing, and leaves only the true exchange polarization given by equation (1).

Let us now examine some of the data available for the hyperfine

fields at non-magnetic impurity atoms in the ferromagnetic transition metals since we expect these fields to arise mainly from the conduction electron polarization. Table 1 shows the hyperfine fields in kilogauss obtained from Mossbauer experiments on 1% tin at ~100°K (Boyle, Bunbury, and Edwards, 1960), and 0.02% gold at 4°K (Shirley, Kaplan, and Axel, 1961) in iron, cobalt, and nickel. For comparison the table also gives the values of H_{eff} corrected to 0°K at impurity iron nuclei from the Mossbauer experiments of Wertheim (1961).

Table I

nucleus	host metal		
Nucleus	Fe	Co	Ni
Fe^{57}	-342	312	280
$Sn^{119\,m}$	- 88(±4)	-26.5(±1.5)	+16.5
Au^{197}	282(±10)	122(±10)	⩽30

Hyperfine fields on gold in iron obtained from gamma-ray experiments are in serious disagreement with the above value. Samoilov et al. (1960) obtained a field of ⩾700 kG at Au^{198} nuclei for 0.3% gold in iron (the values quoted on page 140 should be reduced by 25-35% since a note of the correction at the end of the Russian paper was overlooked). More recently Kogan et al. (1961) have obtained a field of ⩾2,000 kG at Au^{199} nuclei for 0.7% gold in iron. Since these results are, as yet, unexplained, it is planned in Oxford to repeat the gamma-ray experiment for Au^{198} in iron.

One should remember that it is not easy to obtain accurate values of H_{eff} from the gamma-ray method, as illustrated for the Fe-Co alloys in figures 3 and 18.

On the other hand, in the Mossbauer experiments of Shirley et al., the nuclear moment of the excited state of Au^{197} was not actually measured. Its value based on the shell model was assumed to be 1.6 nm.

Certain regularities appear in table I. The numerical value of H_{eff} at Sn and Au nuclei in the host metals increases with increasing atomic number of the solute. It also decreases from iron to nickel for a given solute, probably because of the change in the saturation magnetization.

The experiments of Boyle et al. show that H_{eff} at Sn in iron and in cobalt is negative, whereas the theory outlined earlier predicts positive values for H_c. Boyle et al. have suggested that, apart from negative conduction electron polarization, the negative field may be produced by overlap of the 4s electrons in the tin atoms onto the 3d electrons of the solvent. The latter effect varies more strongly than the conduction electron polarization term from iron to nickel because it depends both on the magnetization and on the distribution of the 3d electrons. If it also causes the large fields on the Au nuclei in iron and in cobalt (Shirley et al., 1961) one expects them to be negative too. The effect would also prevent one from deducing H_c for the matrix atoms in a simple way

from the above results.

The effective field on the hydrogen nuclei in UH_3 (30 kG, page 140) suggests that H_c will be small. But although UH_3 exhibits metallic properties, its structure is different from that of the transition metals and the conduction electrons probably behave differently in this substance. However we know from the following experiments on 3d transition metal alloys that H_c is probably small in these cases also.

Measurements by Wei, Cheng and Beck (1961) for the alloy $V_{33}Fe_{67}$, whose saturation moment is about 1.0 β/atom, show that the value of H_{eff} at the V^{51} nucleus is less than 60.9 kG. Vanadium probably has no localized moment because, according to the model for the bcc structure, it has three conduction electrons in (sp^3) orbitals and two 3d electrons spin paired in t_{2g} bonding orbitals. In addition my own recent measurements (not described in this thesis) for the alloy $Ni_{78}Cu_{22}$, whose saturation moment is about 0.4 β/atom, show that H_{eff} at the copper nuclei is less than 26 kG. In both these cases we have upper limits for H_c. On the other hand, since H_{eff} at tin nuclei in nickel is positive, this field (+16.5 kG) gives a lower limit for H_c in nickel.

It should be emphasized that the above remarks are tentative. Blatt (unpublished) has presented another possible view. In his model the conduction electrons have hybridized d-s wave functions,

and H_c is assumed to be negative in iron and in cobalt but positive in nickel as indicated by the values of H_{eff} on impurity tin nuclei in these metals. If this is so, H_c makes a fair contribution to the negative hyperfine field in iron, and also accounts for the decrease in the field on impurity iron atoms in cobalt and nickel (table I).

The best model for deriving values of H_c is still a matter of conjecture, since at the present time not very many data are available. The following Knight Shift experiments, which we may usefully consider at this point, show however that it may not be possible to describe H_c in the transition metals by means of a simple theory. The Knight shift* is an increase in the nuclear magnetic resonance frequency in a Pauli paramagnetic metal relative to that of the nucleus in non-magnetic surroundings. It is caused by the hyperfine interaction between the nuclear magnetic moments and s-type conduction electrons, and is proportional to the Pauli susceptibility χ_p, and to $|\psi(0)|^2$. Measurements of the Knight shift in dilute alloys of manganese in copper (Owen, Browne, Knight, and Kittel, 1956; Owen, Browne, Arp, and Kip, 1957) have shown it to be unaffected by the presence of manganese, whereas marked effects due to the exchange interactions between the $3d^5$ manganese ion electrons and the 4s conduction electrons of the crystal were expected. Asymmetry in the resonance line shape

* See Knight (1956).

suggested that the polarization falls off with distance from a manganese ion, becoming negligible at about five lattice spaces. This and other experimental evidence lead to an s-d exchange of 1/10th to 1/20th of the free ion value. Theoretical work by Yosida (1957) has shown that the polarization is indeed concentrated around the manganese ions. For a fcc lattice H_c is negative at the nearest neighbour distance and positive at the next nearest neighbour distance.

Finally it should be mentioned that heat capacity measurements for the ferromagnetic V-Fe alloys well below $1^{\circ}K$ might give some useful data. These alloys would be better than the Cu-Ni alloys because the saturation magnetization is larger, the V^{51} nucleus (spin 7/2) has a larger magnetic moment (5.148 nm) than that of copper, and if Goodenough's model is correct, only the conduction electrons are expected to contribute to H_{eff} at the vanadium nucleus. In $V_{25}Fe_{75}$ at $0.2^{\circ}K$, for example, one should be able to detect an effective field as low as 10 kG.

The 3d electrons

The contribution to H_{eff} from electrons on the same atom is given by $H_a = -A\bar{S}/g_N\beta_N$, where A is the hyperfine coupling constant and $\bar{S}$ is the mean spin per atom (page 78). In a pure metal H_a should therefore be proportional to the magnetization. This relation has been verified experimentally by observing that H_{eff} has the same temperature variation as the magnetization. This has

been done for iron both in Mossbauer experiments (Nagle et al., 1960) and from the nuclear magnetic resonance (Robert and Winter, 1960; Budnick et al., 1961), and for cobalt from the nuclear magnetic resonance (Portis and Gossard, 1960; Jaccarino, 1959). The expressions from spin wave theory and from Stoner's collective electron theory both fit the measurements quite well. But for measurements on nickel (NMR. Bruner et al., 1961) the agreement is not so good.

The above remarks are not quite accurate because there is a slight dependence of A on temperature at constant volume. This was shown by Benedek and Armstrong (1961) from measurements of the pressure and temperature dependence of the Fe^{57} nuclear magnetic resonance frequency in ferromagnetic iron. H_a is therefore not strictly proportional to $\bar{S}$. However the change in A between $0^\circ K$ and $300^\circ K$ is less than 1%, so in the following sections A is taken as approximately constant for a given metal.

The pure metals

It is now well known from Mossbauer experiments (Hanna et al. 1960 a) and from nuclear magnetic resonance (Robert and Winter, 1960; Budnick et al., 1961) on Fe^{57}, that the effective magnetic field at the nuclei in metallic iron is 340 kG, corrected to $0^\circ K$, and it has a negative sign (Hanna et al., 1960b). It seems therfore that the main contribution to H_{eff} comes from the inner s-electron polarization (H_{al}, page 120).

Spin polarized Hartree-Fock calculations for iron with d^6 and d^8 configurations give a negative value for H_{al} which is, however, smaller than that required experimentally (see Watson and Freeman, 1961a). As described later Goodenough's model requires five d-electrons in metallic iron. Since H_{al} is sensitive to d-electron behaviour, calculations for this case would be interesting.

Early measurements of H_{eff} in cobalt by gamma-ray anisotropy and by specific heat measurements have been indicated in figure 18. The most accurate measurements, which are by nuclear magnetic resonance, give H_{eff} = -217 kG in fcc cobalt and -227 kG in hcp cobalt, corrected to $0^{\circ}K$ (Portis and Gossard, 1960. Street et al., 1961. Hardy, 1961). These results show that since H_{eff} is almost the same in both cases the interaction between the nuclear and electronic magnetic moments in hexagonal cobalt must be small, and hence H_{a2} is also small (page 78).

Bruner et al. (1961) have measured the nuclear magnetic resonance frequency of Ni^{61} in metallic nickel at $298^{\circ}K$, and $78^{\circ}K$. Their results give an estimate of 170 kG for H_{eff} at room temperature, and 185 kG at $0^{\circ}K$ by extrapolation. The hyperfine coupling constant for nickel is thus roughly twice as large as for iron and cobalt. Expressing it in the form H_{eff}/n_{eff}, where n_{eff} is the number of Bohr magnetons per atom at saturation, we obtain 153 kG/β_B for bcc iron, 132 for hcp cobalt, and 281 for fcc nickel.

Iron-cobalt alloys

The values of H_{eff} at the iron nuclei in the iron-cobalt alloys at room temperature are known from the Mossbauer experiments of Johnson et al.(1961), who expressed their results in terms of the field in pure iron. If we take this to be 340 kG at $0^{\circ}K$, then we find effective fields for the various compositions at $0^{\circ}K$ as shown in figure 29. The field extrapolated to $0^{\circ}K$ found by Wertheim (1961) at impurity iron atoms in cobalt is also shown, and is in agreement with the results of Johnson et al. The slight discrepancy in figure 29 arises because, whereas Wertheim used the cobalt magnetization curve to correct H_{eff} from room temperature to $0^{\circ}K$, we have effectively used the iron magnetization curve for all the alloys. The slight error introduced in this way will not affect the discussion to be given later.

For the field at the cobalt nuclei we refer to figure 18, page 116. The gamma-ray anisotropy measurements, and the specific heat measurements of Arp et al. suggest that H_{eff} for small quantities of cobalt in iron should be ~320 kG. Dash et al.(1960 1961) have shown from the intensity changes of the Fe^{57} Mossbauer spectrum at low temperatures that the hyperfine field at Co^{57} parent nuclei in iron is $-300(\pm 20)$kG. More recently an accurate determinati on of the field has been obtained by nuclear magnetic resonance (Koi and Tsujimura, 1961) yielding the value of 289.7 kG at $0^{\circ}K$ for 1% Co^{59} in iron. As predicted

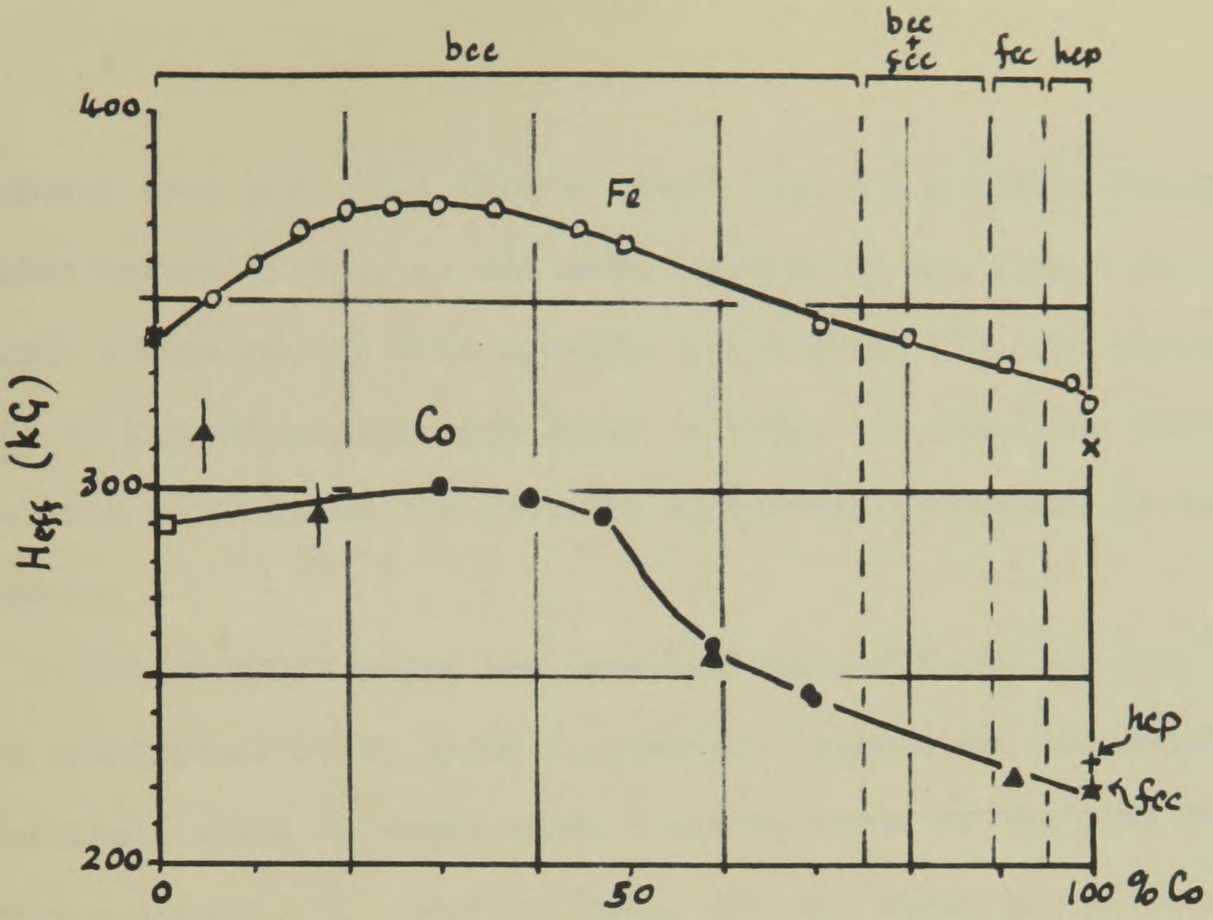

Figure 29 Heff at iron and cobalt nuclei in Fe-Co alloys. o Johnson et al., x Wertheim (Mössbauer). □ Koi and Tsujimura (NMR). ▲ Arp et al., • Exell (specific heat). + NMR results for fcc and hcp cobalt.

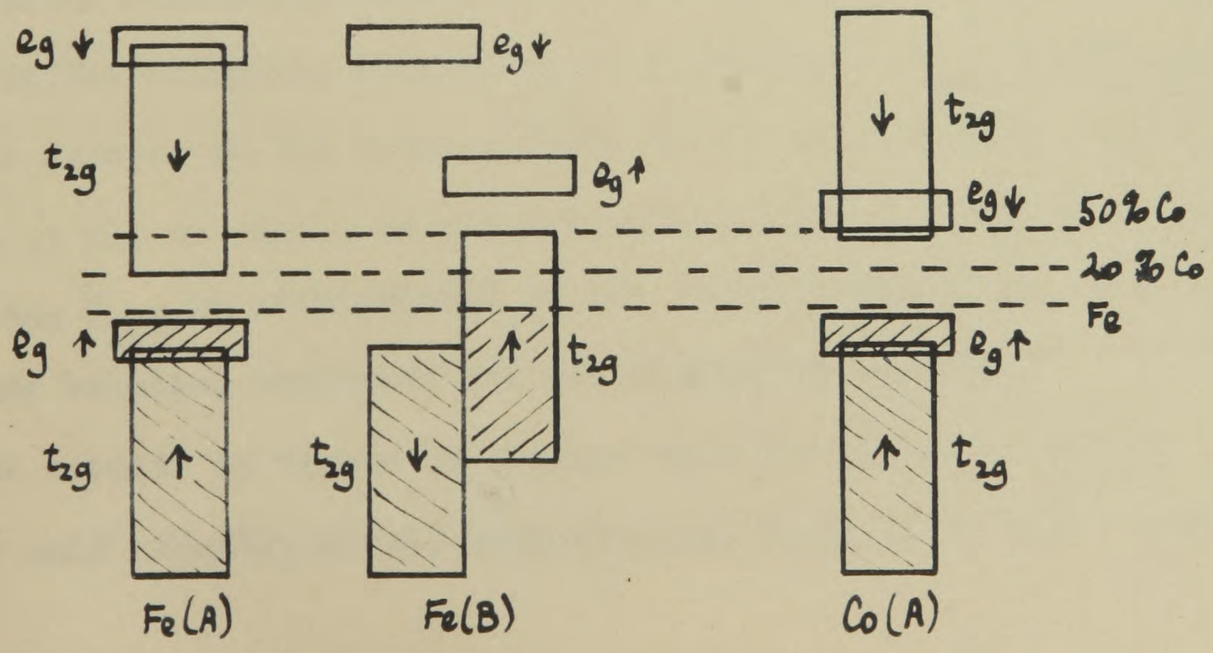

Figure 30 Proposed 3d band structure for bcc Fe-Co alloys.

by Johnson (see page 121) this is lower than the previous determinations. The best values of H_{eff} at the cobalt nuclei in the alloys from nuclear magnetic resonance and from specific heats below $1^{o}K$, are plotted in figure 29 for comparison with those on iron. We shall now discuss these data in terms of the probable electronic structures in the bcc phase.

In Goodenough's model bcc iron has the configuration $(3d)^5(4sp^3)^3$. Since antiferromagnetic order is possible between the two simple cubic sublattices, which we shall label A and B, three of the five 3d electrons occupy a t_{2g} bonding band. The two remaining 3d electrons, which are responsible for the atomic moment, occupy localized e_g states on one sublattice (say A) and antibonding t_{2g} states on the other. For a given iron atom resonance between these two configurations occurs. Figure 30 shows a qualitative diagram of this band structure.

Since we concluded earlier that the contribution to H_{eff} from H_c was probably relatively small for the 3d transition metals, we shall assume in the following discussion that changes in H_{eff} in the alloys indicate changes in the configuration of the 3d electrons. Following Johnson et al. we shall, as a first approximation, assume that for a given atom H_{eff} is proportional to the atomic moment, i.e. that the hyperfine coupling constants are not changed by alloying.

The results in figure 29 suggest that the moment on cobalt changes only slightly in the concentration range 0% to 50%. Cobalt

seems to favour the A-configuration, in contrast with Goodenough's proposal, while the extra 3d electrons go into the $t_{2g}\uparrow$ band on the Fe(B) atoms, thus producing the observed increase in H_{eff} at the iron nuclei. This view is also supported by the drop in the electronic specific heat of these alloys (figure 20, page 124). Beyond 50% cobalt the $e_g\downarrow$ and $t_{2g}\downarrow$ bands of cobalt start to fill and give rise to the steep drop in H_{eff} at the cobalt nuclei, and to the rise in the electronic specific heat. At the same time partial filling of the $t_{2g}\downarrow$ band on the A-atoms of iron may contribute to the slower fall in H_{eff} at the iron nuclei. A sketch of the proposed 3d band structure for cobalt in the bcc Fe-Co alloys is included in figure 30.

Finally it should be mentioned that neutron diffraction data quoted by Goodenough (Shull, unpublished) indicate that in ordered iron-cobalt alloys one type of atom carries a moment of -2.0 β, while the other has -2.9 β. The present model predicts that the higher moment is on the Fe(B) atoms.

Close packed alloys

The only measurement of a hyperfine field in the cobalt-nickel system is that of Arp et al. for $Co_{60}Ni_{40}$ (fcc) where $H_{eff}(Co)$ = 161($\pm$3) kG. The cobalt rich alloys are hcp, and the nickel rich alloys are fcc, with the transition at $Co_{65}Ni_{35}$. In these structures nearest neighbour antiferromagnetic order is not possible so the electrons are in metallic bands, the populations being $(3d)^{9.45}(4s)^{0.55}$

for pure nickel, and $(3d)^{8.25}(4s)^{0.75}$ for pure cobalt. The presence of unpaired locallized d_{z^2} electrons in hcp cobalt, and e_g electrons in fcc nickel, produces spontaneous magnetization in the d-bands.

The value of -80 kG for the effective field at impurity cobalt nuclei in nickel, which has been quoted by Wertheim (1961) and by Shirley et al. (1961) appears to be a linear extrapolation from the specific heat data of Arp et al. and not an actual measurement. Since the change in the average atomic moment is linear between cobalt and nickel, this procedure may give approximately correct results. There are no measurements of the effective field on the nickel nuclei in these alloys.

Values of the hyperfine field at iron nuclei in iron-nickel alloys deduced from the data of Johnson et al. are shown in figure 31. Wertheim's result for a trace of iron in nickel is also indicated. In the bcc region the behaviour is similar to that in the iron-cobalt alloys. This suggests that initial additions of nickel contribute electrons to the $t_{2g}\uparrow$ band of Fe(B). In the fcc region we may compare the values of H_{eff} directly with the atomic moments which are known from the neutron diffraction data of Shull and Wilkinson (1955) - see figure 32. It is obvious that H_{eff} is not proportional to the atomic moment.

The d-band in Goodenough's model for fcc nickel is sketched in figure 33. The observed atomic moments are well explained if

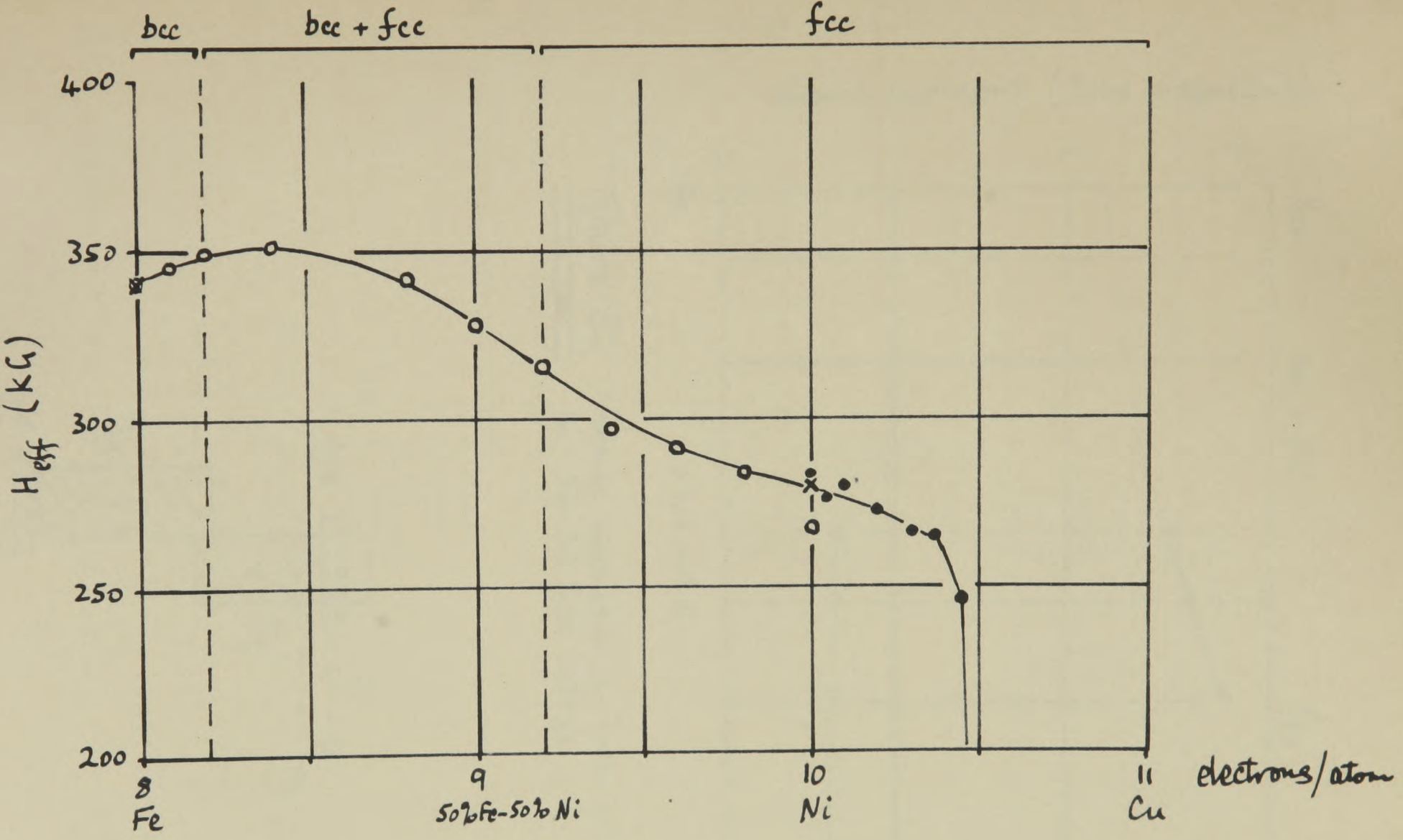

Figure 31 H_{eff} at iron nuclei in Fe-Ni and in Ni-Cu alloys.
o Johnson et al., X Wertheim, • Wertheim and Wernick.

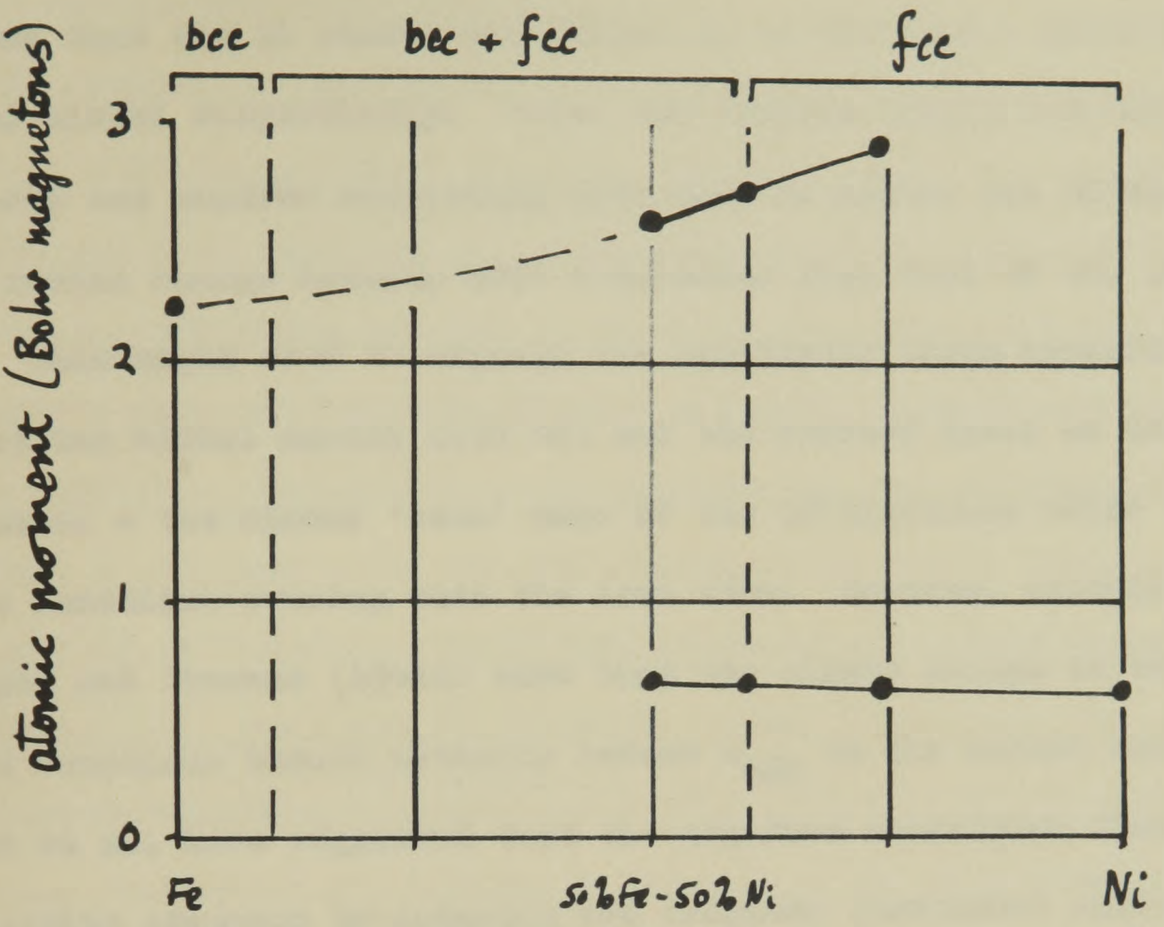

Figure 32 Atomic moments on iron and nickel in Fe-Ni fcc alloys.

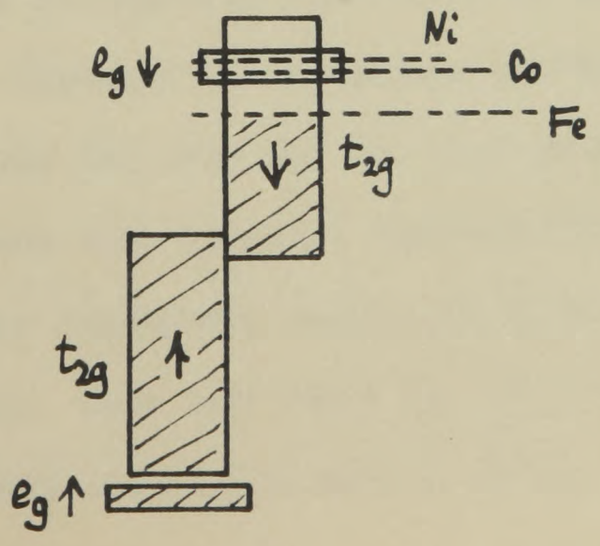

Figure 33 3d band structure for fcc metals.

we assume that the 3d states are filled up to the levels shown for iron and nickel respectively. Weiss and Freeman (1959) have shown from X-ray and neutron scattering data that in nickel the 3d↑electrons have a radial charge density more compressed than that of the 3d↓electrons. This might seem to explain the relatively large hyperfine field at the nickel nuclei (170 kG) and the reduced field on the iron nuclei - the nickel 'sees' more of the 3d↑electrons while the 3d↓wave functions overlap onto the iron atom. However, calculations by Watson and Freeman (1961a) show that the slight change in the 3d wave functions should actually reduce H_{eff} on the nickel nuclei. Johnson et al. have suggested that the negative conduction electron polarization proposed by Anderson and Clogston (mentioned earlier) might account for the reduced hyperfine field on iron. At present these phenomena are not really understood.

Iron impurities in other metals

Mossbauer experiments have shown that there is no observable hyperfine field down to 4°K on impurity iron atoms in the antiferromagnetic transition metals chromium and manganese (Wertheim, 1961). The exchange coupling between the iron and the host metal spins is therefore small. This agrees with magnetic susceptibility measurements for alloys of chromium containing small quantities of iron (Newmann and Stevens, 1959). They show that the iron atoms have a moment of 2 β which is freely orientable down to 90°K.

In Goodenough's model bcc chromium and manganese have a band structure similar to that of Fe(A) shown in figure 30. The lower t_{2g} and e_g subbands overlap slightly. Chromium has 2.99 t_{2g} bonding electrons and 0.01 localized e_g electrons per atom, while manganese has three t_{2g} electrons and one e_g electron per atom. The localized e_g electrons are antiferromagnetically aligned. Newmann and Stevens have tentatively suggested that the presence of iron in chromium stabilizes a structure with two interpenetrating simple cubic sublattices each of which is itself antiferromagnetic. This explains the weak iron-chromium coupling because an impurity iron atom has four nearest neighbour chromium atoms with spin up, and four with spin down. The three t_{2g} bonding electrons on the iron atom would not be preferentially oriented, so the two localized e_g electrons (which are coupled to the t_{2g} electrons by Hund's rule) would not produce a static effective field at the iron nucleus.

We note in passing that one could measure the hyperfine field in manganese by the specific heat method. The value of H_{eff} at the nuclei of the Mn^{2+} ions in MnF_2 is known to be about 660 kG from the low temperature specific heat data of Cooke and Edmonds (1958). For the Mn^{2+} ion S = 5/2. In the case of manganese metal the atomic moment is 1.1 β (Shull and Wollan, 1956), which presumably arises mainly from the single e_g electron. H_{eff} should then be about 130 kG if the hyperfine coupling constant A is the same for the metal as for

the ionic salt. The expected contribution to the specific heat ($\sim 1.0/T^2$ millijoules/mol.deg.) should be distinguishable below 1°K from the rather large electronic contribution (18T millijoules/mol.deg.).

The hyperfine field at impurity iron atoms in some fcc alloys has been determined from Mossbauer experiments. In Co_8Pd_{92}, (Nagle et al., 1960) no hyperfine field was observed above the ferromagnetic Curie point (275°K). Below the Curie point at 88°K, the field was found to be approximately the same as that for pure iron (330 kG). The values of H_{eff} at iron nuclei in nickel-copper alloys at 4°K have also been determined (Wertheim and Wernick, 1961) and are plotted in figure 31.

It seems from the Co-Pd result that the field at the iron nuclei is caused mainly by its own unpaired 3d electrons which have a resultant spin similar to that in iron metal. But in the nickel-copper system the fields at the iron nuclei lie on a curve which is a smooth continuation of the results for the iron-nickel alloys. So in this case the values of H_{eff} at the iron nuclei may be reduced slightly by electrons on the surrounding atoms as discussed earlier. The diagram in figure 33 suggests that it is the localized $e_g\uparrow$ electrons which are stable, while the metallic t_{2g} electrons cause the observed variations of H_{eff} with alloy composition.

PART THREE

LOW TEMPERATURE HEAT CAPACITY OF TITANIUM-IRON AND ZINC-MANGANESE FLUORIDE

CHAPTER ONE

LOW TEMPERATURE HEAT CAPACITY OF TiFe

Introduction

Recent heat capacity measurements on titanium-iron (TiFe) between 1.4°K and 4°K have been found to deviate from the usual law of the form $C = \gamma T + \beta T^3$ at low temperatures (Beck, private communication, 1959). When this law is followed a plot of C/T against T^2 gives a straight line with a positive slope. The experimental result for TiFe sent from Illinois to the Clarendon Laboratory by Professor P.A Beck (1959) and later published by Schroder and Cheng (1960) is sketched in figure 1. An attempt to interpret the high values of C/T at the lower temperatures in terms of the tail of a Schottky anomaly fails. The best fitting law of the form $C = \gamma T + \beta T^3 + \alpha/T^2$ has a negative value of β, which is impossible. Similar results have also been found for Ni-Cu alloys by Guthrie, Friedberg, and Goldman (1959), and for V-Fe and Cr-Mn alloys by Cheng, Wei, and Beck (1960).

To obtain more information on the anomaly Professor Beck sent the TiFe sample to Oxford for heat capacity measurements below 1°K. The results of these measurements are described and discussed in the present chapter.

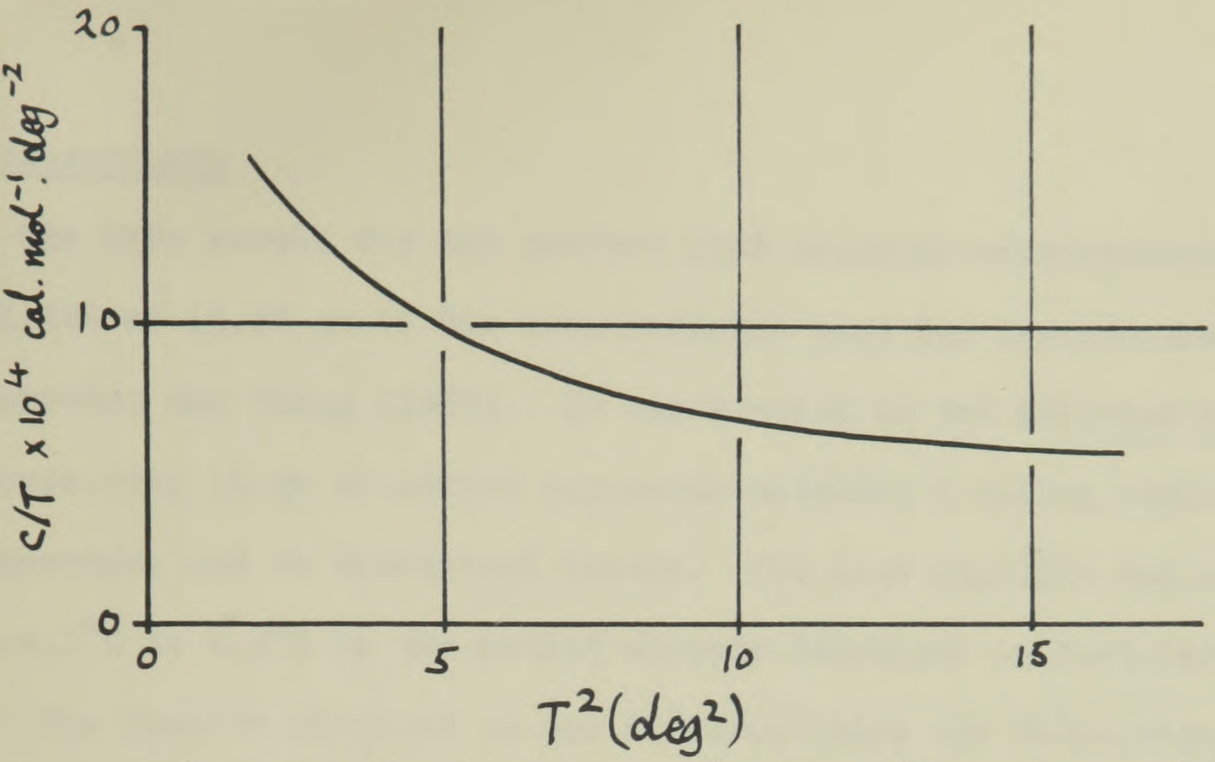

Figure 1 Heat capacity of TiFe (Schroder and Chong)

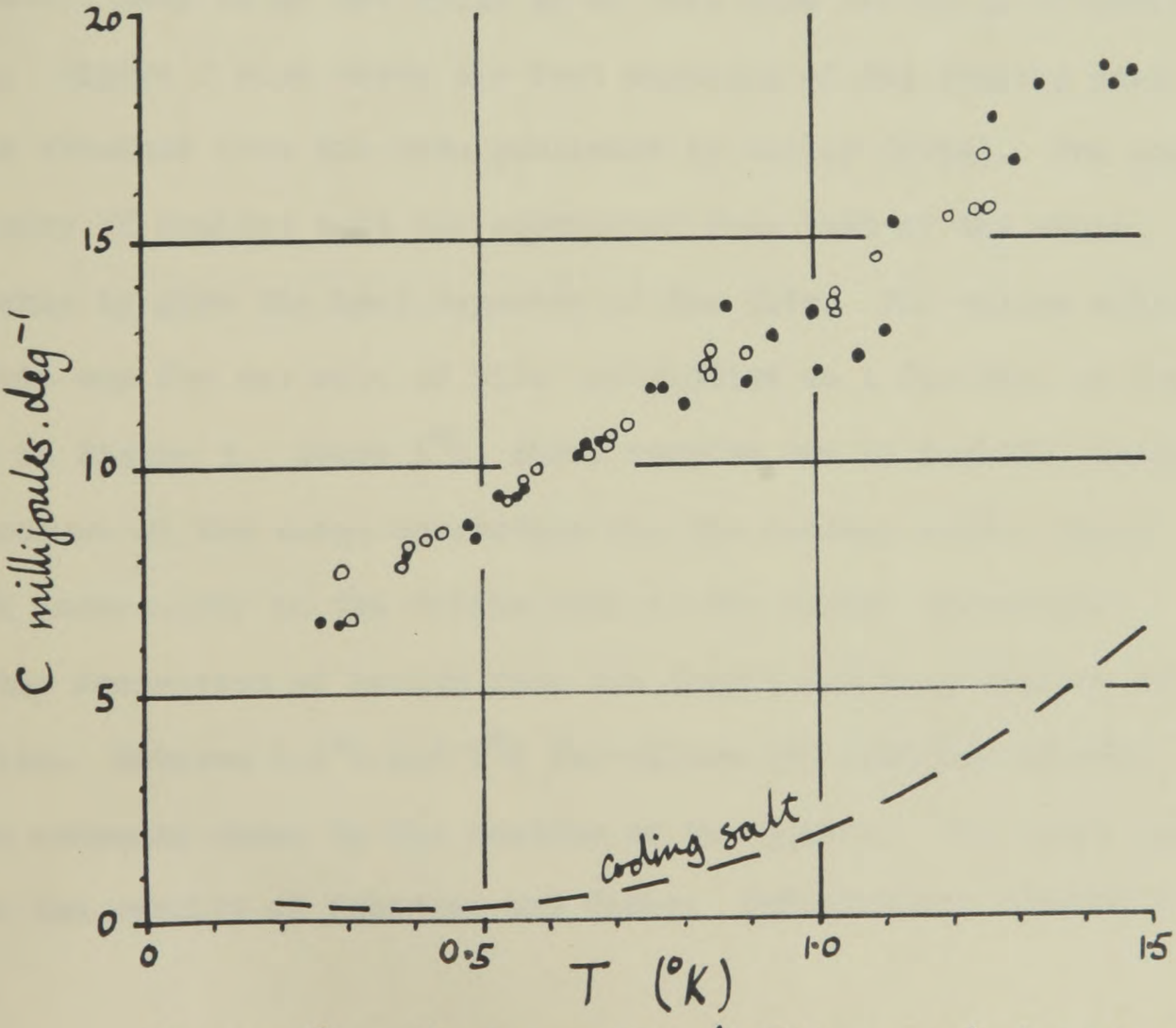

Figure 2 Heat capacity of TiFe sample (15.92 gm) and 15 gm of cooling salt.

The experiments

The TiFe sample for the present heat capacity measurements consisted of 15.92 gm of the same material used for the measurements of Schroder and Cheng (1960). It was mounted in the cryostat with approximately 15 gm of cerium magnesium nitrate, a carbon resistance thermometer, and an electrical heater. The heat capacity was measured from 0.3°K to 1.4°K by the method already described in Part Two.

The results obtained on two different days are shown together in figure 2, those shown by open circles probably being the most accurate. These points represent the total heat capacity of the assembly, that is of the 15.92 gm of TiFe plus the 15 gm of cooling salt. Figure 2 also shows the heat capacity of the cooling salt alone obtained from the data published by Bailey (1959). The heat capacity of cooling salt was subtracted from that of the whole assembly to give the heat capacity of the TiFe. The values obtained in this way for one mole of TiFe are plotted as a function of temperature in figure 3. Above 1°K, these results are of doubtful accuracy on account of the large correction for the cooling salt. Below 0.4°K uncertainty in the calibration of the carbon thermometer and the desorption of helium from the sample may have spoiled the results. Between 0.4°K and 1°K the values are probably correct to an accuracy shown by the scatter of the points. The small crosses show the results of Schroder and Cheng. Satisfactory agreement

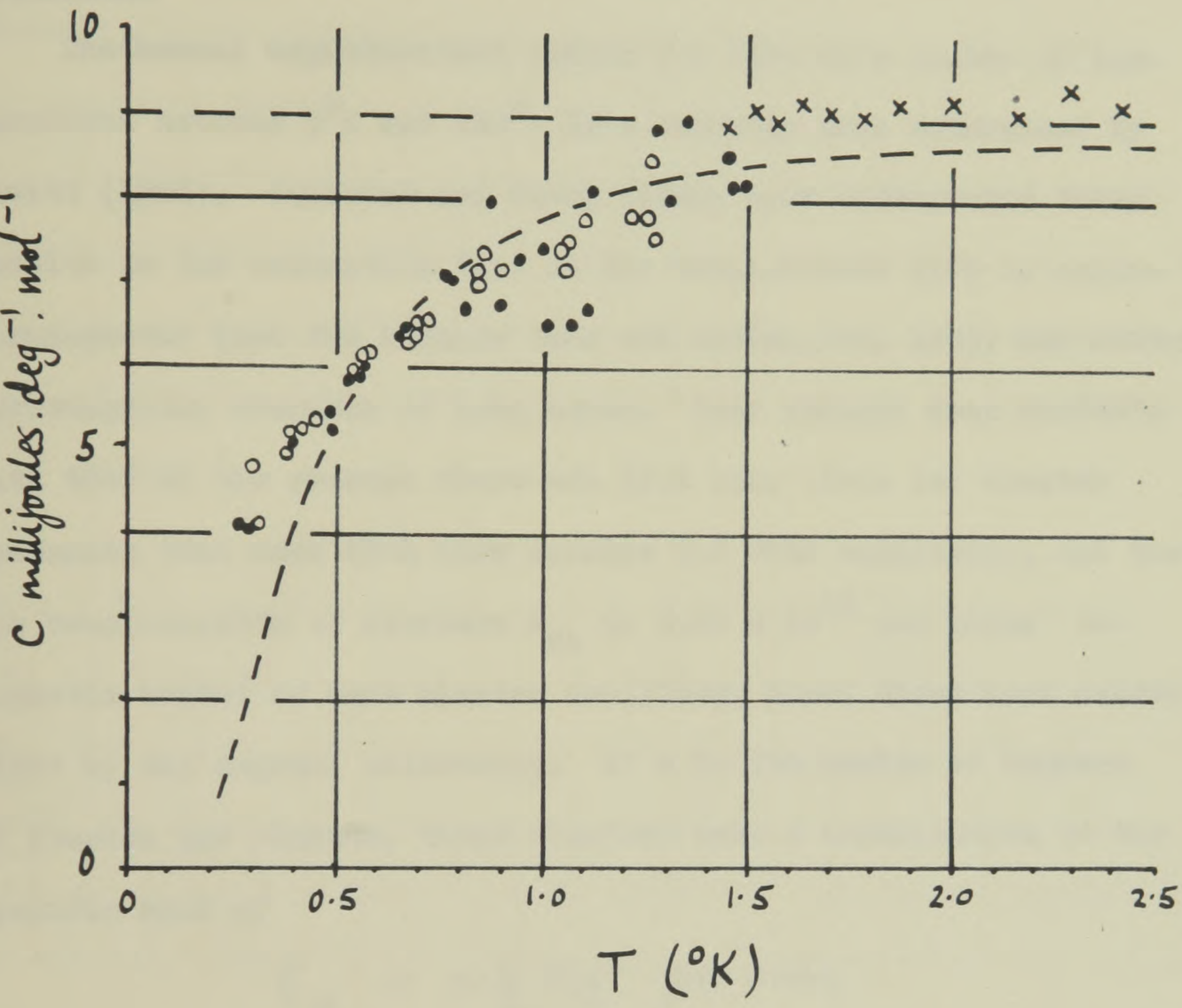

Figure 3 Heat capacity of TiFe. The curve shows an Einstein function for

$C' = C_E(\infty) = 9$ millijoules.deg^{-1}.mol^{-1}

$T_E = 1.3$ deg.

exists between these and the present results.

Discussion

Isothermal magnetization curves for TiFe at a number of temperatures between 9°K and 110°K have recently been determined by Nevitt (1960). Schroder and Cheng (1960) have interpreted these results on the assumption that at low temperatures TiFe is superparamagnetic (see for example Bean and Livingston, 1959) and contains ferromagnetic clusters of iron atoms. They deduced from Nevitt's data that on the average there are 52.8 iron atoms per cluster (assuming that each iron atom carries 2.2 Bohr magnetons), and that the concentration of clusters N_{cl} is 3.26×10^{20} per mole. The magnetic vector of each cluster oscillates about directions determined by the crystal anisotropy. If z is the number of degrees of freedom per cluster, these clusters make a contribution to the specific heat of

$$C_{cl} = z\frac{k}{2}N_{cl} \quad \text{per mole,}$$

where k is Boltzmann's constant.

Schroder and Cheng found that their heat capacity results for TiFe between 1.4°K and 4°K followed a law of the form $C = \gamma T + \beta T^3 + C'$, where

$$C' = 9.0 \text{ millijoules.mol}^{-1}.\text{deg}^{-1}.$$

C_{cl} is practically equal to C' for z = 4, a very reasonable value

which gives strong support to the theory.

This theory has been worked out in more detail recently by Schroder (to be published; private communication by Beck, 1961). The essential details will now be outlined.

The direction of easy magnetization for iron atoms in a cubic lattice is along one of the 100-axes. Suppose that the magnetization vector of a ferromagnetic cluster is deviated from a 100-axis by a small angle α. The crystalline anisotropy energy is then increased by an amount

$$\Delta E = KV \alpha^2,$$

where K is a constant of the order 6×10^5 erg.cm^{-3} for iron at very low temperatures, and V is the volume of a cluster. The cluster acts like a small gyroscope whose magnetization vector rotates around the 100-axis. The magnetic moment μ of this cluster is given by $\mu = n\beta$, where n is the number of free magnetic electrons per cluster, and β is the Bohr magneton. The effect of the crystal anisotropy on the cluster is equivalent to that of a magnetic field H given by

$$\Delta E = \tfrac{1}{2} \alpha^2 \mu H.$$

H must therefore be equal to $2KV/\mu$, which for iron is 700 gauss.

For a cluster of n spins there are $2n + 1$ equally spaced energy levels separated in energy by $\Delta E = 2\beta H$. Since $2n + 1$ is large ($\simeq 233$ for the clusters in TiFe), the heat capacity of a cluster

can be approximated at helium temperatures by an Einstein function. The heat capacity per mole is then given by

$$C_{cl} = z\frac{k}{2}N_{cl}C_E(T_E/T),$$

where

$$C_E\left(\frac{T_E}{T}\right) = \frac{\left(\frac{T_E}{T}\right)^2 \exp\left(\frac{T_E}{T}\right)}{\left(\exp\left(\frac{T_E}{T}\right)-1\right)^2}.$$

The Einstein temperature T_E, which is independent of the cluster size and depends only on the material, is given by

$$kT_E = 2\beta H.$$

The present heat capacity measurements for TiFe below $1^{\circ}K$, described earlier in this chapter and shown in figure 3, may be fitted to an Einstein function. This was done in the following way. The value of C' for TiFe, given by Schroder and Cheng (1960) and equal to 9.0 millijoules.mol^{-1}.deg^{-1}, was taken to be the value of the Einstein heat capacity function at high temperatures, so that

$$C_{cl} \sim C'C_E(T_E/T).$$

A value of T_E was then chosen to give the best agreement between C_{cl} and the measured heat capacity in the neighbourhood of $0.6^{\circ}K$ where the present measurements are probably the most accurate. The dashed straight line in figure 3 shows the value of C', while the dashed curve shows the values of $C'C_E(T_E/T)$ for

$$T_E = 1.3 \text{ deg.}$$

There is fair agreement between this curve and the experimental points.

The "anisotropy field" H acting on the clusters in TiFe is found from the relation $H = kT_E/2\beta$ to be about 10,000 gauss. Since the magnetic moment and volume of the clusters deduced from Nevitt's data are given by $\mu \simeq 1.03 \times 10^{-18}$ erg.gauss^{-1} and $V \simeq 6.3 \times 10^{-22}$ cm^3 respectively, one finds from the above value of T_E that the crystalline anisotropy energy for TiFe at low temperatures is

$$K = \frac{\mu k T_E}{4\beta V} \simeq 8 \times 10^6 \text{ erg cm}^{-3}$$

This is a little over an order of magnetude greater than that of iron.

If we allow for the effect of the finite number of electron spins n per cluster, the heat capacity is given by $C_{cl} = C'(C_E^{(1)} - C_E^{(2)})$, where $C_E^{(1)}$ and $C_E^{(2)}$ denote the Einstein heat capacity functions for quantum harmonic oscillators of frequency $2\beta H/k$ and $(2n + 1)2\beta H/k$ respectively (see Kurti and Simon, 1935). $C_E^{(1)}$ is the same as $C_E(T_E/T)$, while the characteristic temperature of $C_E^{(2)}$ is given by $(2n + 1)T_E$, that is 303 degrees. $C_E^{(2)}$ is then less than 5% of $C_E^{(1)}$ below 45°K, and this confirms Schroder's approximation for liquid helium temperatures.

Schroder pointed out, however, that since the thermal energy of a cluster cannot be larger than the crystalline anisotropy energy,

the heat capacity of the clusters should decrease to zero at a temperature given by $kT_M \sim KV$. We find that T_M expressed in terms of T_B, is of the order $\mu T_B/4\beta$, giving

$$T_M \simeq 29^\circ K$$

from the present results. Nevitt's magnetization curves for TiFe (see Schroder and Cheng, 1960) indicate that the anisotropy energy is comparable with the thermal energy of the clusters near $9^\circ K$, a temperature rather low compared with $29^\circ K$. But the discrepancy between these two figures is not serious because the above calculations are so rough.

CHAPTER TWO

ZINC-MANGANESE FLUORIDE

Introduction

Schulman and Jaccarino (1957) have observed the nuclear magnetic resonance lines of F^{19} in manganese fluoride (MnF_2) in the paramagnetic region. At the Néel temperature 68°K, below which the manganese fluoride becomes antiferromagnetic, the lines disappeared abruptly because the sudden increase in sub-lattice magnetization shifts them beyond the frequency range of the spectrometer. But in some substances the nuclear resonance has been found to disappear at a temperature above the lambda anomaly in the heat capacity associated with the antiferromagnetic transition (see for example Kim and Sugawara, 1958; Robinson and Friedberg, 1960).

Experiments have been done in the Clarendon Laboratory by Baker and Lourens to measure the Néel temperatures of zinc-manganese fluoride crystals (Baker, Lourens, and Stevenson, 1961). The temperature at which the nuclear magnetic resonance of the fluorine nuclei disappeared on cooling from room temperature was determined as a function of manganese concentration in the mixed crystal. Theoretical work predicts that in magnetically dilute systems co-operative phenomena do not occur for concentrations less than a critical value. Baker, Lourens, and Stevenson compared their results

with a theoretical curve of Sato, Arrott, and Kikuchi (1959) and qualitative agreement was found. Since the nuclear resonance does not always disappear at the Néel temperature, it was decided to look for heat capacity anomalies in zinc-manganese fluoride which would mark the transition from the paramagnetic state to the antiferromagnetic state. Heat capacity measurements on a number of samples of different manganese concentrations were accordingly made by Bailey from 1.5°K to 20°K (1960, unpublished), and by myself from 0.5°K to 2.5°K.

Experiments

The preparation of the samples has been described by Baker, Lourens, and Stevenson (1961). Those used in the present work were as follows -

Composition	mass	
$Zn_{0.89}Mn_{0.11}F_2$	0.619 gm	single crystal
$Zn_{0.82}Mn_{0.18}F_2$	5.45 gm	polycrystalline
$Zn_{0.75}Mn_{0.25}F_2$	1.78 gm	polycrystalline
$Zn_{0.57}Mn_{0.43}F_2$	3.23 gm	single crystals

The samples were mounted in the cryostat with an electrical heater, a carbon resistance thermometer, and cerium magnesium nitrate for magnetic cooling. The heat capacity was measured electrically

from about 0.5°K to about 2.5°K. The results, corrected for the heat capacity of the cooling salt, are shown in figures 1, 2, 3, and 4. The heat capacities per mole are plotted as a function of temperature and the results of Bailey are also indicated. They will be discussed later.

Additional measurements on two of the samples were made without any cerium magnesium nitrate present. The $Zn_{0.82}Mn_{0.18}F_2$ sample was found to cool after adiabatic demagnetization. The final temperatures (as measured on the carbon thermometer) after demagnetizations from initial fields up to 13 kG at 1.16°K are shown in figure 5. The susceptibility of this sample, as measured on a ballistic bridge, was found to obey a law of the form $\chi \simeq a/(T + \theta)$, from 0.5°K to 4°K, where a is a constant and $\theta \simeq 2$°K. This behaviour indicates that the sample is paramagnetic at these temperatures.

In the case of $Zn_{0.57}Mn_{0.43}F_2$ no magnetic cooling was observed, and the susceptibility was too small to measure accurately with the bridge. It is unlikely that this sample is paramagnetic at helium temperatures. These results are consistent with those of Baker, Lourens, and Stevenson (1961) who find that, for less than 25% Mn, mixed crystals of Zn-MnF_2 are antiferromagnetic above 2°K at most, while for 43% Mn co-operative behaviour sets in at 17°K.

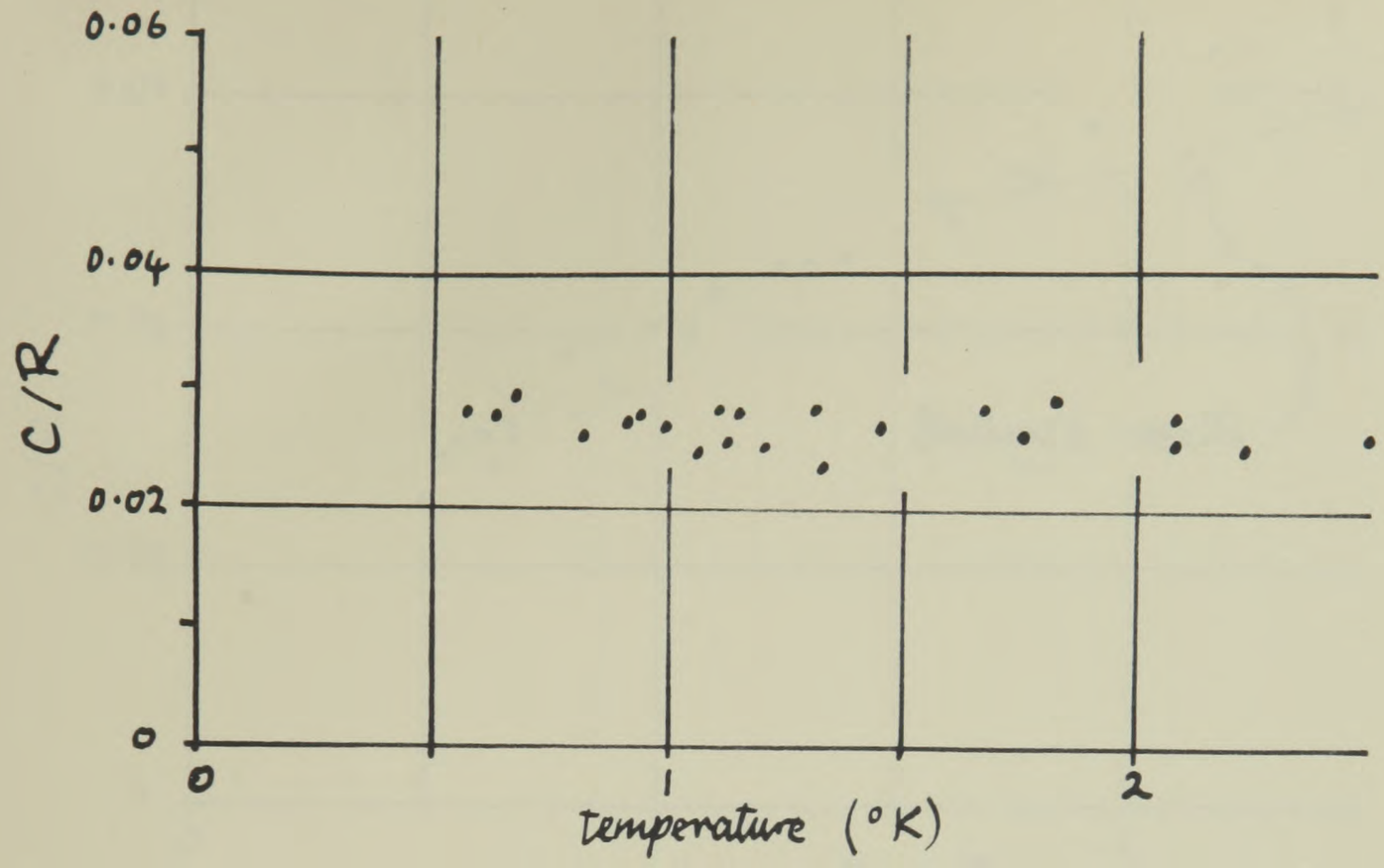

Figure 1 Heat capacity of $Zn_{0.89}Mn_{0.11}F_2$

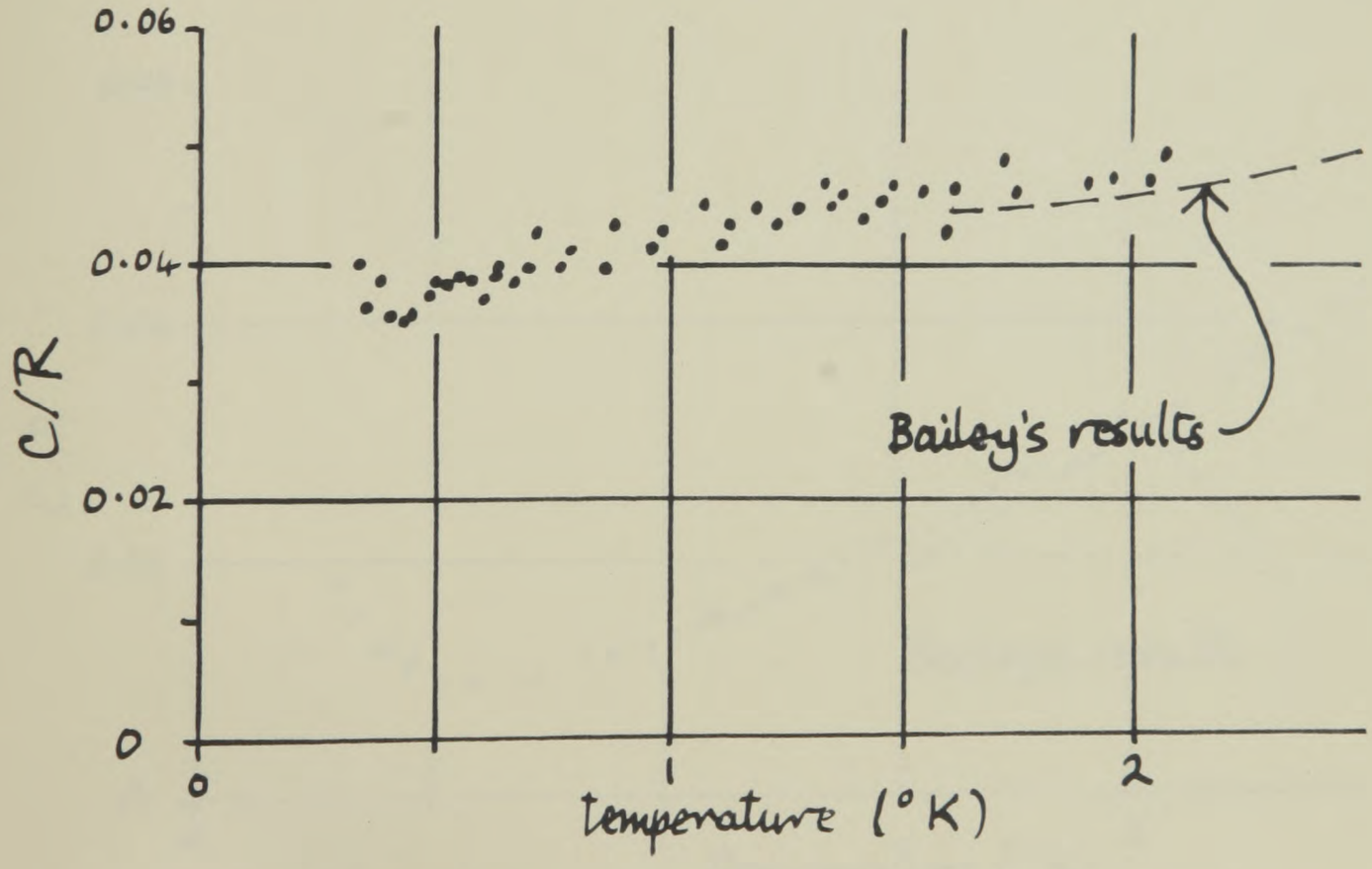

Figure 2 Heat capacity of $Zn_{0.82}Mn_{0.18}F_2$

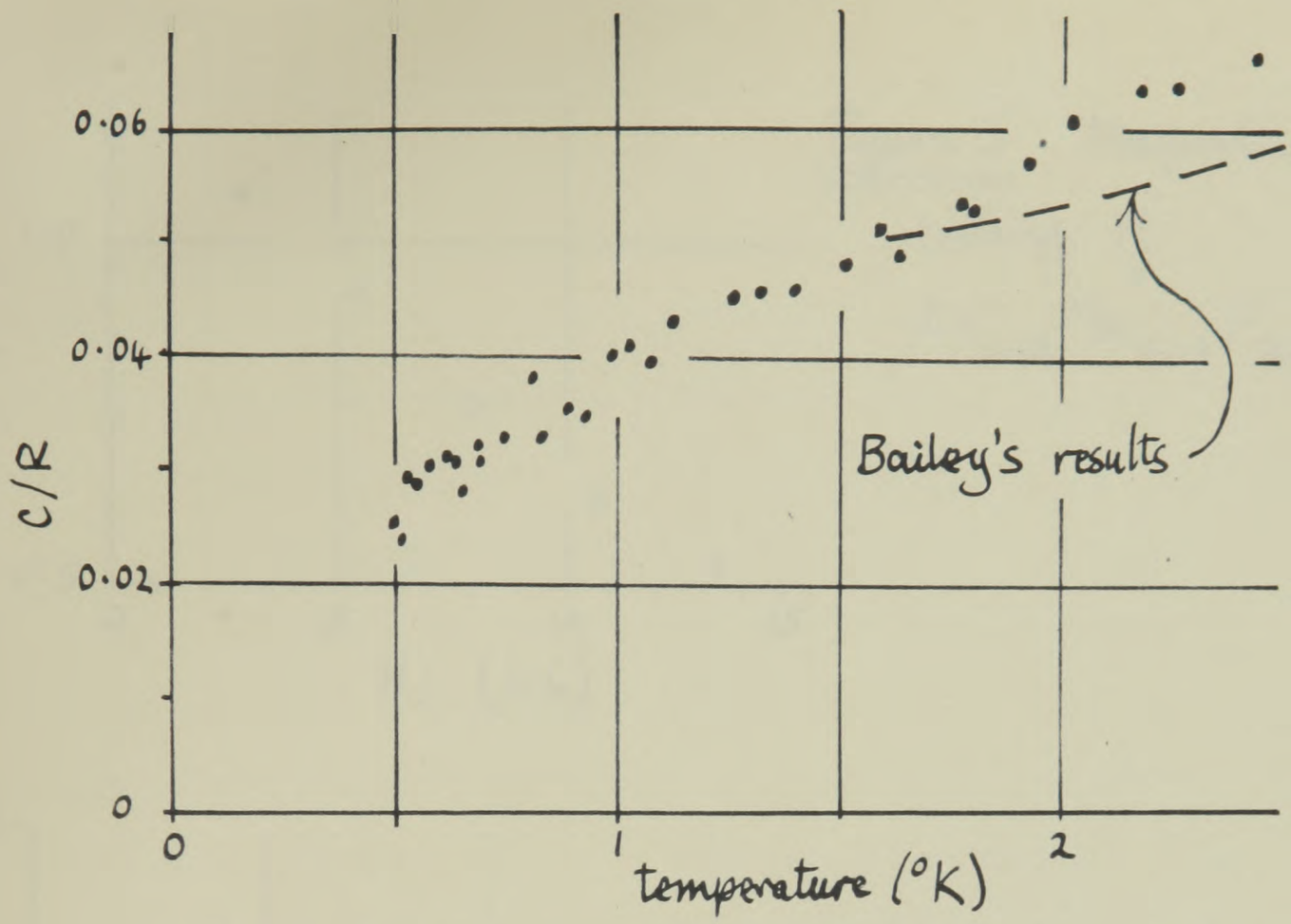

Figure 3 Heat capacity of $Zn_{0.75}Mn_{0.25}F_2$

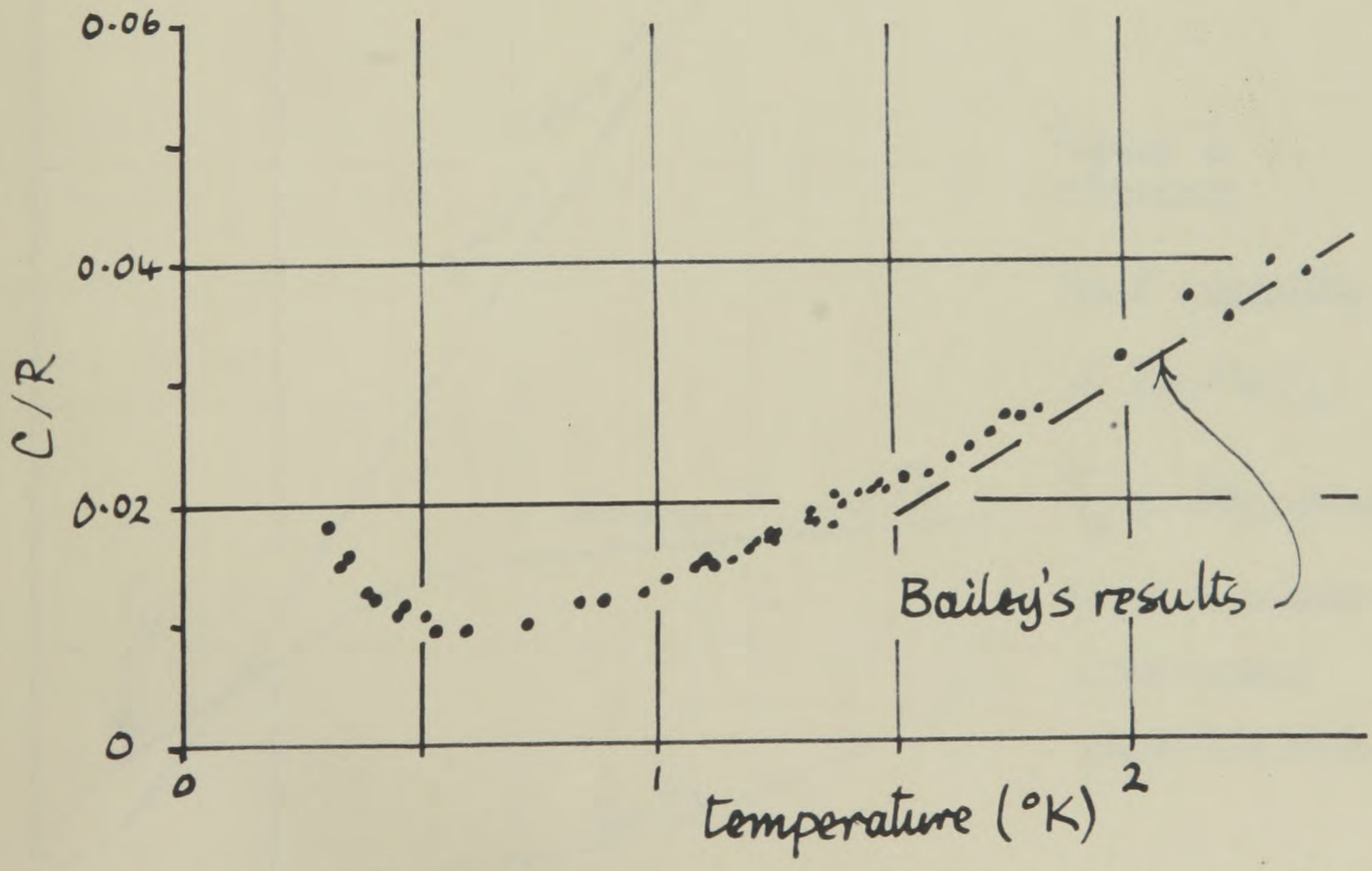

Figure 4 Heat capacity of $Zn_{0.57}Mn_{0.43}F_2$

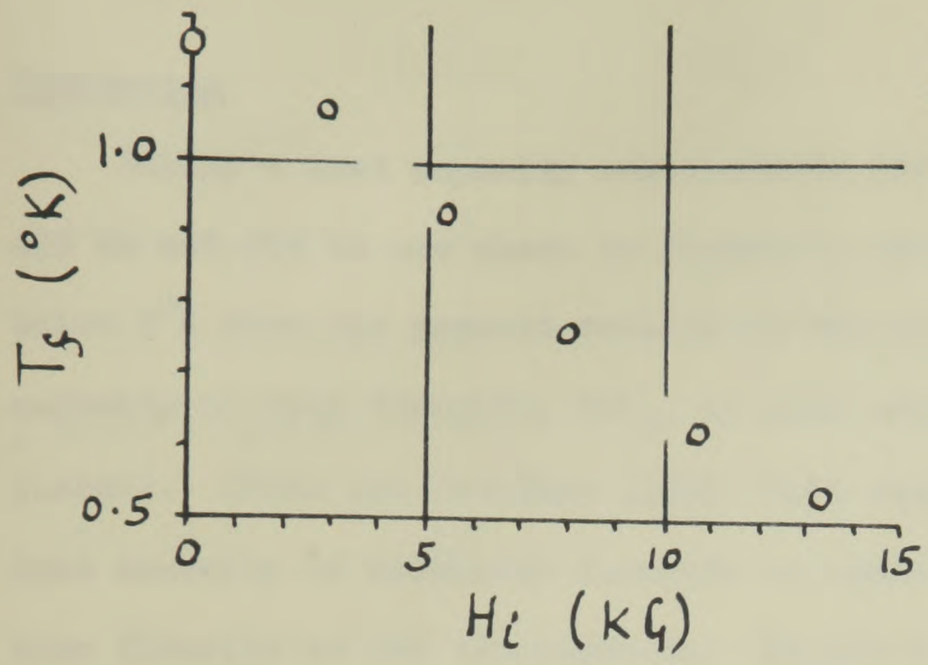

Figure 5 Magnetic cooling of $Zn_{0.82}Mn_{0.18}F_2$

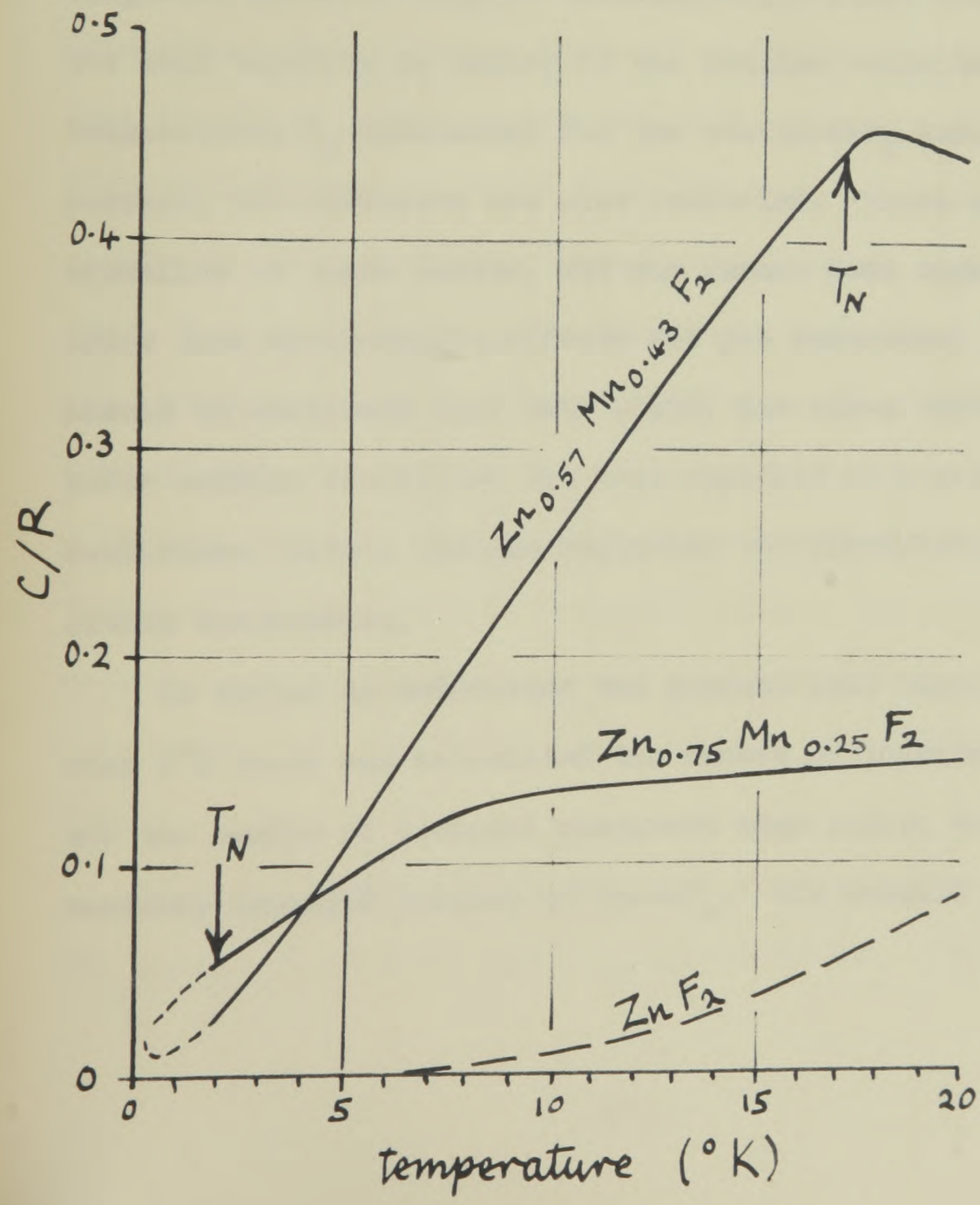

Figure 6

Heat capacities of Zn-MnF_2.

T_N :- Néel points from nuclear resonance experiments.

Discussion

Bailey's heat capacity measurements for the samples containing 43% Mn and 25% Mn are shown in figure 6, while the dotted lines below 2°K show the present results on the same scale. The heat capacity of zinc fluoride, ZnF_2, is also shown (Bailey, 1960, unpublished). Stout and Catalano (1955) have estimated that the lattice heat capacity of manganese fluoride is about 25% more than that of zinc fluoride at low temperatures. Figure 6 shows that the zinc-manganese fluoride samples therefore have large contributions to the heat capacity in excess of the lattice contribution. The Néel temperatures T_N determined for the two $Zn-MnF_2$ samples by Baker, Lourens, and Stevenson are also indicated. There are no sharp lambda anomalies at these points, but the excess heat capacities probably arise from co-operative effects not yet understood in detail. It should be mentioned that Bell (1958) has shown theoretically that under certain conditions the heat capacity of a solid mixture is continuous, with a maximum replacing the discontinuity at the transition temperature.

In trying to understand the present heat capacity measurements near 1°K Baker has calculated the number of isolated manganese atoms, and the number of isolated manganese atom pairs, and so on, in randomly arranged samples of $Zn-MnF_2$. His results are as follows -

	11% Mn	18% Mn	25% Mn	43% Mn
% single atoms	31	14	6	0.4
% atoms in pairs	18	8	3	-
% atoms in threes	10	5	1	-
% atoms in fours	0.4	1	0.1	-
% remainder	40	72	90	99

The solid curve in figure 7 shows smoothed values for the present heat capacity measurements on $Zn_{0.89}Mn_{0.11}F_2$ for one gram atom of manganese. Curve 1 shows the heat capacity of the isolated Mn^{++} ions in the ZnF_2 environment calculated by Baker by computer methods from paramagnetic resonance data (Clogston et al., 1960). Curve 2 shows the heat capacity also computed by Baker, and of the Schottky type, for the Mn^{++} ion pairs coupled by exchange. Unfortunately the exchange energy, estimated at ~ k x 3.5°K from the magnetic data of MnF_2, is subject to a probable error of about ± k x 2°K. A smaller exchange energy would account better for the experimentally observed shape of the heat capacity curve. The rest of the heat capacity probably arises in a similar way from the remainding coupled groups of ions, and from a small nuclear contribution as described below.

Figure 8 shows the present heat capacity measurements on $Zn_{0.57}Mn_{0.43}F_2$ for one gram atom of manganese. The anomaly below

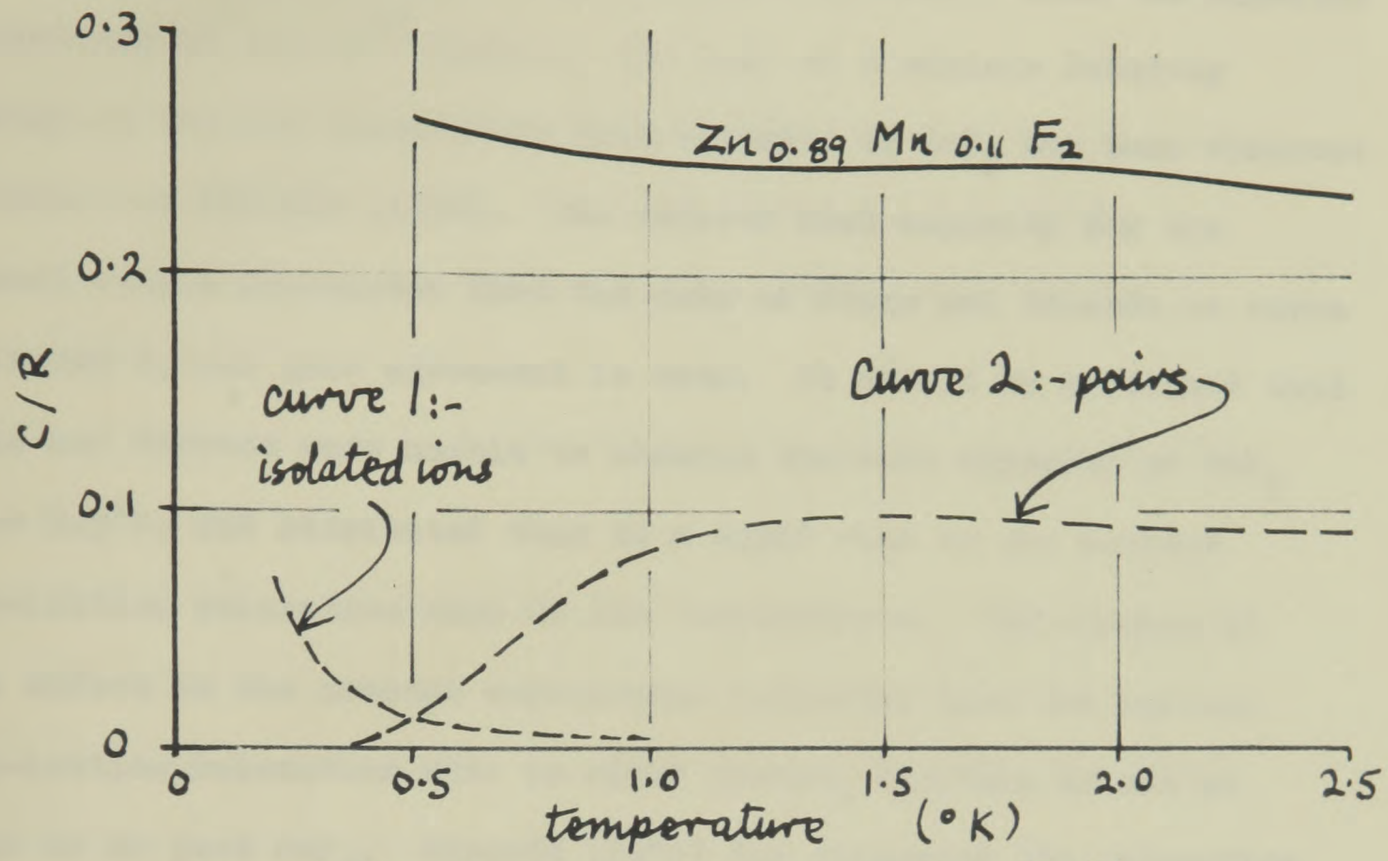

Figure 7 Heat capacity per mole of Mn

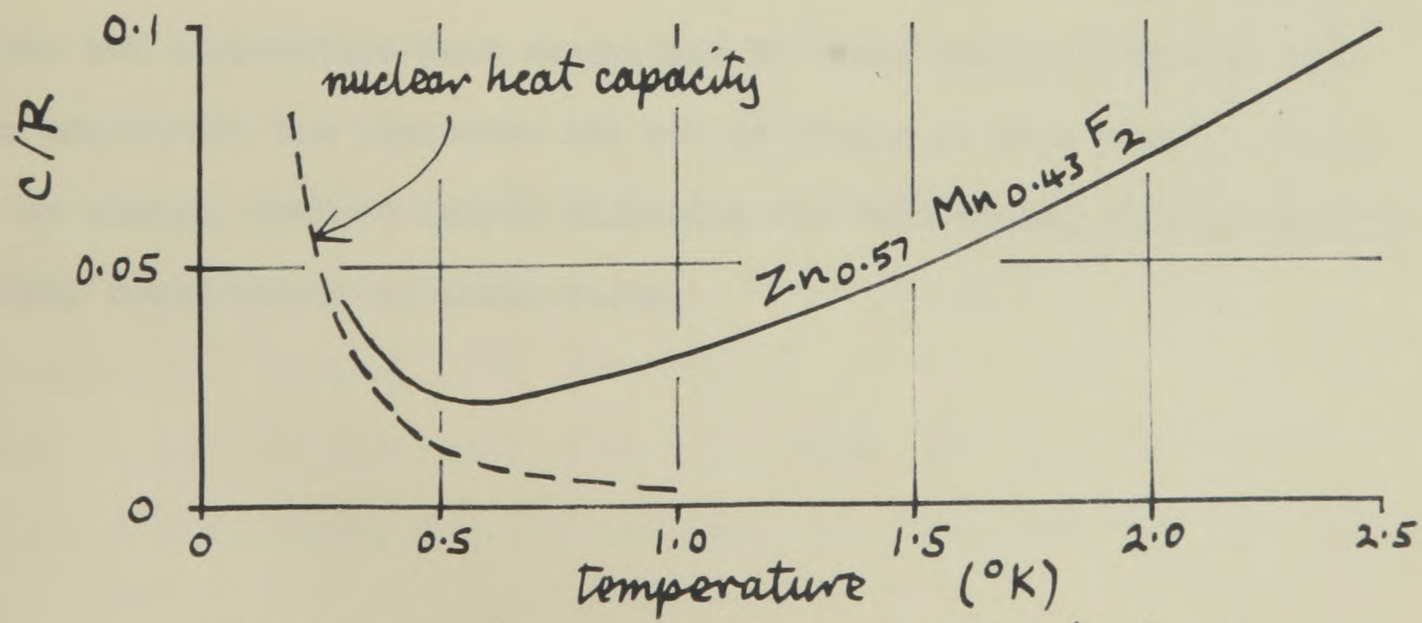

Figure 8 Heat capacity per mole of Mn

$1^{\circ}K$ in this antiferromagnetic sample probably arises from the magnetic interaction of the Mn^{55} nuclei. The tail of a nuclear Schottky anomaly in the low temperature heat capacity of MnF_2 has been observed by Cooke and Edmonds (1958). The nuclear heat capacity for the present sample calculated from the data of Cooke and Edmonds is shown in figure 8, and good agreement is seen. It should be mentioned that Cooke and Edmonds were unable to observe the heat capacity of MnF_2 below $0.5^{\circ}K$, and attributed this to a rapid rise in the nuclear spin-lattice relaxation time at low temperatures. The absence of this effect in the present experiments indicates that the nuclear spin-lattice relaxation time in mixed $Zn-MnF_2$ crystals is not as large as in pure MnF_2. Edmonds (1958) has discussed the relaxation mechanisms and drawn attention to experiments by Bloembergen (1949) which show that paramagnetic impurities greatly reduce the relaxation times.

To conclude this discussion we note that, although some features of the low temperature heat capacities of mixed $Zn-MnF_2$ crystals have been explained, the phenomena are not as simple as been hoped. There are no sharply defined lambda anomalies for determining antiferromagnetic Néel temperatures in these salts.

References

Abragam, A., and Pryce, M.H.L. Proc. Roy. Soc. A 205 135 (1951).

Ambler E., and Hudson, R.P. J. Chem. Phys. 27 378 (1957).

Arp, V., Edmonds, D., and Petersen, R., Phys. Rev. Letters 3 212 (1959).

Arp, V., Kurti, N., and Petersen, R. Bull. Amer. Phys. Soc. II 2 388 (1957).

Bagguley, D.M.S., and Griffiths, J.H.E. Proc. Roy. Soc. A 204 188 (1950).

Bagguley, D.M.S., and Owen, J. Rep. Prog. Phys. 20 304 (1957).

Bailey, C.A. Phil. Mag. 4 833 (1959).

Baker, J.M., Lourens, J.A., and Stevenson, R.W.H. Accepted for publication in Proc. Phys. Soc. (1961). 77, 1038.

Baldock, D.N. D.Phil. Thesis, Oxford (1960).

Batterman B.W. Phys. Rev. Letters 2 47 (1959).

Bean, C.P., and Livingston, J.D. J. App. Phys. Supp. 30 120S (1959).

Bell, G.M. Proc. Phys. Soc. 72 649 (1958).

Bleaney, B.,, and Stevens, K.W.H. Rep. Prog.Phys. 16 108 (1953).

Bleaney, B., and Trenam, R.S. Proc. Roy. Soc. A 223 1 (1954).

Bloembergen, N. Physica 15 386 (1949).

Cheng, C.H., Wei, C.T., and Beck, P.A. Phys. Rev. 120 426 (1960).

Clement, J.R., Logan, J.K., and Caffney, J. Phys. Rev. 100 743 (1955).

Clogston, A.M., Gordon, J.P., Jaccarino, V., Peter, M., and Walker, L.R.,
Phys. Rev. 117 1222 (1960).

Coles, B.R. Advances in Phys. 7 40 (1958).

Cooke, A.H., and Edmonds, D.T. Proc. Phys. Soc. 70 517 (1958).

Cooke, A.H., Meyer, H. and Wolf, W.P. Proc. Roy. Soc. A 233 536 (1956).
Proc. Roy. Soc. A 237 404 (1956).

Croft, A.J. D. Phil. Thesis, Oxford (1952).

Croft, A.J., and Exell, R.H.B. Accepted for publication in Proc.
Roy. Soc. (1961). A 262, 110.

Cutler, P.H. M.Sc. Thesis, Pennsylvania State University (1955).

Daniels, J.M. Proc. Phys. Soc. B 63 1028 (1950).

Daniels, J.M., and Kurti, N. Proc. Roy. Soc. A 221 243 (1954).

Edmonds, D.T. D. Phil. Thesis, Oxford (1958).

Flotow, H.E., Lohr, H.R., Abraham, B.M., and Osborne, D.W.
J. Am. Chem. Soc. 81 3529 (1959).

Freeman, R., Murray, G.R., and Richards, R.E. Proc. Roy. Soc.
A 242 455 (1957).

Gardner, W.E., and Kurti, N. Proc. Roy. Soc. A 223 542 (1954).

Giauque, W.F. Phys. Rev. 92 1339 (1953).

Giauque, W.F., Stout, J.W., Egan, C.J., and Clark, C.W.
J. Amer. Chem. Soc. 63 405 (1941).

Goodenough, J.B. Phys. Rev. 120 67 (1960).

Gossard, A.C., and Portis, A.M. Phys. Rev. Letters 3 164 (1959).

Grace, M.A., Johnson, C.E., Kurti, N., Scurlock, R.G., and Taylor, R.T.
Conf. Phys. Basses Temp. Paris (1955) p.263; Phil. Mag. 4
948 (1959).

Gruen, D.M. J. Chem. Phys. 23 1708 (1955).

Guthrie, G.L., Friedberg, S.A., and Goldman, J.E. Phys. Rev. 113 45 (1959).

Hanna, S.S., Heberle, J., Perlow, G.J., Preston, R.S., and Vincent, D.H. Phys. Rev. Letters. 4 177 and 513 (1960).

Heer, C.V. Bull. Amer. Phys. Soc. II 5 297 (1960).

Heer, C.V. and Erickson, R.A. Phys. Rev. 108 896 (1957).

Henry, W.E. Phys. Rev. 109 1976 (1958).

Herring, C. J. App. Phys. Supp. 31 (5) 3S (1960).

Hull J.R., and Hull, R.A. J. Chem. Phys. 9 465 (1941).

Jacob, C.W. and Warren, B.E. Am. Chem. Soc. J. 59 2588 (1937).

Jarrett, H.S. J. Chem. Phys. 27 1298 (1957).

Khutsishvili, G.R. J.E.T.P. 2 744 (1956).

Kim, P.H., and Sugawara, T. J. Phys. Soc. Japan. 13 968 (1958).

de Klerk, D., and Hudson, R.P. Phys. Rev. 91 278 (1953).

Komura, Y., Tomiie, Y., and Nathans, R. Phys. Rev. Letters 3 268 (1959).

Kurti, N. Conf. Phys. Basses Temp. Paris (1955). Discussion p. 187.

Kurti, N. Nuovo Cimento 6 Suppl. p. 1101 (1957).

Kurti, N. Z. Phys. Chem. Neue Folge 16 281 (1958).

Kurti, N., Rollin, B.V., and Simon, F.E. Physica 3 266 (1936).

Kurti, N., and Safrata, R.S. Phil. Mag. 3 780 (1958).

Kurti, N., and Simon, F.E. Proc. Roy. Soc. A 149 152 (1935).

Lin, S.T., and Kaufmann, A.R. Phys.Rev. 102 640 (1956).

Lipson, H. Proc, Roy. Soc. A 151 347 (1935).

Logan, J.K., Clement, J.R., and Jeffers, H.R. Phys. Rev. 105 1435 (1957).

Lomer, W.M., and Marshall, W. Phil. Mag. 3 185 (1958).

Marshall, W. Phys. Rev. 110 1280 (1958).

Mössbauer, R.L. Z. Physik. 151 124 (1958).

Mott, N. F., and Stevens, K.W. Phil. Mag. 2 1364 (1957).

Nagle, D.E., Frauenfelder, H., Taylor, R.D., Cochran, D.R.F., and Matthias, B.T. Phys. Rev. Letters 5 364 (1960).

Nevitt, M.V. J. App. Phys. 31 155 (1960).

Nicol, J., and Soller, T. Bull. Amer. Phys. Soc. II 2 63 (1957).

Robinson, W.K., and Friedberg, S.A. Phys. Rev. 117 402 (1960).

Rundle, R.E. J. Am. Chem. Soc. 69 1719 (1947); J. Am. Chem. Soc. 73 4172 (1951).

Samoilov, B.N., Sklyarevskii, V.V., and Stepanov, E.P. J.E.T.P. 36 (9) 972 (1959); J.E.T.P. 11 261 (1960).

Sato, H., Arrott, A., and Kikuchi, R. J. Phys. Chem. Solids. 10 19 (1959).

Schmid, L.P., and Smart, J.S. U.S. Naval Ordnance Rep. No. 3640 (1954).

Schroder, K. and Cheng, C.H. J. App. Phys. 31 2154 (1960).

Shulman, R.G., and Jaccarino, V. Phys. Rev. 108 1219 (1957).

Smith, P.L., and Wolcott, N.M. Conf. Phys. Basses Temp. Paris (1955) p.283.

Stout, J.W., and Catalano, E. J. Chem. Phys. 23 2013 (1955).

Trzebiatowski, W., Silwa, A., and Stalinski, B. Roczniki Chem. 26 110 (1952); 28 12 (1954). See Chem. Abstracts 46 10726 (1952); 48 11131 (1954).

Van Dijk, H., and Keesom, W.H. Physica 7 970 (1940).

Van Kranendonk, J., and Van Vleck, J.H. Rev. Mod. Phys. 30 1 (1958).

Weiss, R.J., and DeMarco, J.J. Rev. Mod. Phys. 30 59 (1958).

White, G.K. Experimental Techniques in Low Temperature Physics, Oxford (1959).

Additional References

Anderson P.W., and Clogston A.M. Bull. Am. Phys. Soc. II 6, 124, (1961).

Batterman B.W., Chipman D.R., and deMarco J.J. Phys. Rev. 122, 68, (1961).

Benedek G.B., and Armstrong J. J. App. Phys. Supp. 32, 1065 (1961).

Bogle G.S., Cooke A.H., and Whitley S. Proc. Phys. Soc. A 64, 931, (1951).

Bogle G.S., and Heine V. Proc. Phys. Soc. A 67, 734, (1954).

Boyle A.J.F., Bunbury D.St.P., and Edwards C. Phys. Rev. Letters, 5, 553, (1960).

Bruner L.J., Budnick J.I., and Blume R.J. Phys. Rev. 121, 83, (1961).

Budnick J.I., Bruner L.J., Blume R.J., and Boyd E.L. J. App. Phys. Supp. 32, 120 S, (1961).

Dash J.G., Taylor R.D., Craig P.P., Nagle D.E., Cochran D.R.F., and Keller W.E. Phys. Rev. Letters. 5, 152, (1960).

Dash J.G., Taylor R.D., Nagle D.E., Craig P.P., and Visscher W.M. Phys. Rev. 122, 1116, (1961).

Guthrie G.L., Freidberg S.A., and Goldman J.E. Phys. Rev. 113, 45, (1959).

Hardy W.A. J. App. Phys. Supp. 32, 122 S, (1961).

Jaccarino V. Bull. Am. Phys. Soc. II 4, 461, (1959).

Johnson C.E., Ridout M.S., Cranshaw T.E., and Madsen P.E. Phys. Rev. Letters, 6, 450, (1961).

Knight W.D. Solid State Physics, 2, 93, (1956).

Kogan, A.V., Kul'kov V.D., Nikitin L.P., Reinov N.M., Sokolov I.A., and Stel'makh M.F. J.E.T.P. 13, 78, (1961).

Koi Y., and Tsujimura A. J. Phys. Soc. Japan, 16, 1040, (1961).

Nelson D.T., and Legvold S. Phys. Rev. 123, 80, (1961).

Newman M.M., and Stevens K.W.H. Proc. Phys. Soc. 74, 290, (1959).

Owen J., Browne M.E., Arp V., and Kip A.F. J. Phys. Chem. Solids, 2, 85, (1957).

Owen J., Browne M., Knight W.D., and Kittel C. Phys. Rev. 102, 1501, (1956).

Parks R.D., and Little W.A. Phys. Rev. Letters. 6, 539, (1961).

Portis A.M., and Gossard A.C. J. App. Phys. Supp. 31, 205 S, (1960).

Robert C., and Winter J.M., Compt. Rend. 250, 3831, (1960).

Shirley D.A., Kaplan M., and Axel P. Phys. Rev. 123, 816, (1961).

Shull C.G., and Wilkinson M.K. Phys. Rev. 97, 304, (1955).

Shull C.G., and Wollan E.O. Solid State Physics, 2, 181, (1956).

Street R., Rodbell D.S., and Roth W.L. Phys. Rev. 121, 84, (1961).

Van Dijk H. Physica 12, 371, (1946).

Watson R.E., and Freeman A.J. J. App. Phys. Supp. 32, 118 S, (1961a); Phys. Rev. 123, 2027, (1961b).

Wei C.T., Cheng C.H., and Beck P.A. Phys. Rev. 122, 1129, (1961).

Weiss R.J., and Freeman A.J. J. Phys. Chem. Solids. 10, 147, (1959).

Wertheim G.K. J. App. Phys. Supp. 32, 110 S, (1961).

Wertheim G.K., and Wernick J.H. Phys. Rev. 123, 755, (1961).

Yosida K. Phys. Rev. 106, 893, (1957).